

**THE STRUCTURE AND EVOLUTION OF LOWER
STRATOSPHERIC FRONTAL ZONES**

by

Andrea Angela Lopez Lang

**A dissertation submitted in partial fulfillment of
the requirements for the degree of**

**Doctor of Philosophy
(Atmospheric and Oceanic Sciences)**

at the

UNIVERSITY OF WISCONSIN-MADISON

2011

**© Copyright by Andrea Angela Lopez Lang 2011
All Rights Reserved**

Abstract

The structure and evolution of the lower stratospheric portion of upper level jet-front systems (ULJFs) are examined in a variety of cases. Following a historical overview, the first half of the analysis examines two lower stratospheric frontal zones. The asynchronous evolution of the lower stratospheric and upper tropospheric frontal portions of ULJFs, as well as some substantial differences in lower stratospheric frontal development that occur in southwesterly and northwesterly flow are highlighted.

The northwesterly flow case was characterized by an initially intense but weakening lower stratospheric front along with an initially weak but intensifying upper tropospheric front. Geostrophic cold air advection in the lower stratospheric cyclonic shear supported subsidence within the cold upper troposphere. This subsidence resulted in lower stratospheric frontolysis via tilting and extended downward below the jet core where it is suggested to have played a role in the early stages of upper tropospheric frontogenesis.

The southwesterly flow case was characterized by a strengthening lower stratospheric front and a weakening upper tropospheric front. A deep column of upward vertical motion resulted from the superposition of lower tropospheric ascent associated with convection along a surface cold front and upper tropospheric ascent through the jet core, coincident with geostrophic warm air advection in the lower stratospheric cyclonic shear. The upper tropospheric ascent, on the cold edge of the lower stratospheric front, acted frontogenetically in the lower stratosphere via tilting.

The second half of the analysis highlights four recent southwesterly flow cases and

suggests a role for tropospheric convection in the development of each lower stratospheric front. The analysis suggests that the lower stratospheric frontogenetic ascent may become enhanced in response to a convective destabilization of the upper troposphere. As latent heating associated with surface frontal convection redistributed the thermal field, the static stability of the near-tropopause upper troposphere decreased. Such a destabilization was associated with a robust response to lower stratospheric QG forcing, in the form of ascent within the cold upper troposphere, and led to lower stratospheric frontogenetic tilting in each case. The implications of the lower stratospheric frontogenetic processes on tropical-extratropical interactions and downstream sensible weather are discussed.

Acknowledgements

I first would like to acknowledge my advisor, Dr. Jonathan Martin. I owe Jon so much credit for both his direct and behind-the-scenes efforts to advance my career. He has always been extremely supportive of my efforts, not only as a scientific mentor, but as a confidence booster as well as a promoter of my general interests. Jon, thanks for coming to my track meets and encouraging me in my coaching role throughout my grad school career. Thanks for allowing me to TA 452 so many times, I can honestly say that I learn something new about science, and about how to be a great teacher, every time I sat through the class. Most of all, thanks for the encouragement and the freedom to make this research my own, you have (and will continue to be) been a great mentor to me.

Throughout grad school, I have had an amazing amount of support from my family and friends. Thanks to all my 1421 office mates over the years and the Morgan group. It seems like I've seen many come and go, but during that time it's been great chat, to bounce ideas off of you all, chat some more, commiserate over Jon's handwriting, and chat even more. Thanks for listening! Of course I have to thank my parents for being so supportive, you were always were interested in hearing about what I was working on and what I was going to do next. Finally I have to thanks James for being a supportive and encouraging husband. Thanks for supporting us though the grad school years, for coming to my talks even if you couldn't follow all of them, and for the encouragement (even though our field uses Fortran and the Linux). I would not have been able to finish this accomplishment without all the support! Thanks again!

Table of Contents

Abstract	i
Acknowledgments	iii
Table of Contents	iv
List of Figures	vi
1. Introduction: A history of jet front observation and theory	1
1.1. The discovery of the jet stream	3
1.2. Understanding the jet-front structure	5
1.2a. Arguments for a mesoscale lower stratospheric structure	5
1.2b. Arguments for a synoptic scale lower stratospheric structure	9
1.2c. Resolving the lower stratospheric structure	13
2. Part I: Examples in northwesterly and southwesterly flow	18
2.1. Introduction	18
2.2. Background	22
2.3. Northwesterly flow case	27
2.3a. Synoptic Overview	27
2.3b. Analysis	31

2.4. Southwesterly flow case	38
2.4a. Synoptic Overview	38
2.4b. Analysis	41
2.5. Summary and Conclusions	47
3. Part II: The influence of tropospheric convection on lower stratospheric frontal development	54
3.1. Introduction	54
3.2. Case Overviews	57
3.2a. Case 1: 19-20 November 2008	58
3.2b. Case 2: 8 December 2008	61
3.2c. Case 3: 7 January 2009	63
3.2d. Case 4: 4 March 2009	66
3.3. Analysis I: Overview of common dynamical processes	68
3.3a. Diabatic stability tendency	69
3.3b. Lower stratospheric QG forcing, ascent, and tilting frontogenesis	72
3.4. Analysis II: Vertical cross sections	77
3.4a. Case 1	77
3.4b. Case 2	79
3.4c. Case 3	81
3.4d. Case 4	83
3.5. Summary and Discussion	85
4. Future Research Directions	89

4.1. Overview of future research directions	89
4.1a. Convection, the tropics and ULJFs	90
4.1b. Lower stratospheric fronts and downstream development	91
4.2a. Stratosphere-Troposphere coupling	92
4.2. Research proposal: North Pacific jet circulations during the extratropical transition of western Pacific tropical cyclones	93
5. References	101

Figure Captions

Figure 1.1. A cross section analysis, from Spain (left) to Sweden (right), of temperature (top) and potential temperature (bottom) by Bjerknes and Palmén (1937). The thick double lines represent the location of the polar front and the single thick line represents the tropopause.

Figure 1.2. For 28 Jan. 1948 (a) the observed and contoured temperature distribution at 200 hPa with the hatched (shaded) area represents the coldest (warmest) temperature at that level and (b) the observed and contoured tropopause height in pressure, with the L(H) representing the lowest (highest) geometric height of the tropopause.

Figure 1.3. A cross section through a synoptic scale trough with the cross stream vertical circulations superimposed on the idealized locations of the polar front and tropopause, from Palmén and Nagler (1949).

Figure 1.4. From Reed and Danielsen (1959), a 5 case composite of (a) temperature (dashed) and thermal-wind derived wind field (solid), and (b) potential temperature (dashed) and derived potential vorticity (solid) fields, with thick lines representing the tropopause and

frontal surfaces in both plots.

Figure 1.5. Adapted from Shapiro (1981), this cross sectional analysis of a particularly strong jet front system over the Desert Southwest. Potential temperature (K) is contoured in solid lines, wind (ms-1) in dashed, the tropopause in red, the jet maximum labeled with a “J” and the cyclonic wind shear on the order of 100 km shaded in yellow.

Figure 1.6. For an idealized jet-front system seen in a vertical-cross front cross sectional with potential temperature, (a) the geostrophic forcing in the Sawyer-Eliassen circulation, and (b) the resulting secondary vertical circulation calculated by solving for ψ in the Sawyer-Eliassen circulation.

Figure 2.1. Vertical cross section of isotachs (m s^{-1} , solid) and isentropes (K, dashed) through an ULJF at 0000 UTC 17 April 1976, using NWS radiosonde data from Winslow, AZ (INW), Tuscon, AZ (TUS), and Fraccionamiento, Mexico (FRC) and supplemented with NCAR Sabreliner aircraft data. The regions of locally enhanced baroclinicity, static stability, and horizontal and vertical shear are shaded, representing the upper tropospheric front (UT Front) below the jet core and the lower stratospheric front (LS Front) above the jet core. Bold black line is the 1.5 PVU ($1 \text{ PVU} = 10^{-6} \text{ K m}^2 \text{ kg}^{-1} \text{ s}^{-1}$) identifying the dynamic tropopause. Adapted from Shapiro (1981).

Figure 2.2. Vertical cross section of isotachs (m s^{-1} , solid) and isentropes (K, dashed) from Valentia, Ireland to Hannover, Germany at 0300 UTC 9 November 1949. The shaded area represents a continuous frontal zone as described by Berggren (1952). Adapted from Berggren (1952).

Figure 2.3. Schematic illustration of idealized configurations of potential temperature along a straight jet streak maximum on an upper tropospheric isobaric surface. Geopotential height (thick solid), potential temperature (dashed), isotachs (thin solid filled) with the jet maximum represented by “J,” and a sense of the mid-tropospheric Sawyer-Eliassen vertical motions (up or down) for (a) no thermal advection along the jet (b) geostrophic cold air advection along the jet and (c) geostrophic warm air advection along the jet.

Figure 2.4. (a) – (c) As for Figure 2.3 (a) – (c) but for a lower stratospheric isobaric surface.

Figure 2.5. (a) 200 hPa geopotential height (solid), potential temperature (dashed), and magnitude of the horizontal potential temperature (shaded) from the Eta-104 model analysis valid at 0600 UTC 4 February 2008. Geopotential height is labeled in m and contoured every 200m, isentropes are labeled in K and contoured every 3 K, and the magnitude of the horizontal potential temperature gradient is shaded every $1 \text{ K (100 km)}^{-1}$ beginning at $2 \text{ K (100 km)}^{-1}$. (b) As for Figure 2.5(a) but at 500 hPa. (c) and (d) As for Figure 2.5 (a) and (b) but from the Eta-104 model analysis valid at 1800 UTC 4 February 2008. (e) and (f) As for Figure

2.5 (a) and (b) but from the Eta-104 model analysis valid at 0600 UTC 5 February 2008. (g) and (h) As for Figure 2.5 (a) and (b) but from the Eta-104 model analysis valid at 1800 UTC 5 February 2008

Figure 2.6. (a) 200 hPa geopotential height (thick solid), geostrophic isotachs (thin solid), isentropes (dashed), and geostrophic temperature advection (shaded) from the Eta-104 model analysis valid at 0600 UTC 4 February 2008. Geopotential height is contoured every 200 m, isentropes are labeled in K and contoured every 3 K, isotachs are labeled in m s^{-1} and contoured every 10 m s^{-1} , and dark (light) shading is geostrophic temperature advection contoured in units of K s^{-1} every $-3 (3) \times 10^{-4} \text{ K s}^{-1}$. (b) 200 hPa geopotential height (thick solid), isentropes (dashed), and vertical motion (shaded). Geopotential height is contoured as in Figure 2.6(a), isentropes are labeled and contoured as in Figure 2.6(a), and shaded solid (dashed) contours represent subsidence (ascent) and are contoured in cm s^{-1} every $-2 (2) \text{ cm s}^{-1}$ beginning at $-2 (2) \text{ cm s}^{-1}$. (c) Isentropes (dashed) and tilting frontogenesis (shaded). Isentropes are labeled and contoured as in Figure 2.6(a) and tilting frontogenesis is in units of $\text{K m}^{-1} \text{ s}^{-1}$ and contoured every $5 (-5) \times 10^{-9} \text{ K m}^{-1} \text{ s}^{-1}$ starting at $10 (-10) \times 10^{-9} \text{ K m}^{-1} \text{ s}^{-1}$ with dark (light) shading indicating negative (positive) tilting frontogenesis.

Figure 2.7. Vertical cross section along the line A-A' in Figure 2.6a valid at 0600 UTC 4 February 2008. (a) Potential temperature (thin solid), geostrophic isotachs (dashed), magnitude of the horizontal potential temperature gradient (shaded), and the tropopause (thick solid).

Potential temperature is labeled in K and contoured every 4 K, isotachs are labeled in m s^{-1} and contoured every 10 m s^{-1} beginning at 30 m s^{-1} , the magnitude of the horizontal potential temperature gradient is contoured every 1 K (100km)^{-1} beginning at $2 \text{ K (100 km)}^{-1}$ and the tropopause is represented by the 1.5 PVU contour. (b) Potential temperature (thin light solid), geostrophic isotachs (thin dark solid), geostrophic temperature advection (dashed), vertical motion (shaded), and the tropopause (thick solid). Potential temperature is labeled and contoured as in Figure 2.7(a), isotachs are labeled as in Figure 2.7(a), geostrophic temperature advection contoured in units of K s^{-1} every $-3 (3) \times 10^{-4} \text{ K s}^{-1}$ with dark (light) contours representing cold (warm) air advection. Vertical motions are contoured in cm s^{-1} every $-2 (2) \text{ cm s}^{-1}$ beginning at $-2 (2) \text{ cm s}^{-1}$ with dark (light) shading representing subsidence (ascent), and the tropopause is represented as in Figure 2.7(a).

Figure 2.8. (a)-(c) As for Figure 2.6(a)-(c) but from the Eta-104 analysis valid 1800 UTC 4 February 2008.

Figure 2.9. As for Figure 2.7(b), but from the Eta-104 analysis valid 1800 UTC 4 February 2008 along the line B-B' in Figure 2.8(a).

Figure 2.10. (a) and (b) As for Figure 2.5 (a) and (b), but from the Eta-104 model analysis valid at 0000 UTC 27 February 2008. (c) and (d) As for Figure 2.5 (a) and (b), but from the Eta-104 model analysis valid at 1200 UTC 27 February 2008. (e) and (f) As for Figure 2.5 (a)

and (b), but from the Eta-104 model analysis valid at 0000 UTC 28 February 2008. (g) and (h)

As for Figure 2.5 (a) and (b), but from the Eta-104 model analysis valid at 1200 UTC 28 February 2008.

Figure 2.11. (a)-(c) As for Figure 2.6(a)-(c) but from the Eta-104 analysis valid at 0000 UTC 28 February 2008.

Figure 2.12. As for Figure 2.7(b), but from the Eta-104 analysis valid at 0000 UTC 28 February 2008 along the line C-C' in Figure 2.11(a).

Figure 2.13. (a)-(c) As for Figure 2.6(a)-(c) but from the Eta-104 analysis valid at 1200 UTC 28 February 2008.

Figure 2.14. As for Figure 2.7(b), but from the Eta-104 analysis valid at 1200 UTC 28 February 2008 along the line D-D' in Figure 2.13(a).

Figure 2.15. Schematic illustrating the asynchronous evolution of the lower stratospheric (LSF) and upper tropospheric frontal (UTF) portions of an ULJF within the (a) northwesterly and (b) southwesterly flow portions of a baroclinic wave. The dashed shaded oval in (a) represents the region of geostrophic cold air advection in cyclonic shear. In such a location within an ULJF, the lower stratospheric front experiences frontolysis via vertical tilting and the

upper tropospheric front experiences frontogenesis via tilting. The frontogenesis is associated with extrusion of stratospheric PV into the troposphere and subsequent downstream surface cyclogenesis. The solid shaded oval in (b) represents the region of geostrophic warm air advection in cyclonic shear. In such a location within an ULJF, the lower stratospheric front experiences frontogenesis and the upper tropospheric front experiences frontolysis via tilting. Darker shaded areas represent the jet stream isotachs. Lower stratospheric frontogenesis intensifies the jet and promotes ridge building downstream. See text for additional explanation.

Figure 3.1. Conceptual models of lower stratospheric frontolysis in northwesterly flow and lower stratospheric frontogenesis in southwesterly flow in (a) and (b), respectively, as summarized in the text. (a) With geostrophic cold air advection (shaded), subsidence represented by the arrow, idealized potential temperature (thin line), jet core represented by the “J”. (b) As in (a) but with geostrophic warm air advection shaded and ascent represented by the arrow.

Figure 3.2. (a) 200 hPa geopotential height, θ , and $|\nabla\theta|$ from the GFS analysis valid at 1800 UTC 19 November 2008. Geopotential height (solid) is labeled in m and contoured every 200 m, θ (dashed) is labeled in K and contoured every 3 K, and $|\nabla\theta|$ is in units of $\text{K} (100 \text{ km})^{-1}$ shaded every $1 \text{ K} (100 \text{ km})^{-1}$ beginning at $2 \text{ K} (100 \text{ km})^{-1}$. (b) as in (a) but at 500 hPa, (c) as in (a) but from the GFS analysis valid at 0600 UTC 20 November 2008, and (d) as in (a) but

from the GFS analysis at 0600 UTC 20 November 2008 and at 500 hPa. (e) Sea level isobars (solid), 950 hPa θ_e (dashed) and 950 hPa horizontal frontogenesis (shaded). Isobars labeled in hPa and contoured every 5 hPa, 950 hPa θ_e labeled in K and contoured every 4 K, and shading indicating 950 hPa horizontal frontogenesis exceeding $5 \text{ K (100 km)}^{-1} (3 \text{ h})^{-1}$.

Figure 3.3 (a) and (b) As for Figures 3.2(a) and (b), but from the GFS analysis valid at 0000 UTC 8 December 2008. (c), (d) and (e) as in Figures 3.2(c), (d) and (e), but from the GFS analysis valid at 1200 UTC 8 December 2008.

Figure 3.4. (a) and (b) As for Figures 3.2(a) and (b), but from the GFS analysis valid at 0600 UTC 7 January 2009. (c), (d) and (e) as in Figures 3.2(c), (d) and (e), but from the GFS analysis valid at 1800 UTC 7 January 2009.

Figure 3.5. (a) and (b) As for Figures 3.2(a) and (b), but from the GFS analysis valid at 0600 UTC 4 March 2009. (c), (d) and (e) as in Figures 3.2(c), (d) and (e), but from the GFS analysis valid at 1800 UTC 4 March 2009

Figure 3.6. The 200 hPa potential temperature contoured every 4 K (dashed) and the diabatic static stability tendency at 250 hPa contoured every 1 K day^{-1} with purple (yellow) shading corresponding to a decrease (increase) in static stability. From the GFS analysis valid at (a)

0600 UTC 20 November 2008, (b) 1200 UTC 8 December 2008, (c) 1800 UTC 7 January 2009, and (d) 1800 UTC 4 March 2009.

Figure 3.7. The 200 hPa potential temperature contoured every 4 K (dashed), the geostrophic isotachs every 10 m s^{-1} beginning at 40 m s^{-1} (solid), and the geostrophic temperature advection in pink (blue) shading above $3 \times 10^{-4} \text{ K s}^{-1}$ (below $-3 \times 10^{-4} \text{ K s}^{-1}$) and contoured every $3 \times 10^{-4} \text{ K s}^{-1}$. From the GFS analysis valid at (a) 0600 UTC 20 November 2008, (b) 1200 UTC 8 December 2008, (c) 1800 UTC 7 January 2009, and (d) 1800 UTC 4 March 2009.

Figure 3.8. The 200 hPa potential temperature contoured every 4 K (solid) and vertical motion from the model analysis every 2 cm s^{-1} beginning at 2 cm s^{-1} in red (-2 cm s^{-1} in blue). From the GFS analysis valid at (a) 0600 UTC 20 November 2008, (b) 1200 UTC 8 December 2008, (c) 1800 UTC 7 January 2009, and (d) 1800 UTC 4 March 2009.

Figure 3.9. 200 hPa potential temperature contoured every 4 K (dashed) and positive tilting frontogenesis shaded and contoured every $4 \times 10^{-9} \text{ K m}^{-1} \text{ s}^{-1}$. From the GFS analysis valid at (a) 0600 UTC 20 November 2008, (b) 1200 UTC 8 December 2008, (c) 1800 UTC 7 January 2009, and (d) 1800 UTC 4 March 2009.

Figure 3.10. Vertical cross section along the line A-A' in Figure 3.7(a) of potential

temperature, geostrophic isotachs, geostrophic temperature advection, vertical motions and diabatic stability tendency from the GFS analysis valid at 0600 UTC 20 November 2008.

Potential temperature (thin gray lines) is labeled in K and contoured every 4 K. Geostrophic isotachs (thick black lines) labeled in m s^{-1} and contoured every 10 m s^{-1} beginning at 40 m s^{-1} .

Vertical motion, with upward (downward) motion in the pink (blue) shading, is contoured in every 2 cm s^{-1} beginning at $4 (-4) \text{ cm s}^{-1}$ then contoured every 5 cm s^{-1} after $20 (-20) \text{ cm s}^{-1}$.

Geostrophic temperature advection (dashed lines) contoured every $3 \times 10^{-4} \text{ K s}^{-1}$ beginning at $3 (-3) \times 10^{-4} \text{ K s}^{-1}$ in the red (blue). Negative diabatic static stability tendency contoured and shaded (yellow) in a every 1 K day^{-1} and beginning at -1 K day^{-1} .

Figure 3.11. As for Figure 3.10, but from the GFS analysis valid at 1200 UTC 8 December 2008 and along the line B-B' in Figure 3.7(b).

Figure 3.12. As for Figure 3.10, but from the GFS analysis valid at 1800 UTC 7 January 2009 and along the line C-C' in Figure 3.7(c).

Figure 3.13. As for Figure 3.10, but from the GFS analysis valid at 1800 UTC 4 March 2009 and along the line D-D' in Figure 3.7(d).

Figure 3.14. Conceptual model of the impact of convectively generated latent heat release on

lower stratospheric frontal development as shown in idealized cross sections through jet-front systems (a) without convection and (b) with convection. (a) A dynamically active lower stratospheric front, characterized by geostrophic warm air advection in cyclonic shear (pink shading), forces ascent (red arrow) that can increase the slope of the isentropes (thin lines) and dynamic tropopause (blue line) above the jet core via frontogenetic tilting. (b) Convectively generated latent heat release reduces the stability in the near-tropopause upper troposphere and can enhance the ascent response to the lower stratospheric QG forcing (larger arrow) thereby intensifying the lower stratospheric tilting frontogenesis process, resulting in a steeply sloped tropopause and an intensified tropopause jet. See text for explanation.

Figure 4.1. A cross section the North Atlantic jet off the east coast of North America at 0000 UTC 28 November 2008, highlighting the jet core (marked with a “J”) and associated frontal structures. The upper tropospheric front is labeled “UTF” and the lower stratospheric front is labeled “LSF.” Isotachs are thick lines every 10 m s^{-1} beginning at 50 m s^{-1} , isentropes are thin lines every 4 K, and the magnitude of the horizontal potential temperature gradient is filled every $1 \text{ K (100 km)}^{-1}$ beginning at $2 \text{ K (100 km)}^{-1}$.

Figure 4.2. Valid at 0600 UTC 5 November 2010. Left: Cross section from A-A' in the right panel, with potential temperature every 4 K (gray lines), cross section normal wind speed every 10 m s^{-1} beginning at 50 m s^{-1} (thick lines), tropopause (1.5 PVU, green lines), geostrophic temperature advection every $5 \times 10^{-4} \text{ K s}^{-1}$ beginning at $5 \text{ (-5)} \times 10^{-4} \text{ K s}^{-1}$ in red

(blue) dashed lines, vertical motion every 2 cm s^{-1} beginning at 4 cm s^{-1} (-4 cm s^{-1}) in pink (blue) fills. Right: 850 hPa equivalent potential temperature in K (fill), ~ 175 hPa potential temperature (black lines every 3 K), sea level pressure (white lines, every 5 hPa), and the 70 m s^{-1} isosurface (green).

Chapter 1

Introduction: A history of jet-front observation and theory

Reinforced by the dramatically increasing number of routine surface weather observations across Europe, the early part of the 20th century was a revolutionary period for the science of meteorology. Analysis of the newly expanded network of surface observations steadily increased the ability of researchers to capture the horizontal structure and evolution of midlatitude weather systems. This synoptic perspective led to burgeoning scientific interest and theories regarding the origin of midlatitude sensible weather. By the turn of the century Margules (1903) had already introduced the fundamental hypothesis that the observed pole to equator temperature gradient was the source of energy for the general circulation of the atmosphere. His theory subsequently sparked the curiosity of researchers interested in the contribution made by individual weather systems to the general circulation of the atmosphere. Consequently, the development of the Polar Front Theory and the Norwegian Cyclone Model by Bjerknes (1921) and Bjerknes and Solberg (1922), respectively, became the primary organizing contributions to the science of modern meteorology.

The *polar front* was described as a continuous front, draped across the mid-latitudes of Earth, that separated the cold polar air from warm tropical air and was “imagined” to continue throughout the troposphere. The Norwegian Cyclone Model suggested that along the polar

front, cyclonic disturbances could develop such that their circulation would transport tropical air northward on their eastern side, creating a warm front, while moving polar air southward on their western side, creating a cold front. The warm and cold fronts were connected at the center of the cyclonic disturbance forming a kink in the overall polar front. The fronts could be identified by their characteristic features, including regions of enhanced cyclonic shear, regions of notable temperature contrast, and by regions of enhanced stability as noted in vertical profiles. Though the Polar Front Theory and Norwegian Cyclone Model were developed and used profusely throughout Europe in the 1920s, it took time for these concepts to take hold elsewhere. It was not until the late 1920s that these weather system concepts were applied by Rossby and Weighman (1926) in the first surface frontal analysis of a North American weather system.

As the field of meteorology expanded in both the U. S. and Europe, observations became plentiful at the Earth's surface, while observations of the free atmosphere remained much more sparse. In the late 1920s and early 1930s, the Dines meteorograph (Dines, 1929) was developed and used throughout Europe to take meteorological observations to altitudes as high as 15 km into the free atmosphere. By the mid-1930s, systematic upper air observations were becoming more routine across Europe. The growing abundance of upper air data in campaigns such as the European Serial Ascents Program (ESAP), resulted in one of the first spatial analyses of the vertical structure of the troposphere and lower stratosphere. Using data from the ESAP, Bjerknes and Palmén (1937) constructed a meridionally oriented vertical cross section over Europe focusing on the temperature structure of the troposphere and lower

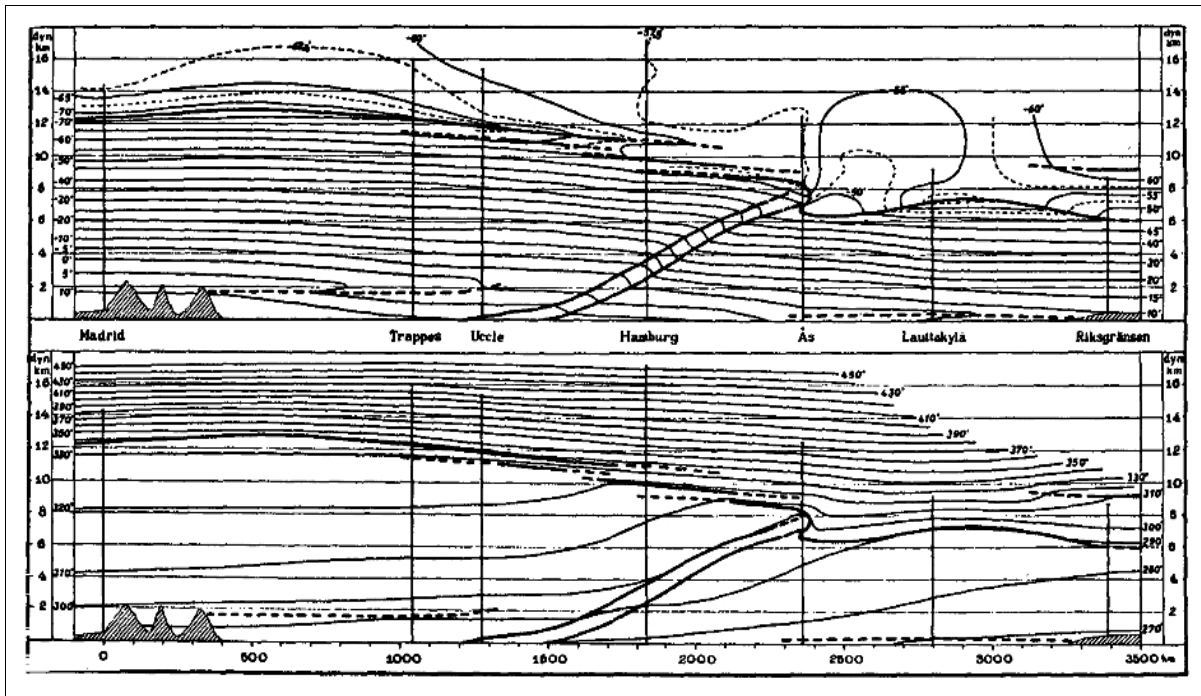


Figure 1.1. A cross section analysis, from Spain (left) to Sweden (right), of temperature (top) and potential temperature (bottom) by Bjerknes and Palmén (1937). The thick double lines represent the location of the polar front and the single thick line represents the tropopause.

stratosphere (Figure 1.1). Their analysis, which depicted the polar front extending from the surface northward and upward through the troposphere, became the first conceptual model of the structure of the tropopause in the vicinity of a front. They suggested that where the polar front met the tropopause, the tropopause surface folded into an “S” shaped curve. Poleward of this intersection the low tropopause was characteristic of the arctic regions, while equatorward of this location the tropopause was notably higher, characteristic of the tropics.

1.1. Discovery of the Jet Stream

By the 1940s, in the midst of World War II, the abundant use of aircraft for military purposes gave rise to an increasing urgency for wide-spread routine upper air observations.

Newly developed aviation technology in U. S. military aircraft allowed pilots to reach altitudes of ~10 km. Thus, forecasting the winds at this “high altitude” flight level became a task for U. S. Air Force Weather Officers around the globe. With knowledge of the thermal wind relationship, meteorologists were able to calculate a theoretical value of the wind speed and direction at some altitude above the ground. This relationship, simply stated, highlights the fact that the vertical shear of the geostrophic wind is directly proportional to the magnitude of the column average horizontal temperature gradient.

According to Bryson (1994), in the fall of 1944 the 20th U. S. Air Force Weather Central stationed on the island of Saipan, was charged with the task of delivering a 20-hour forecast for the winds at 35,000 ft over Tokyo. This was precisely the level at which the newly introduced B-29 bombers would be flying during a proposed air raid mission. Armed with the thermal wind relationship while constructing their forecasts, Weather Officers Bill Plumbly and Reid Bryson were able to overcome the challenges of forecasting in the data sparse Pacific region. Although a wind of this magnitude had never been observed, the officers calculated the flight level winds to be westerly, with speeds of 168 knots (a speed much faster than the B-29s were built to handle). While delivering their forecast they were met with disheartening skepticism as the General (whose name was left out of Bryson's account) disregarded their unprecedented calculation. The following day the B-29 pilots took off toward Japan without scientific guidance provided by the Weather Officers. Upon reaching flight level strong winds kept the aircraft nearly at a standstill in mid-air, where pilots reported observed winds from the west at 170 knots. The airmen failed to reach their targets and the mission was failed. However,

employing their knowledge of the observed frontal positions as well as the the thermal wind relationship, the U. S. Weather Central had both predicted and observed the jet stream for the first time (Bryson, 1994). It was a discovery that many forecasters around the globe were independently making during the war.

1.2. Understanding the Jet-Front Structure

a. Arguments for a mesoscale lower stratospheric structure

After World War II, the implications of the jet stream and its potential interaction with surface weather peaked the interest of a variety of researchers. In a study focusing on cases of developing vs. non-developing cyclones in the lee of the Rocky Mountains, Riehl (1948) concluded that those cases in which particularly intense jet stream winds were observed at 300 hPa were more likely associated with cyclone development than non-jet cases. In his analysis, Riehl gave a particularly detailed description of the tropopause and temperature structure at 200 hPa (Figure 1.2), a level above the jet core. He suggested that both the tropopause topography and the thermal field exhibited a non-linear spacial distribution, such that their evolution could not be the result of horizontal advection alone. Based upon the structure of the tropopause and temperature fields, his analysis led him to conclude that there must be a cross stream vertical circulation above the jet. Similarly, Palmén (1948) noted that the pronounced static stability in the lower stratosphere would allow the effect of any vertical motion in its vicinity to have a great effect on the temperature field. He explained that because of its proximity to the tropopause, the 200 hPa thermal field was especially suitable for studying the

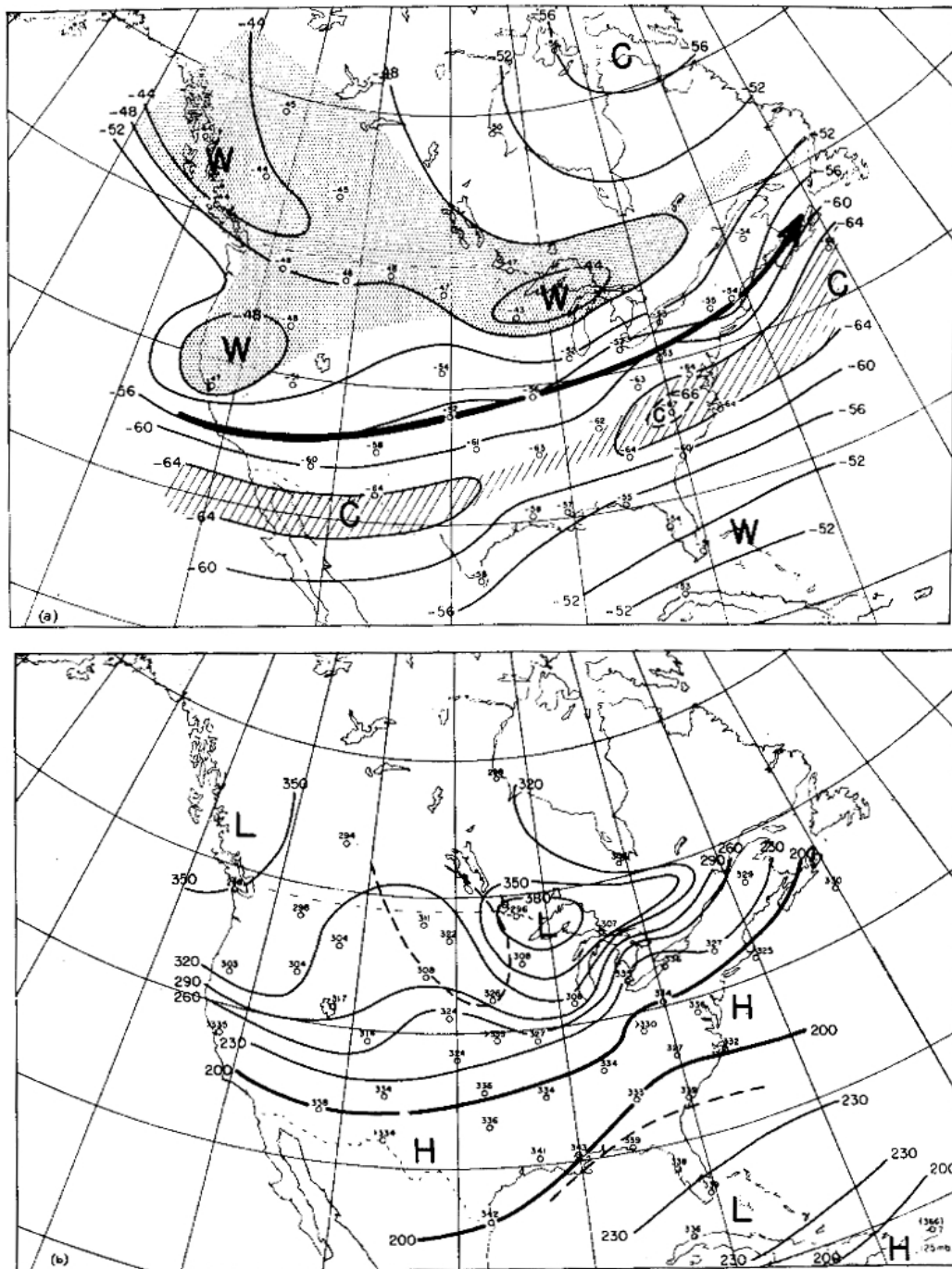


Figure 1.2. For 28 January 1948 (a) the observed and contoured temperature distribution at 200 hPa with the hatched (shaded) area representing the coldest (warmest) temperature at that level and (b) the observed and contoured tropopause height in pressure, with the L(H) representing the lowest (highest) geometric height of the tropopause. From Riehl (1948)

vertical wind field in the vicinity of the jet. Based upon the distribution of the temperature at 200 hPa, he also suggested that the temperature and wind field above the jet were connected with a cross stream vertical circulation superimposed on the zonal jet flow. Thus, soon after its discovery, the jet and its associated thermal field was being associated with vertical circulations in the upper troposphere and lower stratosphere.

The importance of analyzing upper level charts to make the correct interpretation of the surface weather was emphasized by Palmén and Nagler (1949). Their work investigated the unseasonable temperatures and sensible weather that occurred over eastern North America in early February 1947. Using the newly developed U. S. atmospheric sounding network, they examined the temperature and wind fields at both 500 hPa and 200 hPa, along with vertical cross sections orthogonal to the pronounced baroclinic zones at both those levels. Their work introduced an updated conceptual model of the tropopause structure in the vicinity of jets and fronts (Figure 1.3). The model suggested that rather than the “S” shaped configuration of the tropopause in the vicinity of the jet, there was a break in the tropopause at the level of maximum winds, separating the location where the polar front met the high tropical and low polar tropopauses. In addition, based on the distribution of the thermal fields above and below

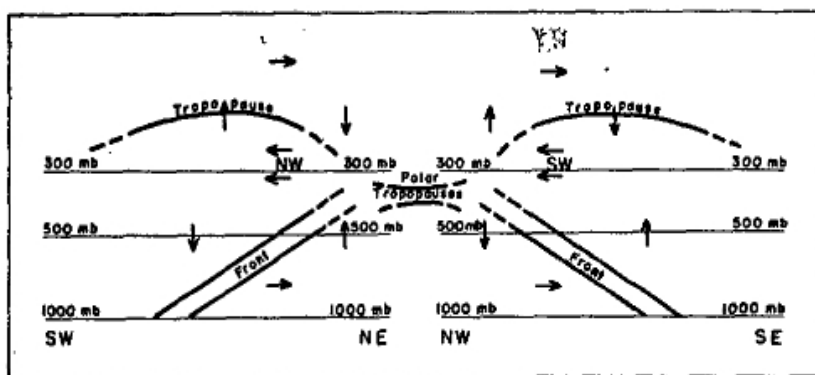


Figure 1.3. A cross section through a synoptic scale trough with the cross stream vertical circulations superimposed on the idealized locations of the polar front and tropopause. From Palmén and Nagler (1949).

the tropopause break region they suggested the existence of two separate vertical circulations, one in the lower stratosphere the other in the upper troposphere.

Not long after Palmén and Nagler's conceptual model was presented, an alternate conceptual model of the frontal structure in the vicinity of the tropopause was proposed by Berggren (1952) (Figure 1.4). His work utilized data from the the high resolution (both spacially and temporally) sounding network over Europe to examine the vertical structure of temperature and wind in several cases that were marked by a notable surface warm front with “active” tropical air. After considering the static stability, the horizontal temperature gradient, and the horizontal wind shear in several vertical sections, Berggren stated that there was no reason not to extend the polar front into the lower stratosphere. He concluded that if the tropical air is active, then the corresponding polar front, which was a warm front in the

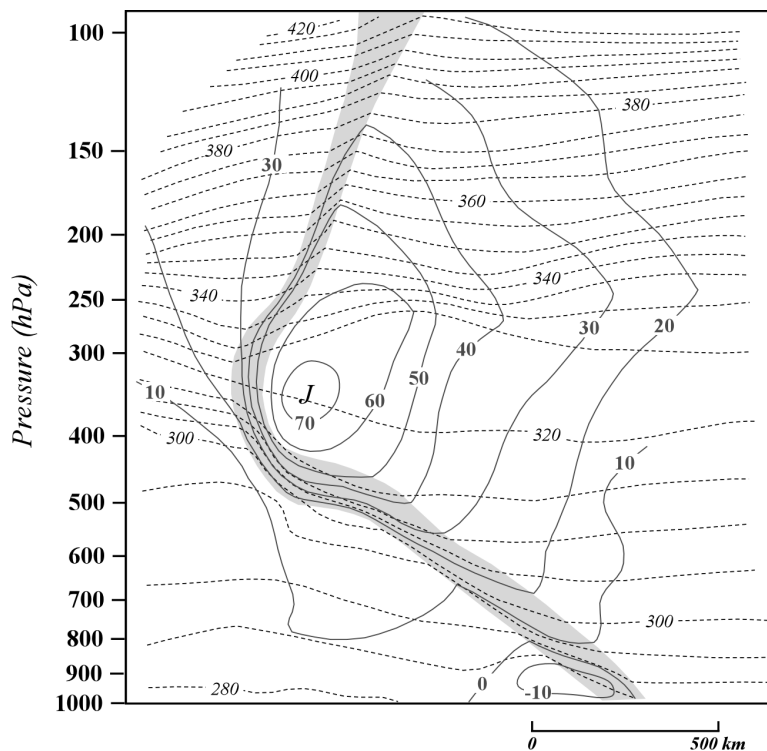


Figure 1.4. Vertical cross section of isotachs ($m s^{-1}$, solid) and isentropes (K , dashed) from Valentia, Ireland to Hannover, Germany at 0300 UTC 9 November 1949. The shaded area represents the continuous polar frontal zone as described by Berggren (1952). Adapted from Berggren (1952).

troposphere (below 400 mb), must be a cold front in the lower stratosphere (above 250 mb), and was characterized by a zone of cyclonic shear at jet level (between 400 and 250 mb).

Berggren and his predecessors had introduced the concept that the cyclonic wind shear and thermal gradients in the lower stratosphere were distributed on the mesoscale, on the order of 100 km, in the vicinity of the polar front and its intersection with the tropopause.

b. Arguments for a synoptic scale lower stratospheric structure

For most of the early 20th century, fronts were considered only in the lower troposphere, where the dense network of surface observations could capture the associated temperature gradients and wind shifts. In an effort to describe the evolution of such frontal features, Petterssen (1936) contributed the two-dimensional frontogenesis equation,

$$\frac{d}{dt}|\nabla\theta| = \left(\frac{\partial}{\partial t} + u\frac{\partial}{\partial x} + v\frac{\partial}{\partial y}\right)|\nabla\theta|, \quad (1.1)$$

in which the rate of change of the magnitude of the potential temperature gradient ($|\nabla\theta|$) was the result of local and horizontal advective tendencies acting on a preexisting temperature gradient. As observations of the free atmosphere became more routine and consistently available, the analysis of such observations led to fresh insights. Accordingly, the concept of a front was extended to include those features observed above the Earth's surface. In an effort to include the effects of vertical motion (ω) in the free atmosphere on frontal evolution, Miller (1948) extended Petterssen's frontogenesis equation into three-dimensions,

$$\frac{d}{dt}|\nabla\theta| = \left(\frac{\partial}{\partial t} + u\frac{\partial}{\partial x} + v\frac{\partial}{\partial y} + \omega\frac{\partial}{\partial p}\right)|\nabla\theta|, \quad (1.2)$$

The three-dimensional frontogenesis function includes the effect of any vertical motion in the vicinity of a baroclinic zone. Specifically, the inclusion of the vertical motion accounted the tilting of a vertical temperature gradient (e.g., a statically stable layer) into a horizontal gradient which can lead to frontogenesis. Accordingly, the additional vertical motion term in the frontogenesis equation is also known as the “tilting” term.

In the mid-1950s there was a paradigm shift in the scientific theory regarding the tropopause structure in the vicinity of jets and fronts. Reed and Sanders (1953) objected to the view from the Norwegian School that fronts extended with more or less equal strength throughout the troposphere. They suggested that strong, unambiguous fronts are generally found along the physical boundary represented by the surface and the thermodynamic boundary represented by the tropopause. In their analysis, they used the Miller frontogenesis equation (2) to investigate the evolution of an observationally well resolved upper tropospheric front. They described the development of the upper tropospheric front as taking advantage of the tilting term in the frontogenesis equation and emphasized that subsidence maximized on the warm side of the upper level front in their case was responsible for frontogenetic tilting. Likewise, the same tilting effect would also act to tilt horizontal vorticity into the a more vertical orientation, increasing the vertical vorticity that characterized the developing upper tropospheric frontal zone.

Reed (1955) extended the analysis by Reed and Sanders (1953), suggesting that not only did these frontal features form as a result of tilting, but that the air within the upper level front was of stratospheric origin. He stated that these upper frontal features did not separate polar

and tropical air masses as the polar front was thought to do, rather they develop entirely within polar air masses. The upper frontogenesis process was associated with descending air which could bring stratospheric values of potential vorticity into the upper troposphere and adiabatically warm the air to the point that its temperature could take on tropical air like characteristics. In addition, Reed began his analysis by explaining how the “frontal problem” needed to be reexamined from a fresh view point, stating that the Polar Front theory was “outdated,” as there had been many types of fronts described in the mid-century literature. He contended that “fronts are merely just zones of relatively strong temperature contrast ... there is little to be gained by marking them in a special manner on maps or cross sections ... the temperature data should speak for itself.” He went on to emphasize the point that our task as scientists is to describe the origin, behavior, and implication of fronts. His bold analysis, while physically meaningful, did not initially receive wide acceptance.

Support for the idea that the dynamics of upper level fronts was strongly tied to the tilting process became the basis for the conceptual model of the jet-front system, presented by Reed and Danielsen (1959). Using the U. S. upper air observation network in a five case composite, they constructed a vertical cross section of the mean jet-front system structure using both temperature (Figure 1.5a) and potential temperature (Figure 1.5b). In their analysis, they emphasized the original hypothesis of the “S” shaped tropopause fold and added that the air within an upper tropospheric front was of stratospheric origin. Their conceptual model was consistent with the tilting frontogenesis theory and the recent observations of stratospheric radioactive fallout (suggesting stratosphere to troposphere transport in the vicinity of jet front

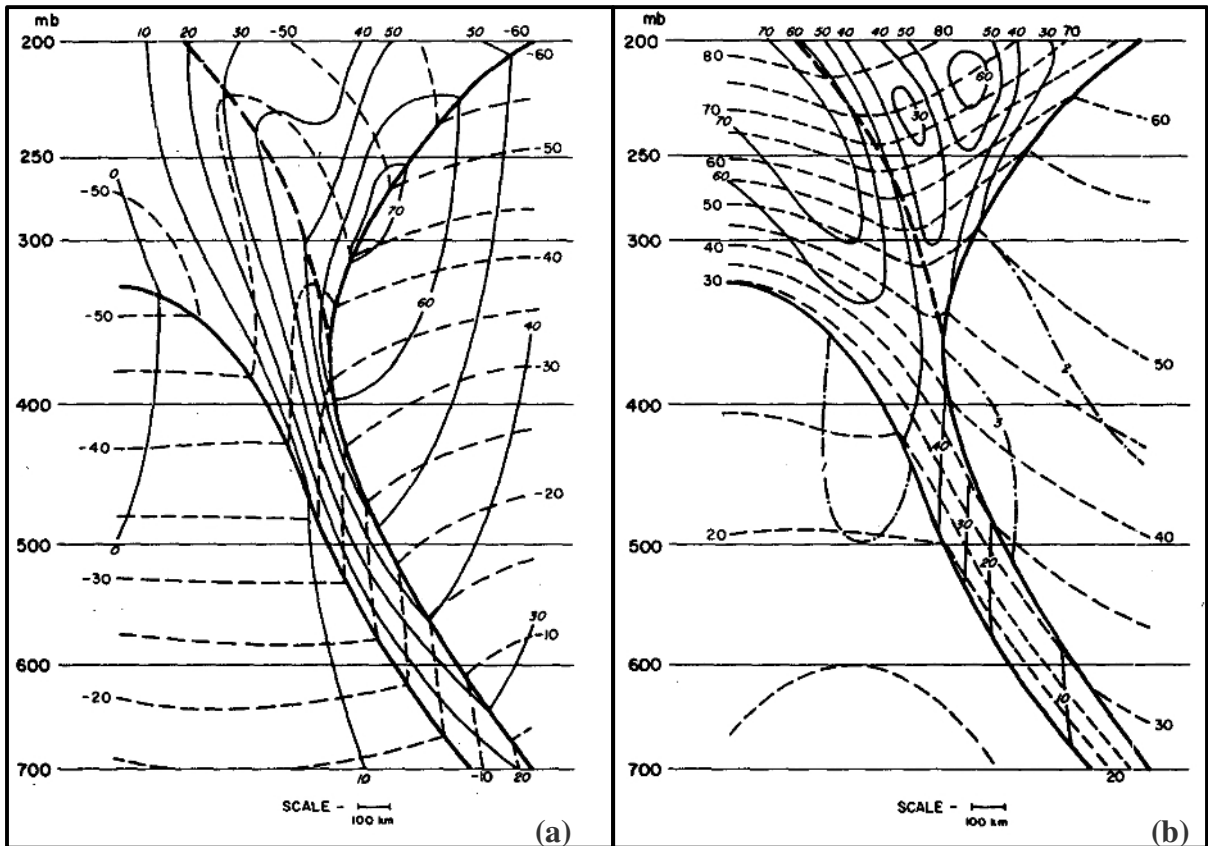


Figure 1.5. From Reed and Danielsen (1959), a 5 case composite of (a) temperature (dashed) and thermal-wind derived wind field (solid), and (b) potential temperature (dashed) and derived potential vorticity (solid) fields, with thick lines representing the tropopause and frontal surfaces in both plots.

systems). However, unlike previous models that had argued for a mesoscale (~ 100 km) cyclonic shear zone in the lower stratosphere, the Reed and Danielsen model spread the cyclonic shear above the tropopause to the synoptic scale (~ 1000 km). Though they used a 5 case composite analysis based on the lower resolution U. S. sounding network data, they argued that there was not enough observational evidence to support the mesoscale contraction of the cyclonic shear above the jet core.

Along with the arguments expanding the scale of the lower stratospheric cyclonic shear, the new paradigm of research on the jet-front system emphasized the dynamics responsible for

the development of its upper tropospheric component. The implications of these newly understood dynamical processes, associated with the tilting frontogenesis theory, went on to become an avenue of research productivity. Research focused on the dynamical processes associated with the upper tropospheric front introduced a number of fundamental insights that explained a variety of atmospheric phenomena, including: (1) stratosphere-troposphere exchange, motivated by the the radioactive fallout problem (e.g. Danielsen, 1964; Shapiro, 1980; Holton et al., 1995; Stohl et al., 2003); (2) clear air turbulence (e.g. Reed and Hardy, 1972; Kennedy and Shapiro, 1975, 1980, Shapiro, 1976; Keller, 1990), and elements of (3) the extra-tropical cyclone life cycle (e.g. Uccellini et al., 1985; Sanders, 1988; Whitaker et al., 1988; Barnes and Colman, 1993; and Lackmann et al., 1997). For a detailed review of the first half-century of research on ULJFs, and the upper tropospheric front, the reader is directed to Keyser and Shapiro (1986).

c. Resolving the lower stratospheric structure

In the early 1960s, there was a growing acceptance of the upper frontogenesis concepts considered in the Reed and Danielsen model. However, there remained one unresolved question: What was the distribution of cyclonic wind shear in the lower stratosphere? Using observational evidence, Riehl (1948), Palmén (1948), Berggren (1952), and Palmén (1958) argued for the mesoscale (~100 km) zone of cyclonic shear, while Reed and Sanders (1953), Newton (1954), Reed (1955), and Reed and Danielsen (1959) argued for the synoptic scale (~1000 km) distribution of cyclonic shear. The more recent Reed and Danielsen model was

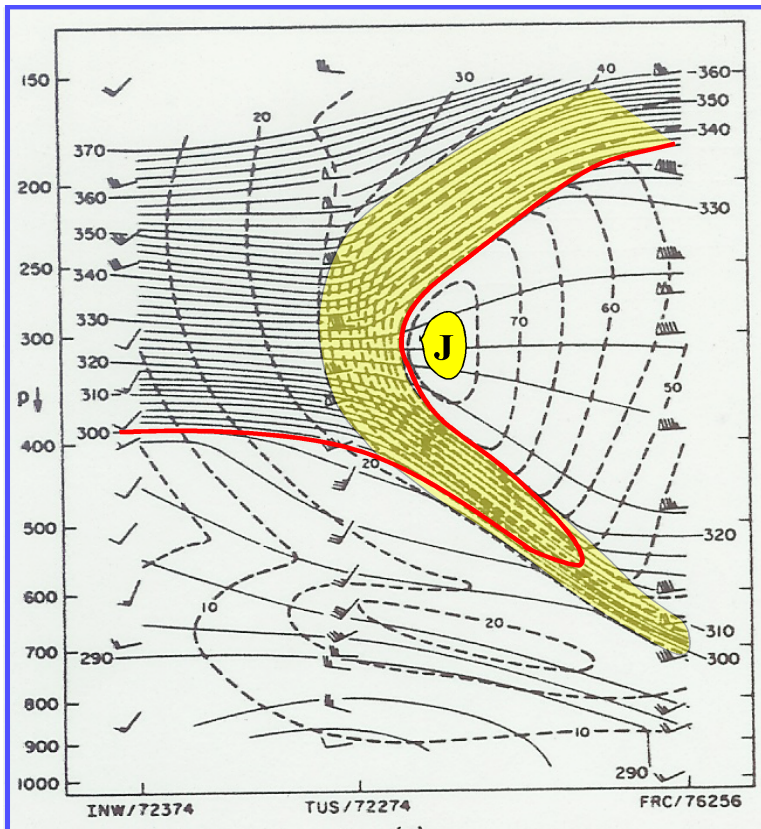


Figure 1.6. Vertical cross section of isotachs ($m s^{-1}$, solid) and isentropes (K , dashed) through an ULJF at 0000 UTC 17 April 1976, using NWS radiosonde data from Winslow, AZ (INW), Tuscon, AZ (TUS), and Fraccionamiento, Mexico (FRC) and supplemented with NCAR Sabreliner aircraft data. Bold red line is the 1.5 PVU ($1 PVU = 10^{-6} K m^2 kg^{-1} s^{-1}$) identifying the dynamic tropopause. The jet maximum labeled with a "J" and the cyclonic wind shear on the order of 100 km shaded in yellow. Adapted from Shapiro (1981).

gaining support as it accounted for the tilting frontogenesis theory, as well as the transport pathway of radioactive debris that originated in the stratosphere yet was observed in the troposphere. However, this debate was reexamined in an analysis conducted by Shapiro (1976), in which he used high resolution research aircraft measurements to analyze the distribution of cyclonic wind shear in the lower stratospheric portion of a jet-front feature. He was motivated to settle the scale resolution problem based upon the implications that the two different distributions of cyclonic shear (e.g., potential vorticity) in the vicinity of the jet had on the evolution of weather systems at the surface. His analysis showed that the cyclonic wind shear was indeed confined to the mesoscale and not the synoptic scale, supporting the idea that

locally high values of potential vorticity should be present adjacent to the jet in the lower stratosphere. Supplementing the U. S. radiosonde data with high resolution aircraft measurements, Shapiro (1981) constructed a new conceptual model of the structure of the jet front system in the vicinity of the tropopause (Figure 1.6). His analysis of the potential temperature and wind fields above the tropopause was similar to that of Berggren (1952), highlighting hypergradients of both temperature and wind in the lower stratosphere. Meanwhile, the distribution of potential temperature and wind fields (i.e. potential vorticity) in the upper troposphere was consistent with the analysis of Reed and Danielsen (1959) and the dynamic implications of the tilting frontogenesis process.

The Sawyer (1956) – Eliassen (1962) equation was the first to make the connection between the primary geostrophic frontogenetic forcing and the creation of a secondary ageostrophic circulation in the vicinity of a frontal zone. Their equation,

$$2\gamma\left(-\frac{\partial u_g}{\partial x}\frac{\partial\theta}{\partial y} + \frac{\partial u_g}{\partial y}\frac{\partial\theta}{\partial x}\right) = \left(-\gamma\frac{\partial\theta}{\partial p}\right)\frac{\partial^2\psi}{\partial y^2} + \left(2\frac{\partial m}{\partial p}\right)\frac{\partial^2\psi}{\partial y\partial p} + \left(\frac{-\partial m}{\partial y}\right)\frac{\partial^2\psi}{\partial p^2}, \quad (1.3)$$

shows that in a coordinate system where the x-direction is oriented along a baroclinic zone, the geostrophic (subscript g) shearing and stretching deformation acting on a baroclinic zone (left-hand side) would force a secondary ageostrophic cross stream circulation (streamfunction ψ in

the right hand side). In their equation m is the geostrophic momentum ($u_g - fy$), $\gamma = \frac{R}{fP_o}\left(\frac{P_o}{P}\right)^{\frac{c_p}{c_v}}$

and is constant on a pressure (P) surface, $\frac{\partial\psi}{\partial y} = \omega$ and $\frac{-\partial\psi}{\partial p} = v_{ag}$. The analysis by Eliassen

(1962) suggested that frontogenesis was a two part process in which (i) the primary geostrophic

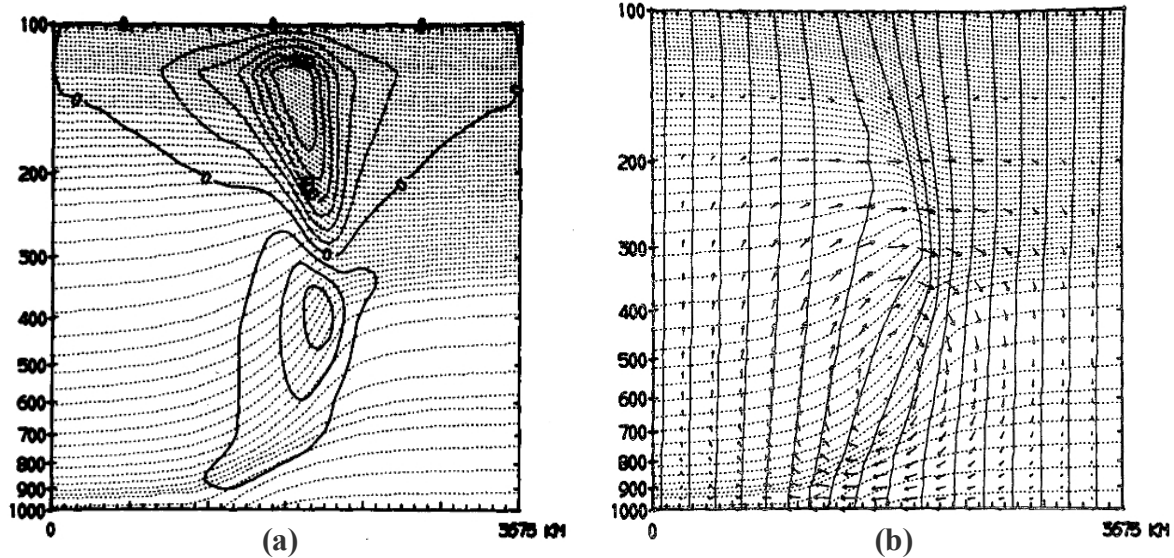


Figure 1.7. For an idealized jet-front system seen in a vertical-cross front analysis with potential temperature (dotted) and, (a) the geostrophic forcing from the Sawyer-Eliassen circulation equation, and (b) the resulting secondary circulation calculated by solving for Ψ the Sawyer-Eliassen equation. From Shapiro (1981)

deformation provides forcing to tighten the temperature gradient, resulting in a secondary ageostrophic circulation, (ii) that secondary ageostrophic circulation could act to further intensify the temperature gradient. He also suggested that the sign of the forcing above and below the jet core could be of opposite sign, but left it to future investigation to solve the second order partial differential equation.

In one of the few investigations in the literature to numerically solve the Sawyer-Eliassen equation, Shapiro (1981) calculated secondary circulations for an idealized front. His analysis considered the geostrophic forcing in a cross front vertical plane, in which he showed that the magnitude of the forcing for the Sawyer-Eliassen circulation was larger above the jet in the lower stratosphere than it was in the upper troposphere (Figure 1.7a). However, his analysis focused on resolving the upper troposphere and the influential vertical motion field in the vicinity of the upper tropospheric front. Thus, the calculated ageostrophic circulation was

obvious in the troposphere and nearly non-existent in the lower stratosphere where poor model resolution existed (Figure 1.7b). Shapiro indicated the strong static stability of the lower stratosphere as the dampening mechanism responsible for the weak secondary circulation above the jet.

Since the analysis by Shapiro, there has been little research attention focusing on the structure, evolution, or dynamics of the lower stratospheric portion of jet-front systems. The goal of this dissertation is to provide a synoptic perspective on the the structure, evolution and dynamics of the lower stratospheric portion of the jet front system. The main research portion of this work is separated into two parts, Chapters 2 and 3, which are presented in the form of individual papers written following the guidelines for submission into the *Quarterly Journal of the Royal Meteorological Society*. Chapter 2 highlights Part I of the analysis of lower stratospheric fronts. This chapter introduces the theory related to lower stratospheric frontal dynamics, and presents two case studies demonstrating the asynchronous evolution of upper tropospheric and lower stratospheric fronts in both the northwesterly and southwesterly flow portions of a baroclinic wave. Chapter 3 presents Part II of the analysis which focuses on several southwesterly flow cases and illustrates what may be a characteristic interplay between the role of tropospheric convection, and associated latent heat release, and the lower stratospheric frontogenesis process. Finally, Chapter 4 highlights some of the implications of this line of research and provides a proposal for future research investigating the role of the lower stratospheric frontogenesis process in distributing energy across the tropical-extratropical interface.

Chapter 2

Part I: Examples in Northwesterly and Southwesterly Flow

2.1. Introduction

Upper level jet-front (ULJF) systems are ubiquitous dynamic and thermodynamic features found in the vicinity of the mid-latitude tropopause. These systems are characterized by a local wind speed maximum (i.e., the jet core) along the sloping mid-latitude tropopause surface. The regions of vertical shear located above and below the jet core are directly associated with attendant baroclinic zones (i.e., the fronts) via the thermal wind relationship (Figure 2.1). Since the mid 20th century, the structure, evolution, and life cycle of these ULJF systems have been studied in the context of clear air turbulence (e.g., Reed and Hardy, 1972; Kennedy and Shapiro, 1975, 1980, Shapiro, 1976; Keller, 1990), stratosphere-troposphere exchange and chemical transport (e.g., Danielsen, 1964; Shapiro, 1980; Holton et al., 1995; Stohl et al., 2003), and the extra-tropical cyclone life cycle (e.g., Uccellini et al., 1985; Sanders, 1988; Whitaker et al., 1988; Barnes and Colman, 1993; and Lackmann et al., 1997). For a detailed review of the first half-century of research on ULJFs the reader is directed to Keyser and Shapiro (1986).

To date, research into ULJFs has centered on the life cycle and associated implications

of the upper tropospheric component of these systems, known as upper level fronts or upper tropospheric fronts (labeled “UT Front” in Figure 2.1). A number of studies, including Uccellini et al. (1985), Sanders (1988), Whitaker et al. (1988), Barnes and Colman (1993), and Lackmann et al. (1997), have demonstrated the role of upper tropospheric frontogenesis in the development of surface cyclones. These studies suggested that the ageostrophic transverse vertical circulation associated with a dynamically active ULJF not only provides the cross-stream differential subsidence required to intensify the upper level front, but simultaneously steepens and lowers the dynamic tropopause below the jet core. This process forces a thin wedge of stratospheric air, characterized by large (small) values of potential vorticity (water vapor), downward into the upper and middle troposphere. Within the upper troposphere the

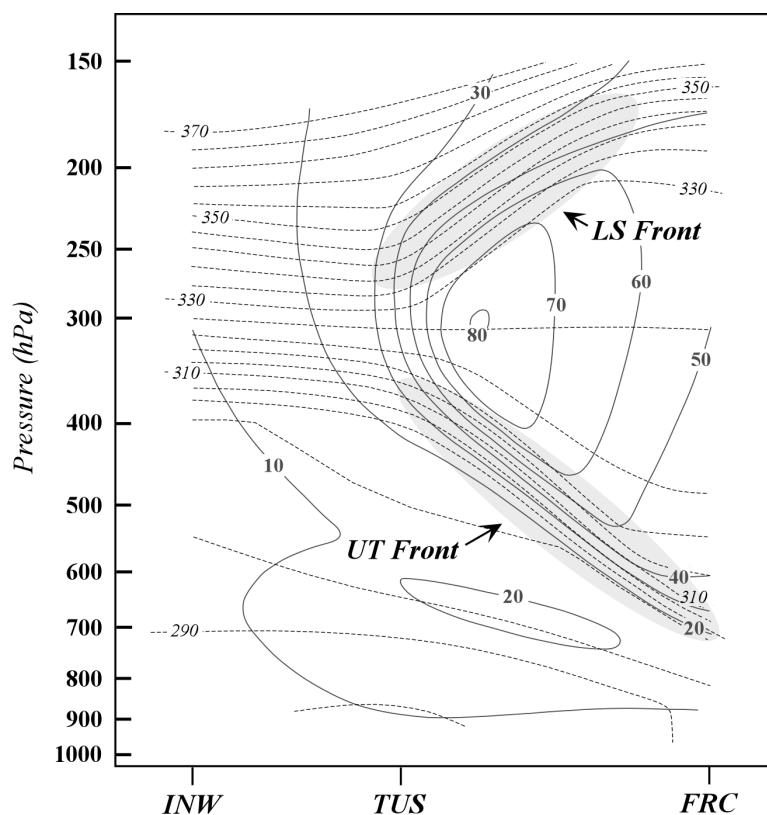


Figure 2.1. Vertical cross section of isotachs ($m s^{-1}$, solid) and isentropes (K , dashed) through an ULJF at 0000 UTC 17 April 1976, using NWS radiosonde data from Winslow, AZ (INW), Tuscon, AZ (TUS), and Fraccionamiento, Mexico (FRC) and supplemented with NCAR Sabreliner aircraft data. The regions of locally enhanced baroclinicity, static stability, and horizontal and vertical shear are shaded, representing the upper tropospheric front (UT Front) below the jet core and the lower stratospheric front (LS Front) above the jet core. Bold black line is the 1.5 PVU ($1 PVU = 10^{-1} K m^{-2} kg^{-1} s^{-1}$) identifying the dynamic tropopause. Adapted from Shapiro (1981).

large potential vorticity is manifest as a local maximum in absolute vorticity, providing an upper level precursor disturbance to a wave scale surface cyclogenesis event and implicating ULJFs in the incipient stages of the extra-tropical cyclone life cycle.

Additionally, the folding of the dynamic tropopause in association with intense upper tropospheric frontogenesis has been cited as one of the most efficient and dominant forms of stratosphere-troposphere exchange in the mid-latitudes (Mohanakumar, 2008). The role of individual ULJFs, specifically the upper tropospheric front, in stratosphere-troposphere exchange has been well documented (e.g., Danielsen, 1968; Shapiro et al., 1987; Lamarque and Hess, 1994; Eisel et al., 1999). The substantial displacements of the dynamic tropopause on isentropic surfaces that occurs within tropopause folds facilitate the exchange of mass across the tropopause (Stohl et al., 2003). As a result of the synoptic and mesoscale processes in the vicinity of a tropopause fold, dry, ozone-rich stratospheric air descends into the troposphere and can irreversibly mix with tropospheric air. It is hypothesized that at least 10% of global tropospheric ozone originates from the stratosphere via intense upper tropospheric frontogenesis and tropopause folding (Mohanakumar, 2008).

As deep, three-dimensional, features centered about the tropopause, ULJF systems have significant vorticity and thermal structures residing both in the upper troposphere *and* in the lower stratosphere (lower stratospheric front, labeled “LS Front” in Figure 2.1). While the majority of research attention regarding ULJFs has been focused on the upper tropospheric portions of these systems, little synoptic research attention has been given to the portions of these structures that reside above the jet core, within the lower stratosphere. The importance of

the lower stratospheric portion of mid-latitude ULJF systems has, for the most part, only been considered in so far as it is manifested in a zonally averaged sense and on seasonal timescales. As summarized by Shepherd (2002), the zonally averaged meridional temperature gradient, associated with the sloping mid-latitude tropopause, is coupled (via thermal-wind) to the zonal wind field at and above the tropopause. The zonal wind field there determines the propagation characteristics of atmospheric waves into the stratosphere, thus effecting the large scale stratospheric circulation and the seasonal scale stratosphere-troposphere exchange accomplished via the wave-driven Brewer-Dobson circulation. However, on shorter synoptic timescales the details of the structure, evolution, and dynamics of the lower stratospheric frontal portions of individual ULJF systems, remains incomplete. Similarly, the comprehensive role of ULJFs in the cyclone life cycle remains incomplete so long as the portions of ULJF systems that reside within the lower stratosphere continue to receive scant research attention. This chapter will provide a contribution toward developing a more comprehensive view of the synoptic dynamics of the mid-latitude lower stratosphere by examining the structure, evolution, and dynamics of the lower stratospheric portions of two recently observed cases of ULJFs.

This chapter is structured in the following manner: A history of research regarding the lower stratospheric portion of ULJFs and a background on frontogenesis is provided in Section 2.2. A case study of ULJF evolution in northwesterly flow is presented in Section 2.3. A case of ULJF evolution in southwesterly flow is presented in Section 2.4. Finally, a summary and discussion of the analyses are provided in Section 2.5.

2.2. Background

In one of the first conceptual models of an upper level jet-front system, Berggren (1952) proposed that a continuous frontal zone (the polar front) stretched upward from the surface, through the upper troposphere and into the lower stratosphere (Figure 1.4). This proposed model, which included mesoscale structures at and above the jet core, was largely dismissed due to lack of consistent balloon observation of the lower stratosphere (Palmén, 1958), allowing subsequent research attention to remain focused on the more consistently and conveniently observable upper tropospheric half of these systems. It was not until the 1960s, when instrumented research aircraft observations in field campaigns became a routinely available supplement to conventional radiosonde data, that a much improved resolution of ULJF structures was afforded (e.g., Danielsen, 1964; Shapiro, 1976). Using such high resolution aircraft measurements, Shapiro (1976) confirmed that there was indeed a mesoscale (~100 km) confinement of cyclonic wind shear below, at, and above the jet core. His analysis supported Berggren's hypothesis of a mesoscale frontal structure extending from the upper troposphere through the level of maximum wind, to the lower stratosphere. The regions of the ULJF that contained larger than background gradients of either potential temperature or cyclonic shear (or both) were termed “frontal” by Berggren (1952) and Shapiro (1976).

In his extension of Sawyer's (1956) study on jet circulation dynamics, Eliassen (1962, his Figure 4) considered the forcing for two separate secondary circulation cells, one above and one below the jet core, associated with geostrophic deformation as described in the Sawyer

(1956)-Eliassen (1962) equation. These two ageostrophic circulations were centered about the baroclinic zones lying above and below the level of maximum wind. Though the notion of one continuous “frontal” region extending through the tropopause was thus suggested (e.g. Berggren, 1952; Shapiro, 1976), theoretical and idealized studies (e.g., Eliassen, 1962; Shapiro, 1981) of ULJFs support the notion that two separate centers of frontogenetic forcing are vertically separated by the jet core. In fact, true fronts are regions characterized by both vertical *and* horizontal shear, as well as locally enhanced static stability (e.g., Newton and Trevisan, 1984; Hobbs et al., 1990; and Martin, 2006). Thus, the baroclinic zones in the upper troposphere and lower stratosphere can be characterized as two separate fronts, while the cyclonic shear region at the jet level, characterized as “frontal” by Berggren (1952) and Shapiro (1976), lacks the characteristics of a true frontal zone.

In his analysis, Shapiro (1982) considered the secondary circulations associated with idealized variations of the geostrophic shearing and stretching deformation forcings in the vicinity of the tropospheric half of the ULJF. He illustrated that in the absence of temperature advection (e.g., a case of pure stretching deformation), the Sawyer-Eliassen circulations in the jet entrance and exit regions resulted in the traditional four-quadrant model; a thermally direct (indirect) circulation in the entrance (exit) region (Figure 2.2a). In cases where cold air advection was present through the jet core, the thermally direct (indirect) circulation in the jet entrance (exit) region was shifted toward the anticyclonic (cyclonic) side of the jet, so that subsidence characterized the jet core (Figure 2.2b). Such a distribution of subsidence is consistent with that attributed to negative vorticity advection by the thermal wind (i.e.,

Sutcliffe, 1947; Trenberth, 1978), which exists along the jet axis when geostrophic cold air advection is present along an ULJF. Keyser and Pecnik (1987) showed that subsidence through the jet core is upper frontogenetic, thus the establishment of geostrophic cold air advection along the jet has been described as an important aspect of the upper front life cycle (Rotunno et al., 1994; Schultz and Doswell, 1999; Lang and Martin, 2010). An environment characterized by geostrophic warm air advection through the jet core shifts the thermally direct (indirect) circulation in the jet entrance (exit) region toward the cyclonic (anticyclonic) side, so that the jet core is conversely characterized by ascent (Figure 2.2c).

Figure 2.3 extends the Figure 2.2 conceptual model to the *stratospheric* half of an ULJF, where the geostrophic vertical shear and horizontal temperature gradient are reversed and illustrates the vertical motions forced by the idealized geostrophic stretching and shearing deformation *above the level of maximum winds*. An environment of pure geostrophic stretching deformation, illustrated as a straight jet streak in the absence of thermal advection, is shown in Figure 2.3a. Resembling the traditional tropospheric four-quadrant model, the thermally direct entrance region and thermally indirect exit region are evident. However, in this lower stratospheric version of the four-quadrant model, the jet entrance (exit) region ascent is located on the cyclonic (anticyclonic) shear side of the jet, opposite to its location in the corresponding environment below the jet core. Figure 2.3b shows the resulting circulations forced by geostrophic cold air advection along an idealized jet. In this case, the thermally direct (indirect) circulation shifts toward the cyclonic (anticyclonic) shear side of the entrance (exit) region. Despite this altered distribution, the same outcome is produced in the lower

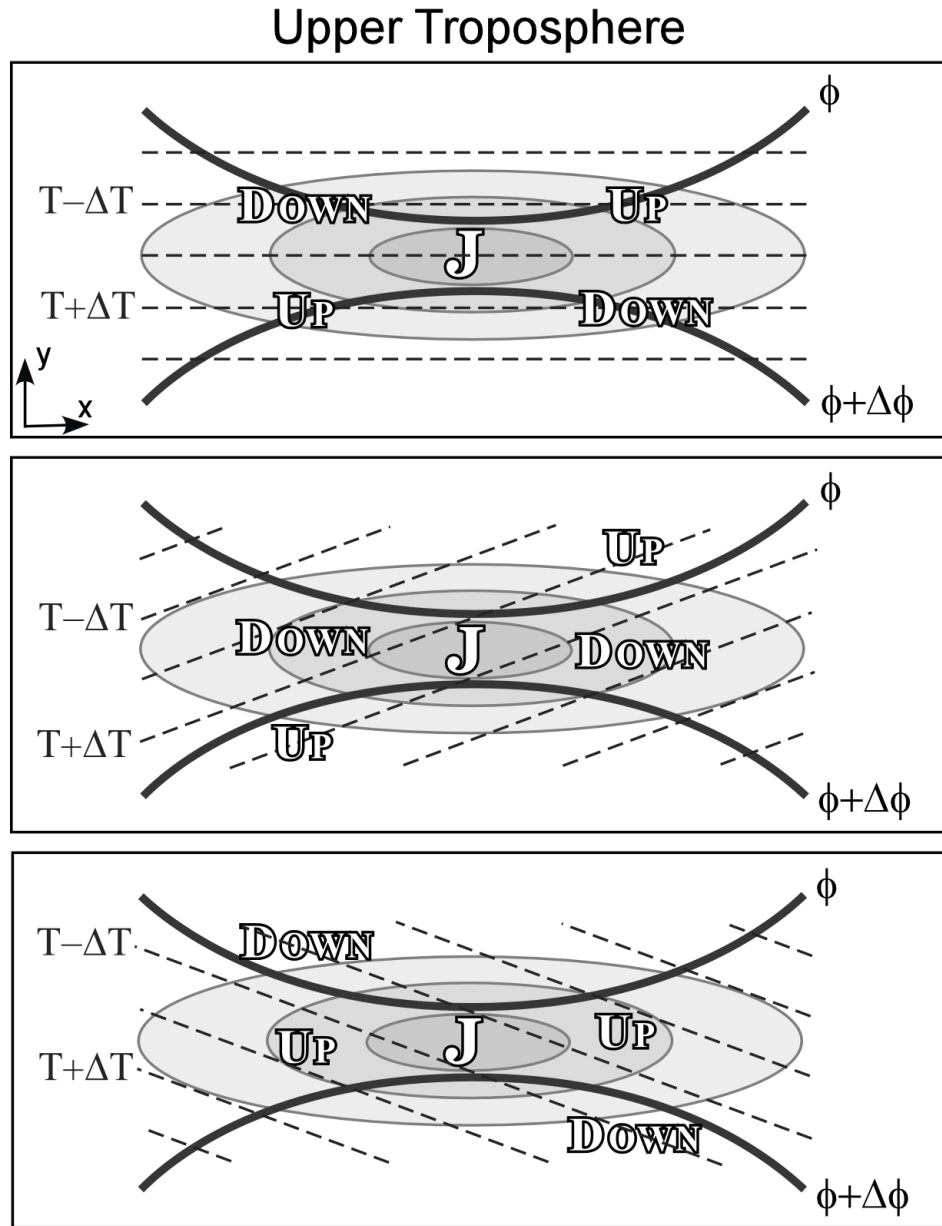


Figure 2.2. Schematic illustration of idealized configurations of potential temperature along a straight jet streak maximum on an upper tropospheric isobaric surface. Geopotential height (thick solid), potential temperature (dashed), isotachs (thin solid filled) with the jet maximum represented by “J,” and a sense of the mid-tropospheric Sawyer-Eliassen vertical motions (up or down) for (a) no thermal advection along the jet (b) geostrophic cold air advection along the jet and (c) geostrophic warm air advection along the jet.

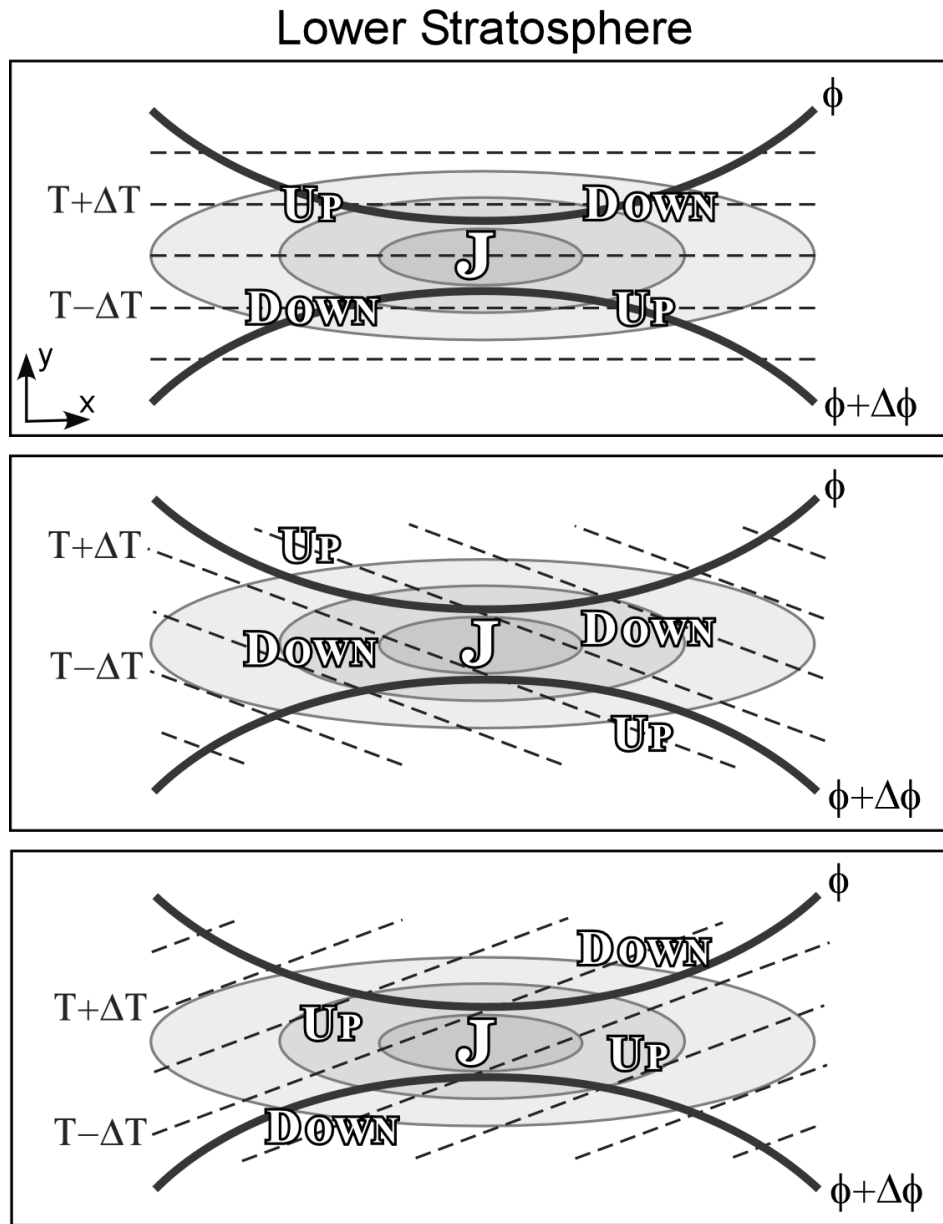


Figure 2.3. (a) – (c) As for Figure 2.2 a – c but for a (lower stratospheric) isobaric surface above the level of maximum winds.

stratosphere as in the upper troposphere, subsidence through the local jet maximum. Finally, the case of geostrophic warm air advection along the jet is illustrated in Figure 2.3c. As in the cold air advection case, though the entrance and exit region circulations shift in opposition to their counterparts below the jet core, the net result is a band of ascent through the local jet axis.

2.3. *Northwesterly Flow Case*

a. Synoptic Overview

During the first week of February 2008, an ULJF associated with the polar jet was situated in northwesterly flow over the west coast of the United States. As this ULJF rounded the base of an upper level trough between 4-5 February an intense upper tropospheric front developed. This upper tropospheric front was associated with the intensification of a mid-tropospheric shortwave that served as a precursor disturbance to a surface cyclogenesis event that brought several states in the Midwest upwards of 30 cm of snow on 5-6 February 2008. The focus of the present analysis is the northwesterly flow lower stratospheric frontal structure associated with the polar jet, prior to and during the early development of the upper tropospheric front. Using gridded model analyses from the National Centers for Environmental Prediction's (NCEP's) Eta model (Eta-104 grid), the evolution of the magnitude of the 200 hPa horizontal potential temperature gradient will be used to represent the lower stratospheric front, as it was consistently located above the level of maximum winds of the northwesterly flow polar jet. The magnitude of the horizontal potential temperature gradient at

500 hPa will serve as a measure of the intensity of the upper tropospheric front.

At 0600 UTC on 4 February the 200 hPa flow was strongly baroclinic over the western United States (Figure 2.4a). Both the northwesterly and westerly flow around a broad trough were characterized by a long baroclinic zone, with a maximum magnitude of $\sim 8 \text{ K (100 km)}^{-1}$ slightly upstream of the trough axis, off the coast of California. The warmest potential temperatures at this level were located over the Great Basin, while the coldest potential temperatures were found in a region equatorward of and parallel to this main baroclinic zone. At 500 hPa, the upper tropospheric front associated with the polar jet was located in the same general area as its lower stratospheric counterpart, but its intensity was weaker, with a magnitude of only $\sim 6 \text{ K (100 km)}^{-1}$ over the California-Arizona border (Figure 2.4b).

By 1800 UTC 4 February, the amplitude of the 200 hPa trough had increased (Figure 2.4c). Off the coast of California, the lower stratospheric front was the noteworthy feature within the northwesterly flow with a magnitude that remained constant ($\sim 8 \text{ K (100 km)}^{-1}$). The magnitude of the thermal contrast decreased downstream of the trough axis. Though the amplification of the trough was notable at 200 hPa, at 500 hPa (Figure 2.4d) the baroclinicity associated with the upper tropospheric front actually weakened slightly as its maximum intensity dropped to $\sim 4 \text{ K (100 km)}^{-1}$. Clearly, through this time in the life cycle of this ULJF system, the upper tropospheric front was much weaker than its robust lower stratospheric counterpart.

At 0600 UTC 5 February, the lower stratospheric front was oriented nearly north-south within the northwesterly flow, from Nevada to Baja California (Figure 2.4e). The maximum

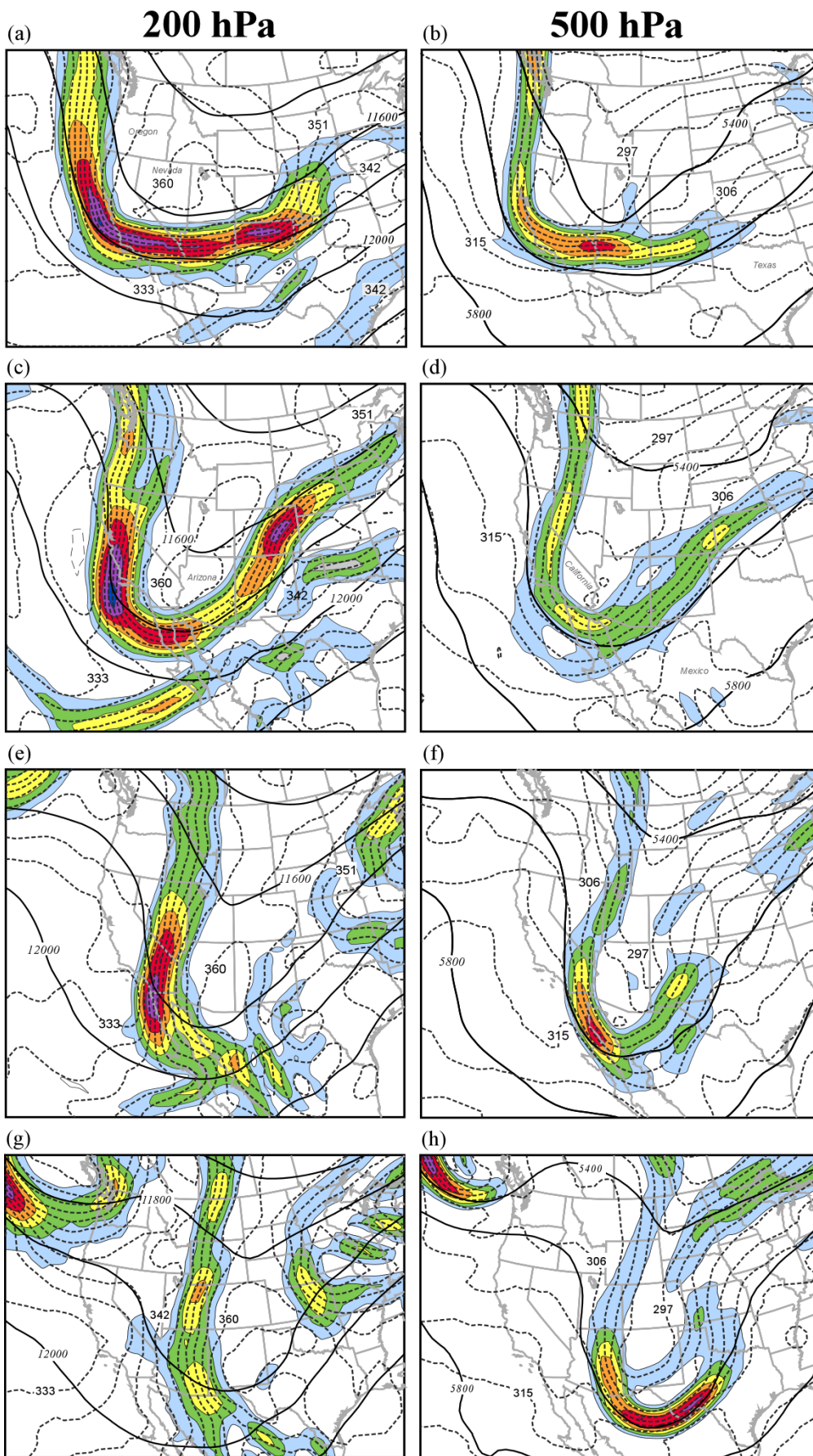


Figure 2.4. (On previous page) (a) 200 hPa geopotential height (solid), potential temperature (dashed), and magnitude of the horizontal potential temperature (shaded) from the Eta-104 model analysis valid at 0600 UTC 4 February 2008. Geopotential height is labeled in m and contoured every 200m, isentropes are labeled in K and contoured every 3 K, and the magnitude of the horizontal potential temperature gradient is shaded every 1 K (100 km)⁻¹ beginning at 2 K (100 km)⁻¹. (b) As for Figure 2.4(a) but at 500 hPa. (c) and (d) As for Figure 2.4 (a) and (b) but from the Eta-104 model analysis valid at 1800 UTC 4 February 2008. (e) and (f) As for Figure 2.4 (a) and (b) but from the Eta-104 model analysis valid at 0600 UTC 5 February 2008. (g) and (h) As for Figure 2.4 (a) and (b) but from the Eta-104 model analysis valid at 1800 UTC 5 February 2008.

intensity of the lower stratospheric front had weakened slightly to $\sim 7 \text{ K (100 km)}^{-1}$ and it was centered over the California-Mexico border, upstream of the trough axis. The baroclinicity downstream, within the southwesterly flow, had nearly disappeared. While the lower stratospheric front began to weaken, the upper tropospheric front at 500 hPa became more coherent within the northwesterly flow immediately upstream of the trough axis, having strengthened to $\sim 6 \text{ K (100 km)}^{-1}$ while moving to northern Baja California (Figure 2.4f).

By 1800 UTC 5 February, the amplitude of the 200 hPa trough had decreased (Figure 2.4g). Within the northwesterly flow, the roughly north-south oriented lower stratospheric front had further weakened in magnitude to $\sim 4 \text{ K (100 km)}^{-1}$ along the Arizona-Mexico border. Simultaneously, at 500 hPa, the upper tropospheric front continued to intensify, reaching a magnitude of $\sim 7 \text{ K (100 km)}^{-1}$ over the Big Bend region of Texas (Figure 2.4h). Continued strengthening of the upper tropospheric front (reaching a magnitude of $\sim 9 \text{ K (100 km)}^{-1}$ by 00 UTC 6 February, not shown) and erosion of the lower stratospheric part reinforced the growing disparity in baroclinicity that characterized these two features throughout the northwesterly flow portion of the ULJF system life cycle. Associated with the upper tropospheric

development was the production of an upper level vorticity maximum (not shown) which acted as a precursor to surface cyclogenesis, a process described by Lackmann et al. (1997).

b. Analysis

The analysis focuses on 4 February, the period during the evolution of this ULJF in which the upper tropospheric front remained relatively weak while the lower stratospheric front was the dominant of the two frontal structures. Quasi-geostrophic (QG) theory was used to diagnose regions of vertical motion forcing in the vicinity of the polar jet's lower stratospheric (200 hPa) frontal zone. The full model vertical motion from the Eta-104 analyses, available every 6 hours, was used in calculations of tilting frontogenesis¹, F_{tilt} , where

$$F_{tilt} = -\frac{1}{|\nabla\theta|} \frac{\partial\theta}{\partial p} \left\{ \frac{\partial\omega}{\partial x} \frac{\partial\theta}{\partial x} + \frac{\partial\omega}{\partial y} \frac{\partial\theta}{\partial y} \right\}. \quad (2.1)$$

At 0600 UTC 4 February, geostrophic cold air advection characterized the ULJF in the entrance region of the northwesterly jet at 200 hPa (Figure 2.5a). A maximum in geostrophic cold advection (geostrophic temperature advection of $-12 \times 10^{-4} \text{ K s}^{-1}$) was located on the cyclonic shear side of the jet entrance region and in the vicinity of the most intense portion of the lower stratospheric front, just off the coast of central California. Coincident with this QG forcing for descent, subsidence was maximized (-8 cm s^{-1}) on the cold side of the lower stratospheric front and in the vicinity of the 200 hPa polar jet core (Figure 2.5b). As a consequence of this large region of subsidence, negative tilting frontogenesis ($\sim -32 \times 10^{-8} \text{ K}$

¹ Tilting frontogenesis was calculated at 175 hPa as the vertical motion at this level was less “noisy” than at 200 hPa.

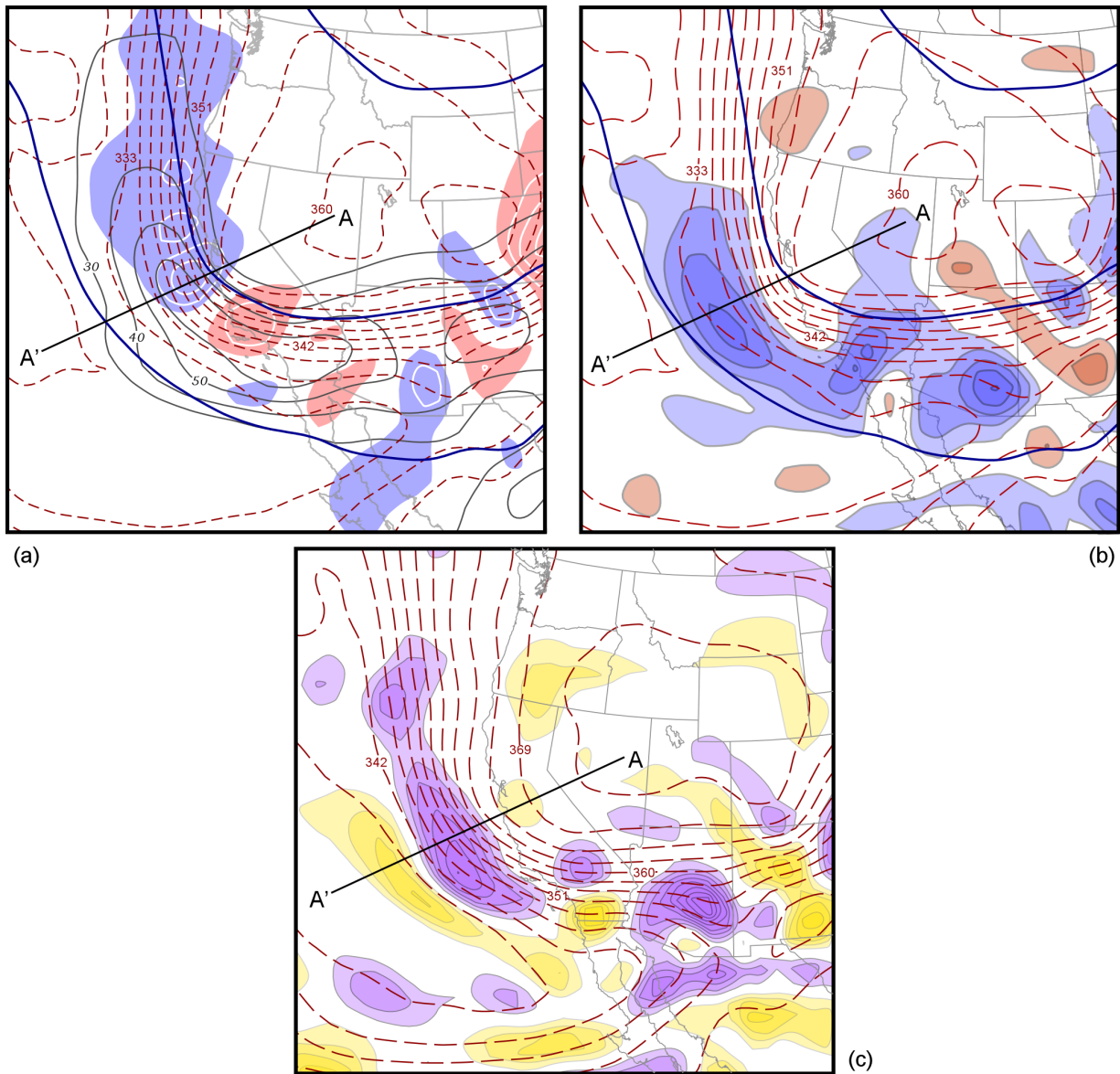


Figure 2.5. (a) 200 hPa geopotential height (thick solid), geostrophic isotachs (thin solid), isentropes (dashed), and geostrophic temperature advection (shaded) from the Eta-104 model analysis valid at 0600 UTC 4 February 2008. Geopotential height is contoured every 200 m, isentropes are labeled in K and contoured every 3 K, isotachs are labeled in $m s^{-1}$ and contoured every $10 m s^{-1}$, and dark (light) shading is geostrophic temperature advection contoured in units of $K s^{-1}$ every $-3 (3) \times 10^{-4} K s^{-1}$. (b) 200 hPa geopotential height (thick solid), isentropes (dashed), and vertical motion (shaded). Geopotential height is contoured as in Figure 2.5(a), isentropes are labeled and contoured as in Figure 2.5(a), and shaded solid (dashed) contours represent subsidence (ascent) and are contoured in $cm s^{-1}$ every $-2 (2) cm s^{-1}$ beginning at $-2 (2) cm s^{-1}$. (c) Isentropes (dashed) and tilting frontogenesis (shaded). Isentropes are labeled and contoured as in Figure 2.5(a) and tilting frontogenesis is in units of $K m^{-1} s^{-1}$ and contoured every $5 (-5) \times 10^{-9} K m^{-1} s^{-1}$ starting at $10 (-10) \times 10^{-9} K m^{-1} s^{-1}$ with dark (light) shading indicating negative (positive) tilting frontogenesis.

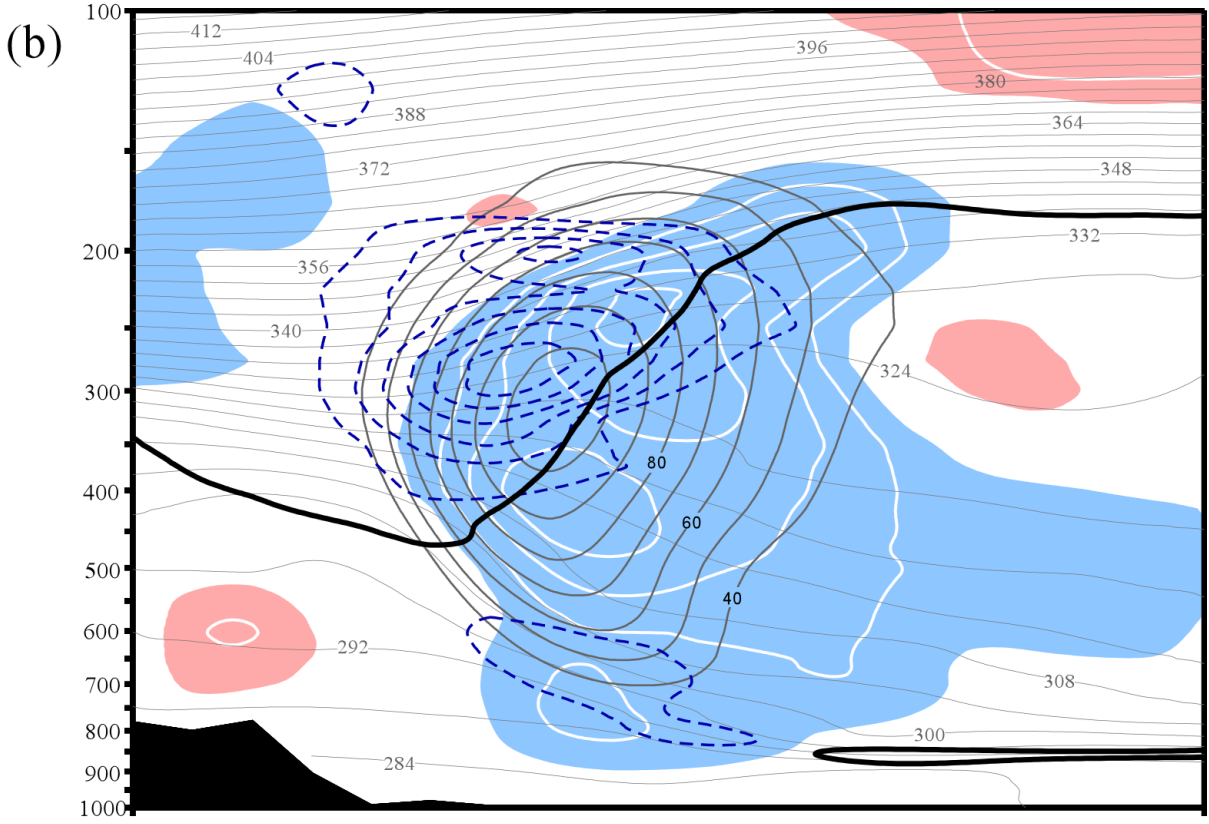
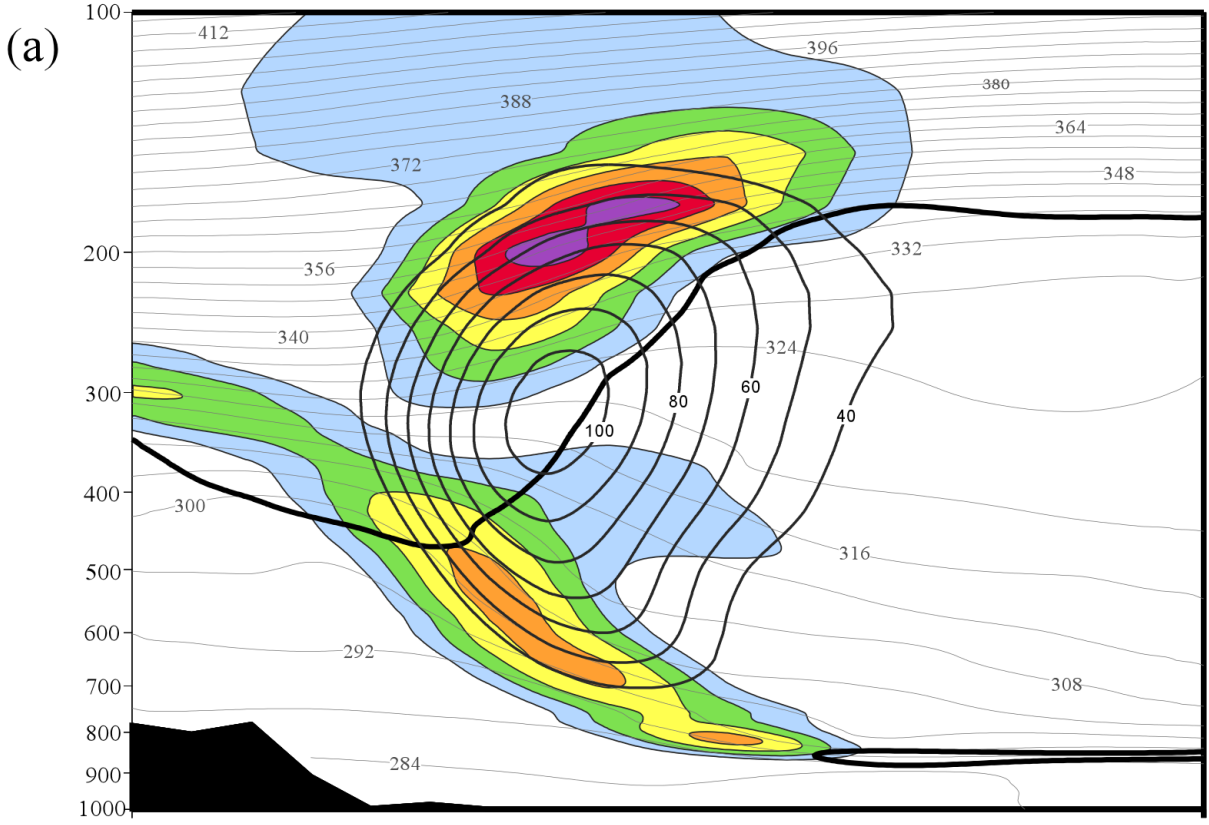


Figure 2.6. (On previous page) Vertical cross section along the line A-A' in Figure 2.5 valid at 0600 UTC 4 February 2008. (a) Potential temperature (thin solid), geostrophic isotachs (dashed), magnitude of the horizontal potential temperature gradient (shaded), and the tropopause (thick solid). Potential temperature is labeled in K and contoured every 4 K, isotachs are labeled in $m s^{-1}$ and contoured every 10 $m s^{-1}$ beginning at 30 $m s^{-1}$, the magnitude of the horizontal potential temperature gradient is contoured every 1 K $(100km)^{-1}$ beginning at 2 K $(100 km)^{-1}$ and the tropopause is represented by the 1.5 PVU contour. (b) Potential temperature (thin light solid), geostrophic isotachs (thin dark solid), geostrophic temperature advection (dashed), vertical motion (shaded), and the tropopause (thick solid). Potential temperature is labeled and contoured as in Figure 2.6a, isotachs are labeled as in Figure 7a, geostrophic temperature advection contoured in units of $K s^{-1}$ every $-3 (3) \times 10^{-1} K s^{-1}$ with dark (light) contours representing cold (warm) air advection. Vertical motions are contoured in $cm s^{-1}$ every $-2 (2) cm s^{-1}$ beginning at $-2 (2) cm s^{-1}$ with dark (light) shading representing subsidence (ascent), and the tropopause is represented as in Figure 2.6a.

$m^{-1} s^{-1}$) characterized the majority of the northwesterly flow portion of the lower stratospheric front (Figure 2.5c) as sinking cold air acted frontolytically along the lower stratospheric front.

A vertical cross section taken through the polar jet along the line A-A' in Figure 2.5 is shown in Figure 2.6. The lower stratospheric and upper tropospheric fronts associated with the polar jet are apparent, though, the lower stratospheric front is the more intense of the two frontal features at this time (Figure 2.6a). The cyclonic shear side of this lower stratospheric front was also characterized by geostrophic cold air advection, with a maximum of $-18 \times 10^{-4} K s^{-1}$ at ~ 275 hPa (Figure 2.6b). At ~ 230 hPa and within the largest wind speed at that level, there was a local maximum in subsidence ($-10 cm s^{-1}$) coinciding with the QG forcing along the lower stratospheric front. This subsidence was maximized above the jet core and to the cold side of the lower stratospheric front. Such subsidence decreased the slope of the isentropes and thus decreased the intensity of the lower stratospheric front above the jet core. The column of subsidence, most strongly forced in the lower stratosphere, extended downward through the weakly stratified jet core into the upper troposphere (Figure 2.6b) where it was

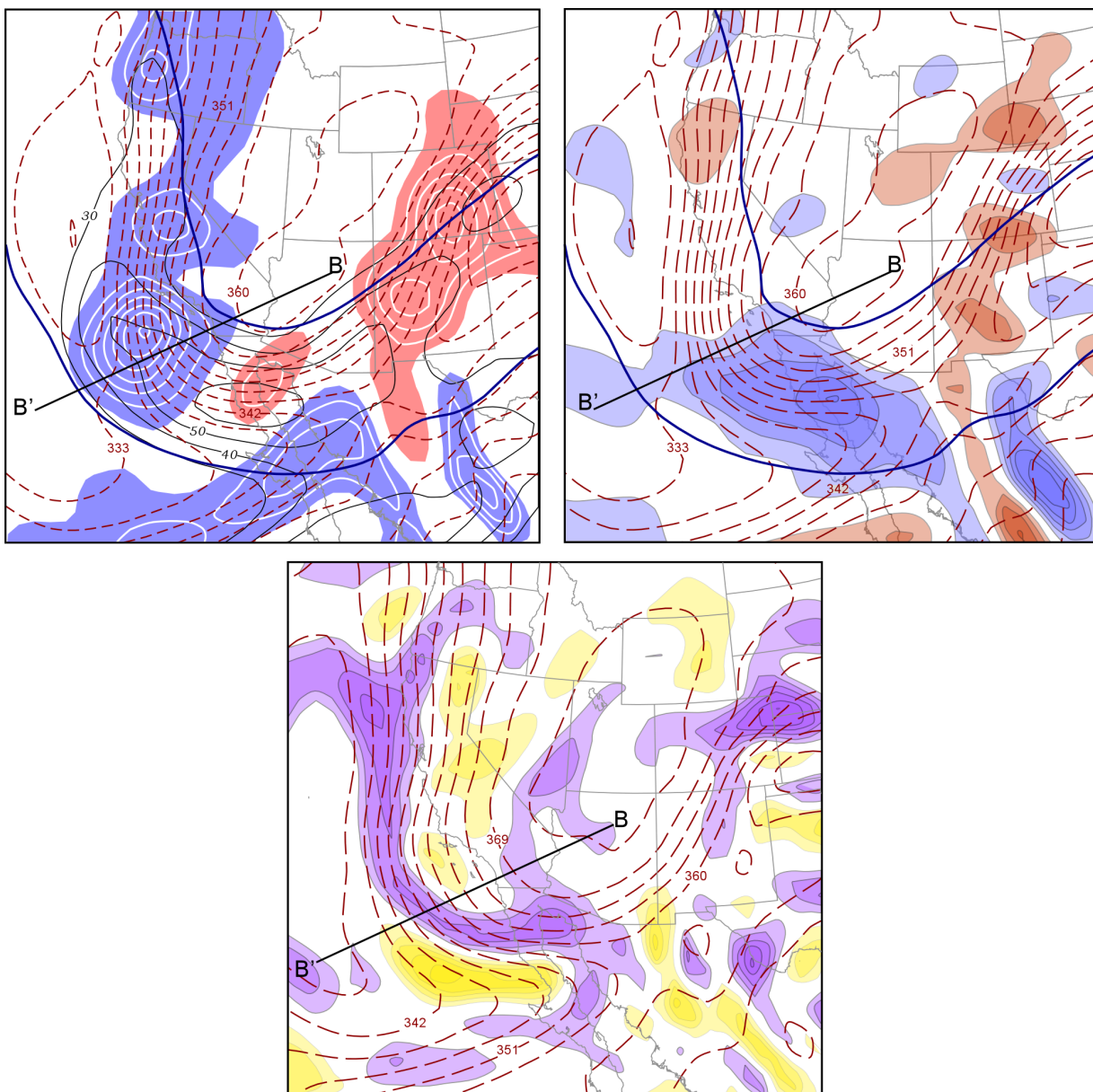


Figure 2.7. (a)-(c) As for Figure 6(a)-(c) but from the Eta-104 analysis valid 1800 UTC 4 February 2008.

maximized on the warm side of the upper tropospheric front and acted frontogenetically via tilting (not shown).

By 1800 UTC 4 February, geostrophic cold air advection had intensified and characterized the majority of the northwesterly flow lower stratospheric frontal zone, from

Oregon to off the west coast of northern Mexico (Figure 2.7a). The geostrophic cold air advection was generally confined to the cyclonic shear side of the geostrophic jet entrance region, with a maximum (geostrophic temperature advection of $-21 \times 10^{-4} \text{ K s}^{-1}$) west of the California-Mexico border. The baroclinic zone associated with a subtropical jet crossing southern Baja California was also characterized by geostrophic cold air advection ($-12 \times 10^{-4} \text{ K s}^{-1}$). Subsidence was maximized (-10 cm s^{-1}) over northern Baja California, with a finger of locally larger values reaching upstream to the cold side of the lower stratospheric front (Figure 2.7b). The gradient of vertical motion along the lower stratospheric front was associated with a linear band of negative tilting frontogenesis ($\sim -24 \times 10^{-8} \text{ K m}^{-1} \text{ s}^{-1}$), from the California-Oregon border south and east to the northern Gulf of California (Figure 2.7c). Similar to the prior period, geostrophic cold air advection on the cyclonic shear side of the geostrophic jet entrance region was coincident with subsidence on the cold side of the lower stratospheric front. This subsidence acted frontolytically via tilting and acted to decrease the baroclinicity within the lower stratospheric front during this period.

A second vertical cross section taken along the line B-B' in Figure 2.7 is shown in Figure 2.8. At this time, a majority of the lower stratospheric front above the jet core was characterized by geostrophic cold air advection in cyclonic shear. Geostrophic cold air advection stretched vertically from 350 hPa to 150 hPa and was maximized (geostrophic temperature advection of $\sim -18 \times 10^{-4} \text{ K s}^{-1}$) at the 250 hPa level. Coincident with this forcing was a maximum in subsidence (-8 cm s^{-1}) at 250 hPa, within the local wind speed max and to

the cold side of the lower stratospheric front. Subsidence on the cold side of the lower stratospheric front acted to decrease the slope of the isentropes above the jet core and continued to decrease the baroclinicity of the lower stratospheric front. Though this subsidence cannot be a result of QG processes associated with the upper tropospheric region of geostrophic warm air advection in cyclonic shear, it was located on the warm side of the weak upper tropospheric front and acted frontogenetically via tilting (not shown).

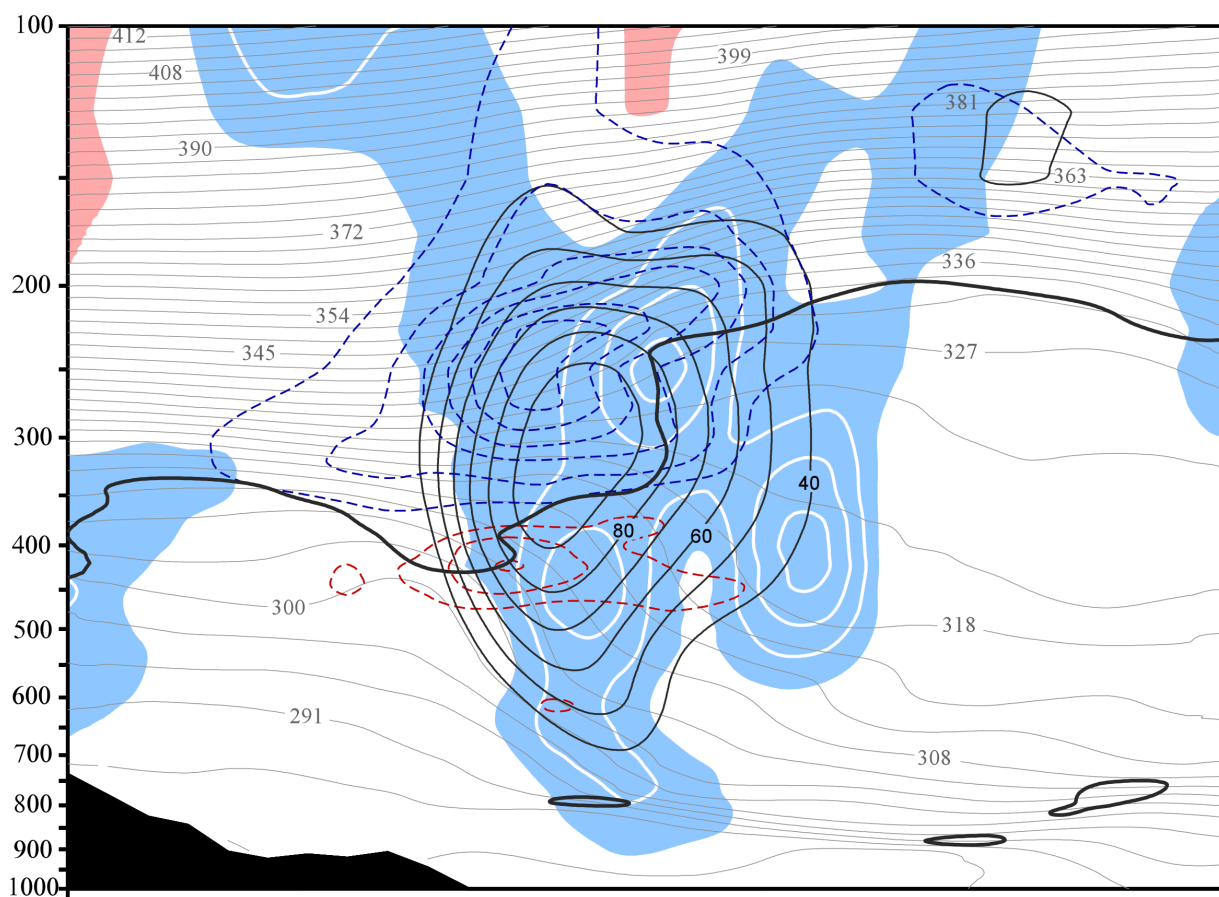


Figure 2.8. As for Figure 2.6b, but from the Eta-104 analysis valid 1800 UTC 4 February 2008 along the line B-B' in Figure 2.7.

2.4. Southwesterly Flow Case

a. Synoptic Overview

Between 26-28 February 2008, a strong winter storm moved northeastward along the east coast of the United States (not shown). The cyclone prompted Winter Storm Warnings from North Carolina to Maine and left nearly 30 cm of snow in many areas of the Northeast. Further south, an intense squall line associated with an active trailing cold front brought severe thunderstorms and power outages to the southeastern states. Temperatures in the wake of this cyclone were 15-20°F colder than normal for much of the East Coast. Using Eta-104 analyses, the deep baroclinic structure that developed within the upper troposphere and lower stratosphere in association with this cyclone will be investigated for the period between 27-28 February 2008.

At 0000 UTC 27 February, general southwesterly flow existed over the east coast of the United States (Figure 2.9). Within the southwesterly flow at 200 hPa, an enhanced baroclinic zone stretched from the southeast states toward Maritime Canada (Figure 2.9a). At this time, the lower stratospheric front had an intensity of $\sim 7 \text{ K (100 km)}^{-1}$ over the state of Maryland. The warmest temperatures at this level were found within the trough over the western Great Lakes region, while the coldest temperatures were found ahead of the lower stratospheric front, off the mid-Atlantic coast. At 500 hPa, the thermal structure was less coherent, with a weak upper tropospheric front over the southeastern states and weak regions of baroclinicity downstream (Figure 2.9b). The intensity of the upper tropospheric front was $\sim 5 \text{ K (100km)}^{-1}$ over the southern Appalachian Mountains. In the vicinity of the southeastern states, the lower

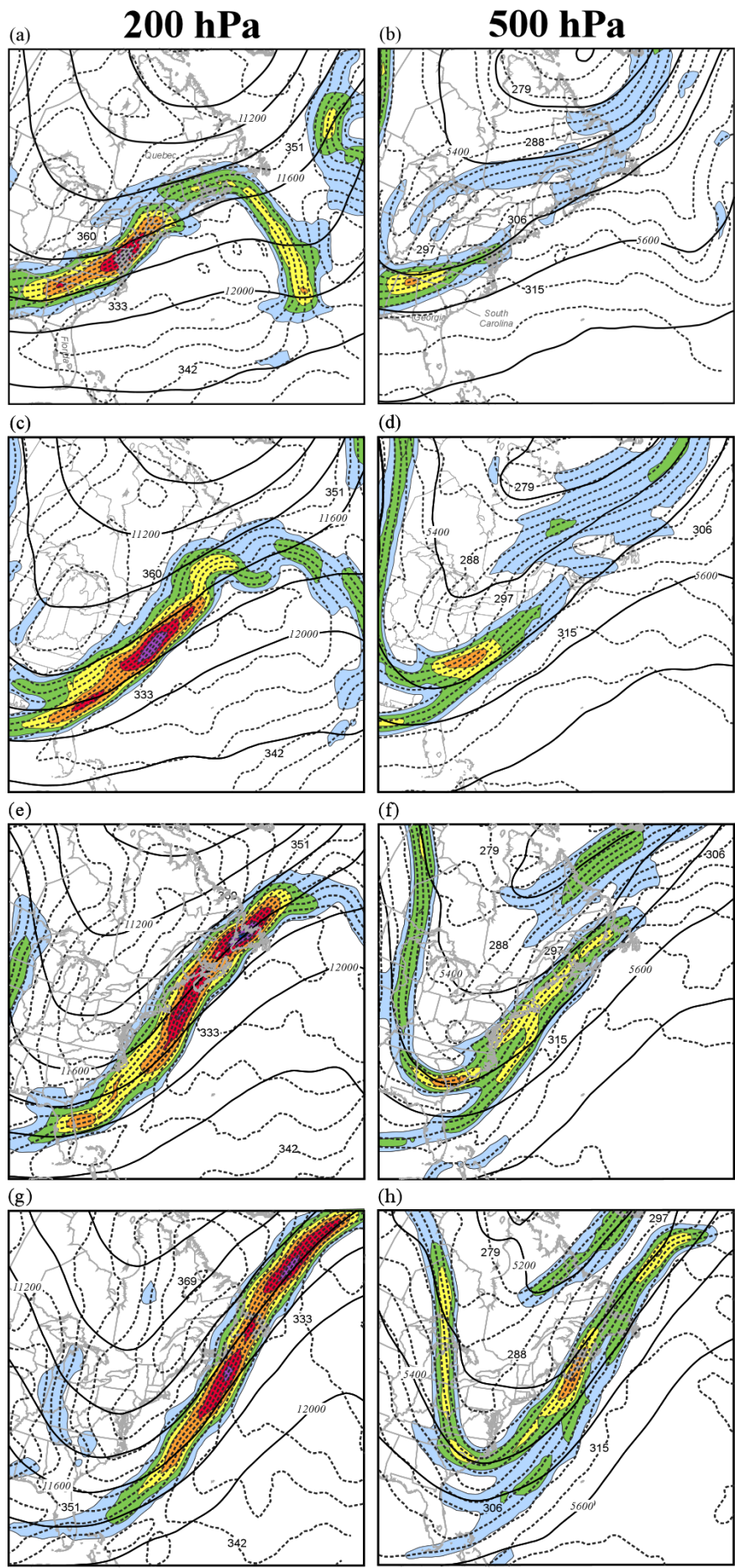


Figure 2.9. (On previous page) (a) and (b) as for Figure 2.4 (a) and (b), but from the Eta-104 model analysis valid at 0000 UTC 27 February 2008. (c) and (d) as for Figure 2.4 (a) and (b), but from the Eta-104 model analysis valid at 1200 UTC 27 February 2008. (e) and (f) as for Figure 2.4 (a) and (b), but from the Eta-104 model analysis valid at 0000 UTC 28 February 2008. (g) and (h) as for Figure 2.4 (a) and (b), but from the Eta-104 model analysis valid at 1200 UTC 28 February 2008.

stratospheric and upper tropospheric fronts were generally parallel, however, at this particular time the lower stratospheric front was more intense than its tropospheric counterpart.

By 1200 UTC 27 February, the lower stratospheric front stretched from the Georgia-Florida border to Maritime Canada (Figure 2.9c). The maximum intensity of the lower stratospheric front remained constant ($\sim 7 \text{ K (100 km)}^{-1}$), however, the area characterized by such magnitude had grown substantially in the intervening 12-hours. A cold trough became more apparent immediately to the east of the lower stratospheric front, the upper troposphere-lower stratosphere equivalent of the thermal ridge ahead of a surface cold front. At 500 hPa, the most intense portion of the upper tropospheric front was found downstream of the confluence in the flow, over the southeastern US (Figure 2.9d). The intensity of the potential temperature gradient associated with the upper tropospheric front had not changed since the previous time ($\sim 5 \text{ K (100 km)}^{-1}$). The upper tropospheric and lower stratospheric fronts were both fairly linear features, over the east coast of the US, with the lower stratospheric front being the more intense of the two fronts.

At 0000 UTC 28 February, the southwesterly flow over the east coast of North America was characterized by an intensifying lower stratospheric front (Figure 2.9e) with a maximum intensity of $\sim 8 \text{ K (100 km)}^{-1}$ over Maritime Canada. Immediately downstream of the 200 hPa

trough axis, from the eastern Great Lakes northward into central Quebec, were the warmest potential temperatures at this level. Ahead of the lower stratospheric front, the thermal trough remained a robust feature, with the coldest temperatures just east of the most intense portion of the front. At 500 hPa, the upper tropospheric front weakened, with only two small regions in which $|\nabla\theta|$ was $\sim 5 \text{ K (100 km)}^{-1}$, over New Jersey and the South Carolina-Georgia border (Figure 2.9f). Over Maritime Canada, where the lower stratospheric front was at its most intense, the upper tropospheric front was nearly non-existent with a $|\nabla\theta|$ of $\sim 3 \text{ K (100 km)}^{-1}$.

By 1200 UTC 28 February, the lower stratospheric front stretched along the east coast of North America from the Bahamas to the region south of Greenland (Figure 2.9g). At 200 hPa, the region of intense baroclinicity ($|\nabla\theta| > \sim 6 \text{ K (100 km)}^{-1}$) characterized a larger area at this time and was flanked by the warmest potential temperatures ($\sim 369 \text{ K}$), over Newfoundland and the coldest potential temperatures ($\sim 330 \text{ K}$), over the northwestern Atlantic. In the upper troposphere, the southwesterly flow was characterized by a lengthy baroclinic zone with $|\nabla\theta| \sim 5 \text{ K (100 km)}^{-1}$ off the east coast of Maine (Figure 2.9h). The upper tropospheric front stretched from the Carolinas to south of Greenland, however, the lower stratospheric front remained the more intense of the two frontal features.

b. Analysis

The interaction of the constituent frontal zones of the ULJF on 28 February is examined next. This period represents the time when the lower stratospheric front was at its maximum intensity and covered the largest geographic area.

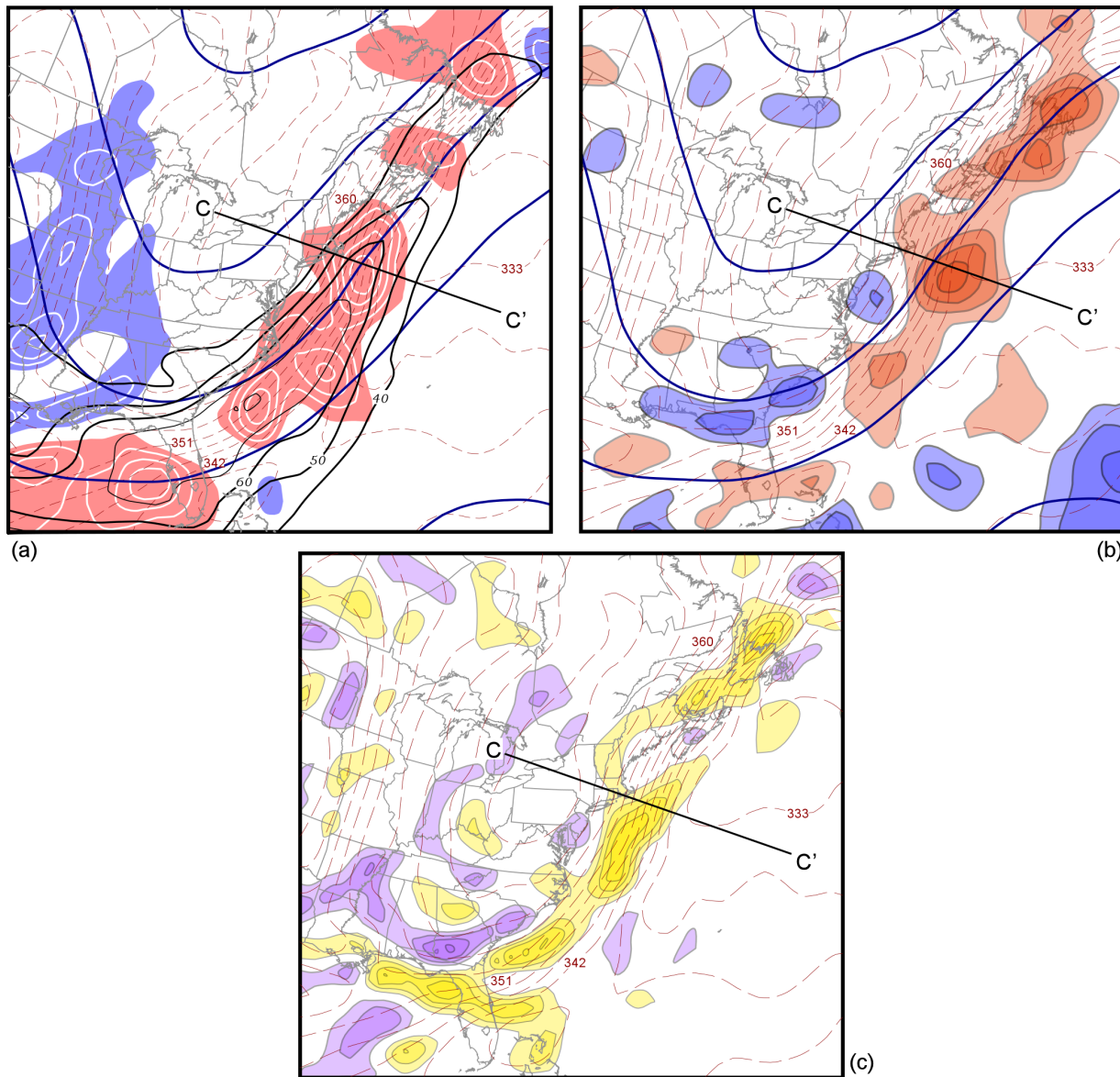


Figure 2.10. (a)-(c) As for Figure 2.5a-c but from the Eta-104 analysis valid at 0000 UTC 28 February 2008.

At 0000 UTC 28 February, southwesterly geostrophic flow was present along the east coast of North America, with a geostrophic jet max greater than 70 m s^{-1} off the southeast coast of the United States (Figure 2.10a). A majority of the cyclonic shear side of the southwesterly flow was characterized by geostrophic warm air advection, with a maximum in the jet exit

region of $\sim 15 \times 10^{-4} \text{ K s}^{-1}$ east of New Jersey. Coincident with this geostrophic forcing, was a linear band of ascent on the cold side of the lower stratospheric front, over Florida and from east of the Carolinas to east of Newfoundland (Figure 2.10b). Ascent was greatest to the east and to the cold side of the maximum in geostrophic warm air advection. With ascent adiabatically cooling the cold side of the 200 hPa front, a nearly continuous band of positive tilting frontogenesis characterized the southwesterly flow lower stratospheric frontal zone from Florida to Newfoundland (Figure 2.10c). Several regions, including Florida, east of Maryland, and east of Newfoundland, had values of tilting frontogenesis greater than $20 \times 10^{-8} \text{ K m}^{-1} \text{ s}^{-1}$.

A cross section taken at 0000 UTC 28 February, perpendicular to the lower stratospheric front, along the line C-C' in Figure 2.10 is shown in Figure 2.11. Below the level of maximum winds, the tropospheric front was characterized by weak geostrophic cold air advection ($-6 \times 10^{-4} \text{ K s}^{-1}$). A plume of upward vertical motion was located immediately east of the surface cold front, was maximized at 500 hPa, and was associated with positive frontogenesis in the lower troposphere (not shown). However, within the lower stratospheric front, a maximum ($15 \times 10^{-4} \text{ K s}^{-1}$) in geostrophic warm air advection was present in the cyclonic shear centered at roughly 200 hPa. Immediately to the cold side of the lower stratospheric front and to the west of the lower tropospheric plume, was a second plume of ascent, with a maximum greater than 12 cm s^{-1} . Ascent in this location acted to increase the slope of the isentropes above the jet core (positive tilting frontogenesis) and acted to increase the slope of the tropopause above the jet core. The two plumes of vertical motion within this

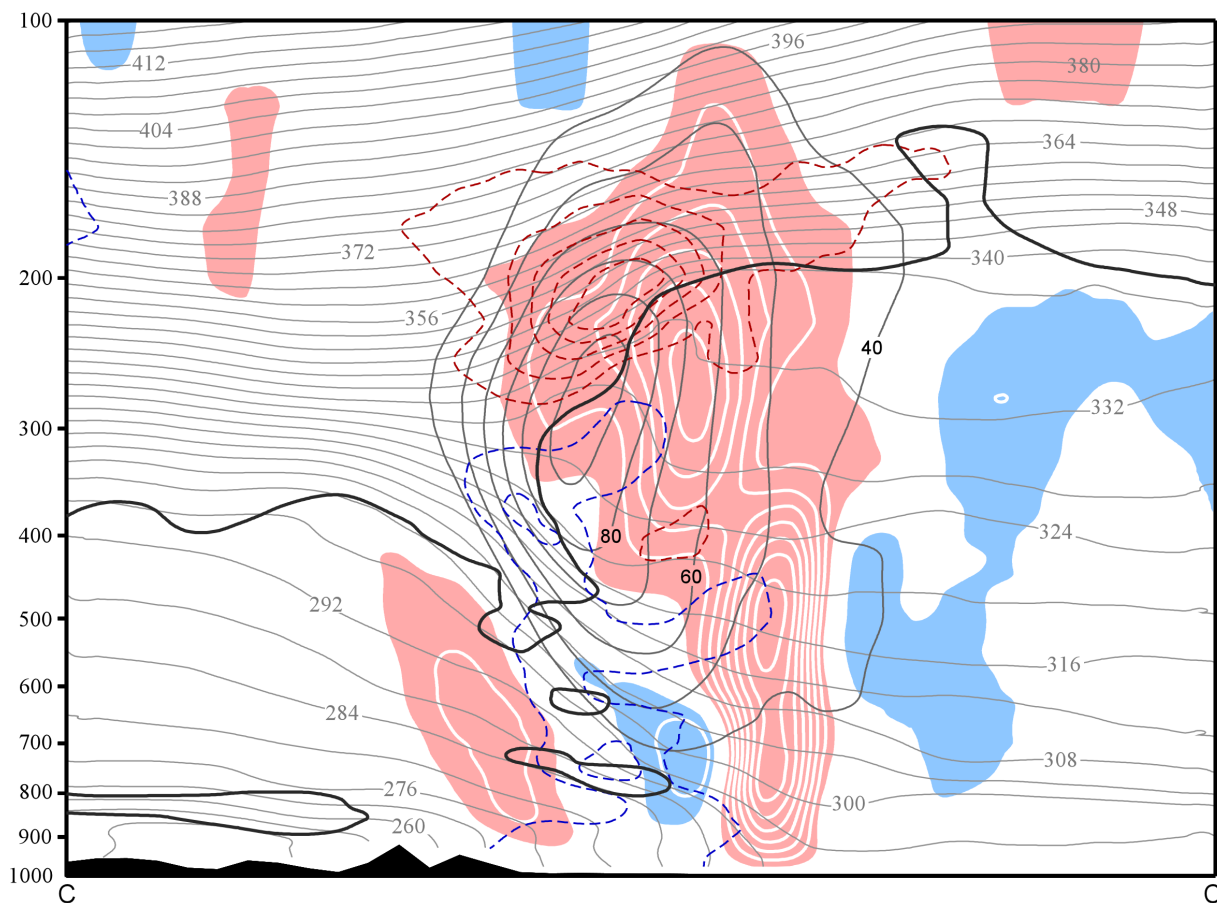


Figure 2.11. As for Figure 2.6b, but from the Eta-104 analysis valid at 0000 UTC 28 February 2008 along the line C-C' in Figure 2.10.

cross section were associated with two separate frontal circulations. One plume responded to frontogenetic forcing associated with the surface front in the lower troposphere while the other was coincident with QG forcing associated with the lower stratospheric front. Together these two plumes created a nearly vertically stacked column of ascent that reached from the surface to above the 150 hPa level and served to weaken the baroclinicity in the troposphere while strengthening it in the lower stratosphere.

By 1200 UTC 28 February, the 200 hPa geostrophic jet had intensified to 80 m s^{-1} off

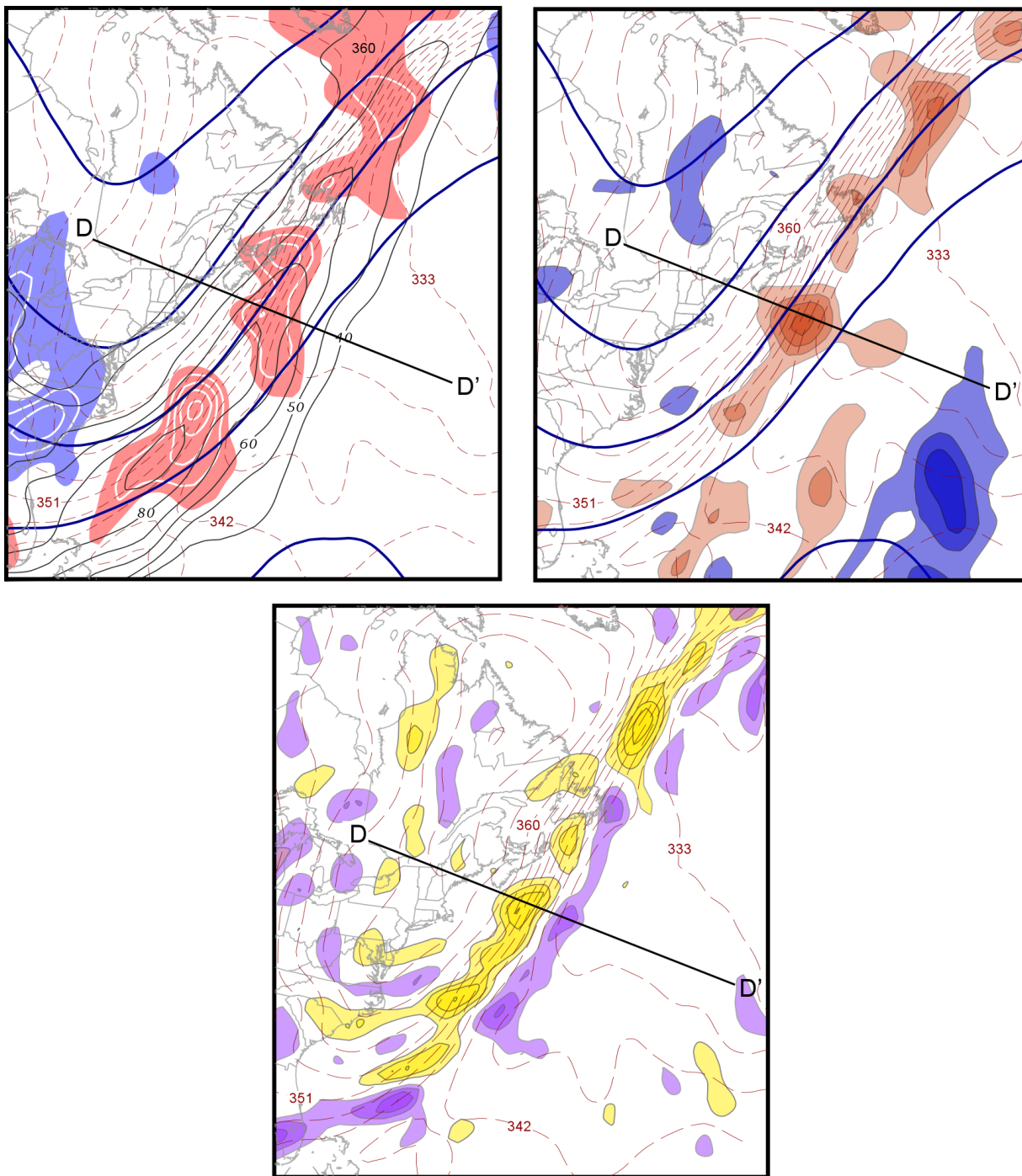


Figure 2.12. (a)-(c) As for Figure 2.5(a)-(c) but from the Eta-104 analysis valid at 1200 UTC 28 February 2008.

the southeast coast of the United States (Figure 2.12a). Primarily downstream of the jet max, geostrophic warm air advection in cyclonic shear persisted through the majority of the southwesterly flow baroclinic zone. There were several maxima off the east coast of North America with values of geostrophic warm advection greater than $12 \times 10^{-4} \text{ K s}^{-1}$. In the vicinity of this QG forcing, a nearly continuous band of ascent characterized a large portion of the southwesterly flow, with the maximum roughly confined to the region of the jet core (Figure 2.12b). As a result, the tilting contribution to frontogenesis was positive and formed a roughly linear band from east of the Mid-Atlantic States to the region south of Greenland (Figure 2.12c).

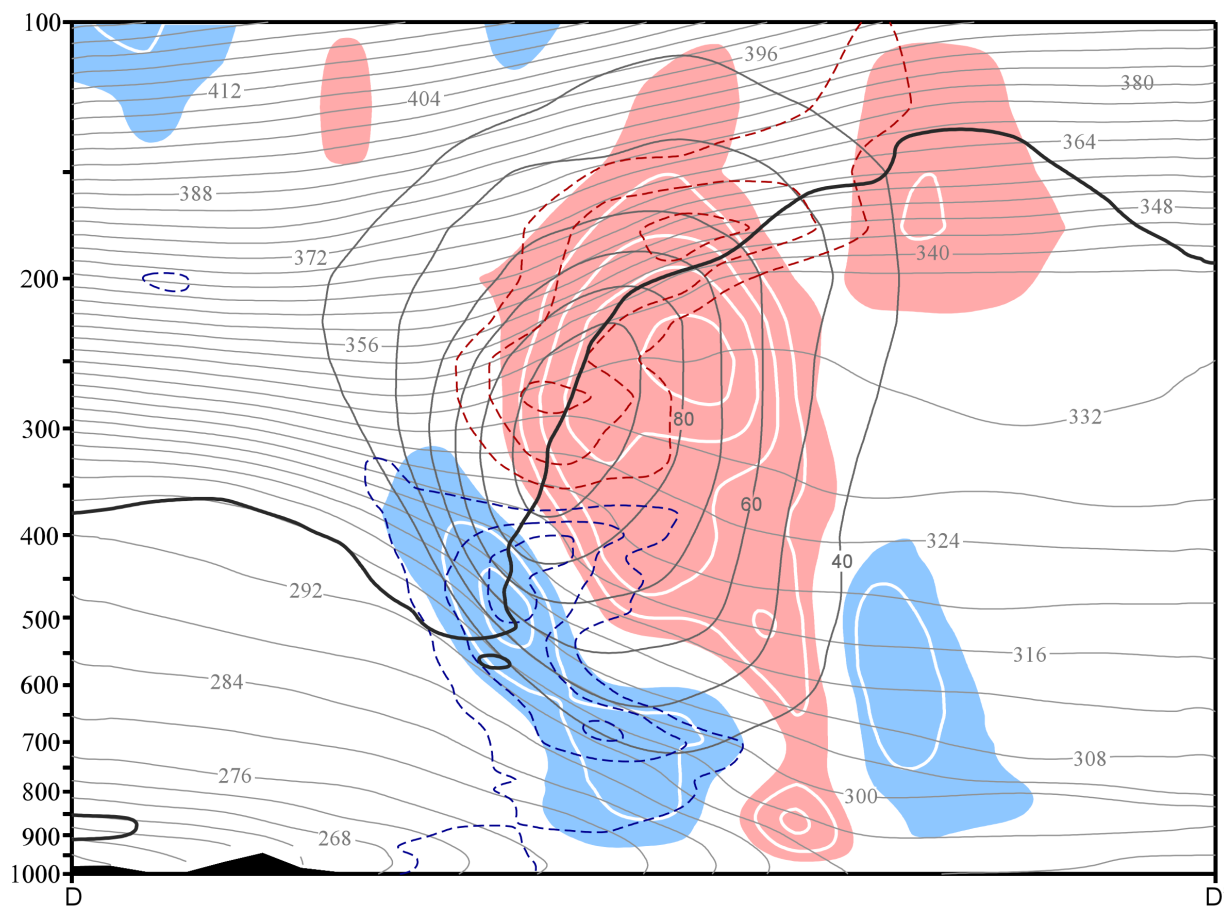


Figure 2.13. As for Figure 2.6b, but from the Eta-104 analysis valid at 1200 UTC 28 February 2008 along the line D-D' in Figure 2.12.

A cross section was taken at 1200 UTC 28 February, along the line D-D' in Figure 2.12, through the straight southwesterly flow off the coast of Nova Scotia (Figure 2.13). The jet had reached 90 m s^{-1} at roughly 250 hPa. Below the jet core, the broad, tropospheric-deep cold front was characterized by geostrophic cold air advection, with the greatest intensity ($-9 \times 10^{-4} \text{ K s}^{-1}$) located at ~ 450 hPa within the upper tropospheric portion of the front. This portion of the front was also characterized by subsidence. In the region above the jet core, geostrophic warm air advection characterized the cyclonic shear side of the jet and the lower stratospheric front. A large plume of ascent (10 cm s^{-1}), in the vicinity of the QG forcing in the lower stratosphere, was centered at roughly 225 hPa on the cold side of the lower stratospheric front. Ascent in the region continued to increase the slope of the isentropes above the jet core and tilt the dynamic tropopause into a more vertical orientation. By this time, the dynamic tropopause above the jet core had risen to ~ 150 hPa and the overall tropopause structure in the vicinity of the ULJF had become more steeply sloped.

2.5. *Summary and Discussion*

Upper-level jet front (ULJF) systems are ubiquitous features of the mid-latitude atmosphere consisting of an upper tropospheric frontal zone beneath the jet core, the jet core itself, and a lower stratospheric frontal zone above the jet core. Given their relevance to the extratropical cyclone life cycle, stratosphere/troposphere exchange, and clear air turbulence, the upper tropospheric portion of these ULJFs have been afforded considerable research attention in the past 60 years. Surprisingly little consideration has been given to the structure, evolution

and dynamics associated with their lower stratospheric counterparts or the interaction between these separate frontal zones in the context of the ULJF life cycle. This chapter provides fresh insights into these issues by emphasizing the lower stratospheric front as a distinct entity within the ULJF and highlighting its structure, evolution, and dynamical interaction with its upper tropospheric counterpart.

Consideration of the lower stratospheric portion of an ULJF as a distinct front encourages the extension of many of the concepts of upper tropospheric frontal dynamics to regions above the level of maximum wind. Analogous to Reed's (1955) description of an upper tropospheric front, the lower stratospheric baroclinic zone is best considered a frontal structure, with its own distinct frontal circulation, that separates stratospheric air from tropospheric air. Above the level of maximum winds, where the pole to equator temperature gradient reverses, the lower stratospheric front represents a boundary separating cold mid-latitude upper tropospheric air from warmer mid-latitude lower stratospheric air. Frontogenetic tilting across a lower stratospheric frontal zone will result from a combination of subsidence maximized in the warm lower stratosphere or ascent maximized in the cold upper troposphere, a thermally indirect circulation. Analogous to the situation in the upper troposphere, these differential vertical motions will result in the deformation of the tropopause above the level of maximum wind, where positive tilting frontogenesis is associated with a more steeply sloped tropopause. Based upon the examination of two cases, both observed in February 2008, the analysis presented here suggests that, though the governing dynamics for their developments (tilting frontogenesis) are the same, the upper tropospheric and lower stratospheric fronts can develop

asynchronously within the evolution of an ULJF through the northwesterly and southwesterly flow portions of a baroclinic wave.

In the northwesterly flow case, the ULJF was originally characterized by a vigorous lower stratospheric frontal zone and a weak upper-tropospheric frontal zone, as measured by the magnitude of the potential temperature gradients at 200 and 500 hPa, respectively. The lower stratospheric front was characterized by geostrophic cold air advection in cyclonic shear (particularly in the jet entrance region) throughout the evolution. This circumstance was associated with subsidence on the cold side of the lower stratospheric frontal zone which, in turn, led to a decrease in its intensity. This subsidence, presumably forced by lower stratospheric frontal processes, protruded downward to sufficient depth to reach the warm side of the weak upper tropospheric front, gradually intensifying that feature. Thus, forcing for subsidence within the decaying lower stratospheric frontal environment is hypothesized to have been a contributing factor in an already favorable environment for the initial development of the upper tropospheric frontal portion of the ULJF. Furthermore, as the lower stratospheric front continued to weaken, the upper tropospheric front intensified demonstrating a clearly asynchronous, yet dynamically interactive developmental relationship between the two component frontal zones of the ULJF.

In the southwesterly flow case, the lower stratospheric front experienced a period of intensification coincident with the weakening of its upper tropospheric counterpart. In that case, the lower stratospheric front was characterized by a nearly continuous band of geostrophic warm air advection on the cyclonic shear side of the jet. Such a circumstance

promotes QG forcing for ascent through the jet core, on the cold side of the lower stratospheric front. Such ascent was frontogenetic above the jet core increasing both the slope of the isentropes and the slope of the tropopause above the jet core. The ascent coincident with the lower stratospheric forcing was discernibly separate from the ascent associated with lower tropospheric frontal forcing. Their nearly vertical superposition, however, created a tropospheric deep column of ascent that acted frontolytically in the middle and upper troposphere but frontogenetically in the lower stratosphere.

The results presented here appear to be characteristic of a number of other ULJF evolutions examined in the course of this research. A conceptual model highlighting some common characteristics of northwesterly flow cases is presented in Figure 2.14a. In northwesterly flow characterized by geostrophic cold air advection in cyclonic shear, the lower stratospheric frontal zone experiences frontolysis while its upper tropospheric counterpart experiences frontogenesis. Attendant with the upper tropospheric frontogenesis is an extrusion of stratospheric PV and O₃ into the upper troposphere. The extruded stratospheric PV is manifest as an upper tropospheric absolute vorticity maxima that can serve as a precursor to surface cyclogenesis.

In southwesterly flow characterized by geostrophic warm air advection in cyclonic shear, the upper tropospheric frontal zone weakens while its lower stratospheric counterpart intensifies via forced ascent through the jet core (Figure 2.14b). As a result, tropospheric water vapor is exported into the lower stratosphere and low values of PV, from the lower troposphere, flood the upper troposphere/lower stratosphere on the anticyclonic shear side of a

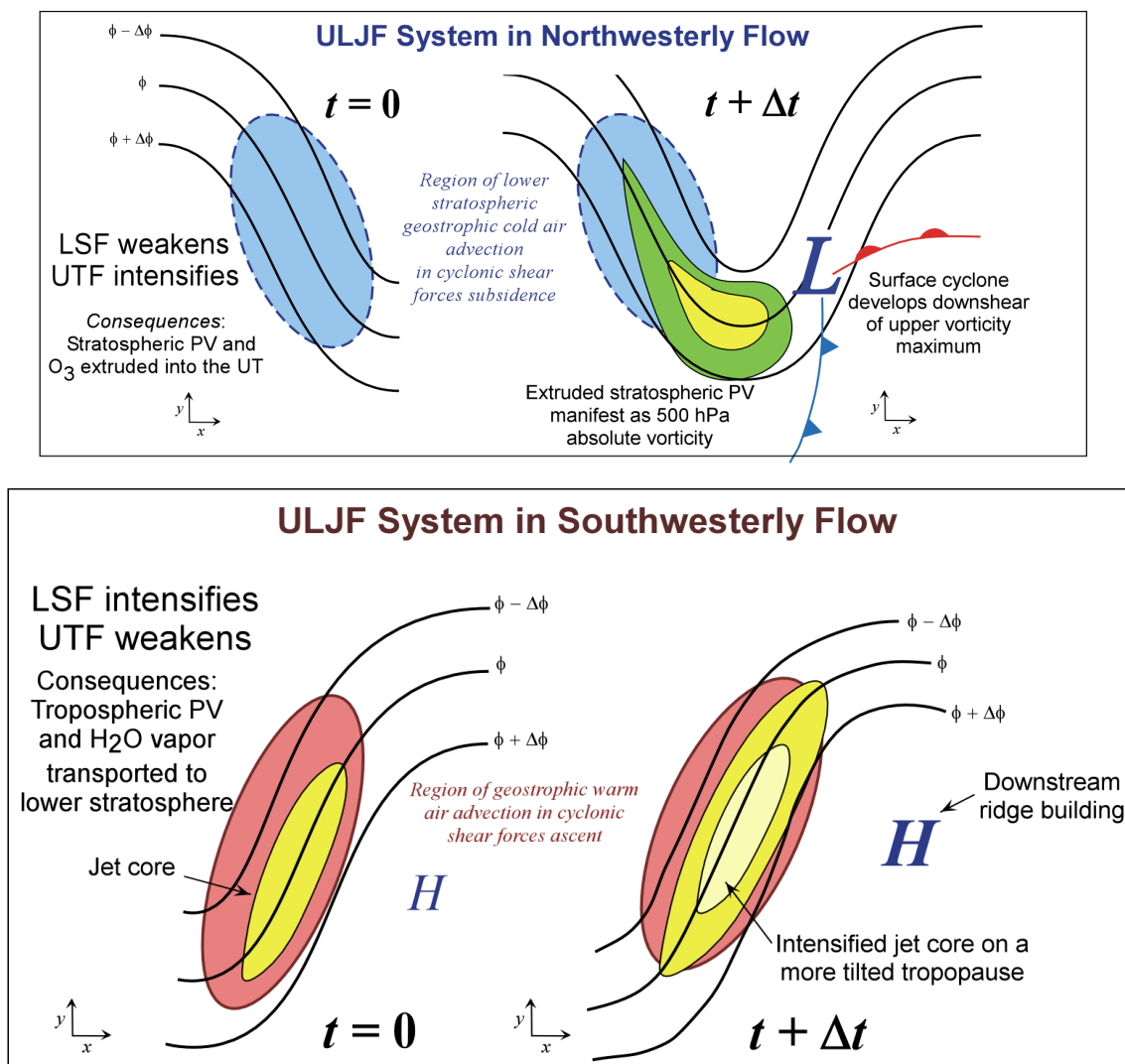


Figure 2.14. Schematic illustrating the asynchronous evolution of the lower stratospheric (LSF) and upper tropospheric frontal (UTF) portions of an ULJF within the (a) northwesterly and (b) southwesterly flow portions of a baroclinic wave. The dashed shaded oval in (a) represents the region of geostrophic cold air advection in cyclonic shear. In such a location within an ULJF, the lower stratospheric front experiences frontolysis via vertical tilting and the upper tropospheric front experiences frontogenesis via tilting. The frontogenesis is associated with extrusion of stratospheric PV into the troposphere and subsequent downstream surface cyclogenesis. The solid shaded oval in (b) represents the region of geostrophic warm air advection in cyclonic shear. In such a location within an ULJF, the lower stratospheric front experiences frontogenesis and the upper tropospheric front experiences frontolysis via tilting. Darker shaded areas represent the jet stream isotachs. Lower stratospheric frontogenesis intensifies the jet and promotes ridge building downstream. See text for additional explanation.

strengthening southwesterly jet. In this case, this process led to the amplification of the ridge at upper tropospheric levels and to anticyclonogenesis in the lower troposphere downstream of the intensified jet. The analysis of several southwesterly flow cases documented during the 2008-2009 North American winter will be highlighted in Part 2 of this study.

This study strongly suggests that consideration of the separate evolution of the lower stratospheric and upper tropospheric frontal zones associated with an ULJF system can lead to a better understanding of the comprehensive life-cycle of an ULJF through a baroclinic wave. It is left to future research to investigate how lower stratospheric frontal processes are explicitly connected to upstream or downstream sensible weather. For example, is lower stratospheric geostrophic warm air advection in cyclonic shear consistently tied to ridge building and blocking in the way that geostrophic cold air advection in the cyclonic shear within an upper tropospheric front is tied to upper level trough and cyclone development? Similarly, to the extent that lower stratospheric and lower tropospheric frontal circulations are vertically aligned, the kinetic energy released in any convective ascent along the tropospheric front can enhance the effect of the frontogenetic tilting already present in the lower stratospheric frontal circulation and thus further increase the slope of the dynamic tropopause associated with an intensifying lower stratospheric front. The role that tropospheric convection plays in the intensification of the lower stratospheric thermal gradient in southwesterly flow cases remains an outstanding question.

The changes to the thermal field at and above the tropopause associated with lower stratospheric frontogenesis are also associated with variation in the structure of the vertical

shear within the lower stratosphere. Thus, fully understanding lower stratospheric frontogenesis has further implications for the coupling between the stratosphere and troposphere by potentially explaining some of the variation in the environment governing the vertical propagation of atmospheric waves as the Sawyer-Eliassen forcing is the synoptic-scale version of the larger-scale Eliassen-Palm flux convergence. Perhaps consideration of lower stratospheric frontal processes will provide further insight into the not-yet-completely-understood role of synoptic scale baroclinic waves in transmitting the downward propagating anomalies, associated with the Northern Annular Mode (NAM), from the stratosphere to the troposphere (e.g., Baldwin and Dunkerton, 1999, 2001; Haynes, 2005; Breiteig, 2008).

Chapter 3

Part II: The influence of tropospheric convection on lower stratospheric frontal development

3.1. Introduction

A midlatitude upper level jet-front system (ULJF) consists of three component parts: (1) a jet core and attendant frontal structures in (2) the upper troposphere and (3) the lower stratosphere, associated (via thermal wind) with the vertical shear in those locations (Figure 2.1). In Chapter 2, it was shown that consideration of the separate evolution of the lower stratospheric front and upper tropospheric front is necessary in order to fully understand the comprehensive life-cycle of an ULJF within a baroclinic wave. Upon the examination of two cases, the Chapter 2 analysis shows that while they have common governing dynamics, namely tilting frontogenesis, the upper tropospheric and lower stratospheric fronts develop asynchronously within the evolution of an ULJF through the northwesterly and southwesterly flow portions of a baroclinic wave.

The dynamical underpinning of the analyses presented in Chapter 2 is the fact that geostrophic temperature advection in the lower stratospheric cyclonic shear portion of the ULJF provides considerable forcing for quasi-geostrophic (QG) vertical motion above the jet core. This QG forcing, centered within the lower stratospheric portion of an ULJF, is tied to

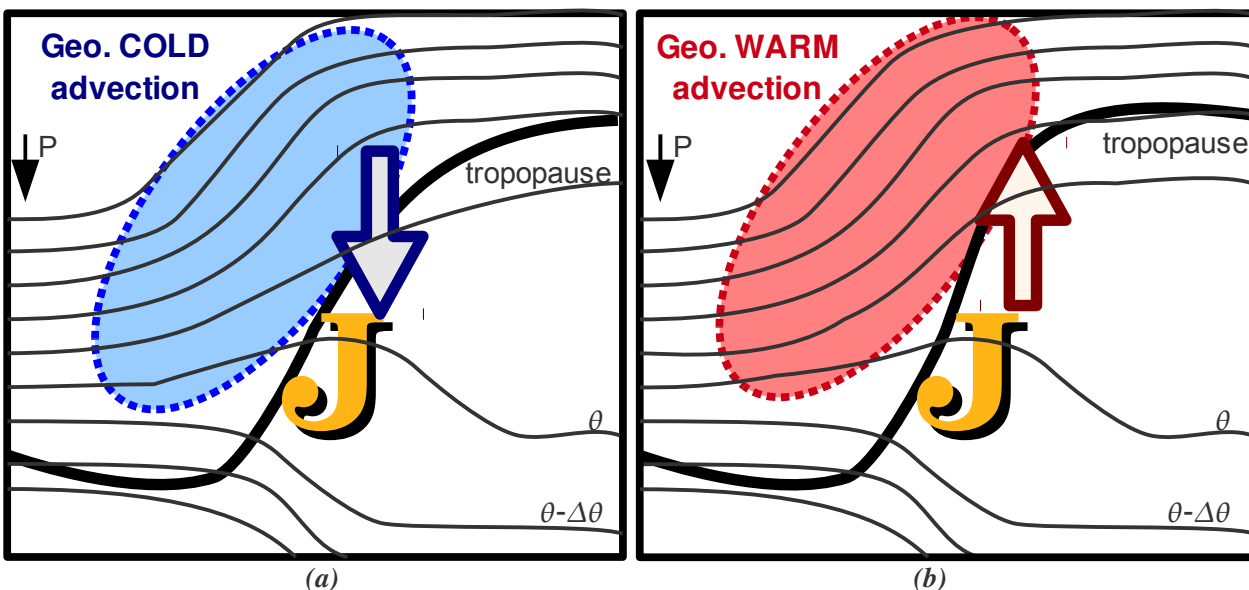


Figure 3.1. Conceptual models of lower stratospheric frontolysis in northwesterly flow and frontogenesis in southwesterly flow in (a) and (b), respectively, as summarized in the text. (a) With geostrophic cold air advection (shaded), subsidence represented by the arrow, idealized potential temperature (thin line), jet core represented by the “J”. (b) As in (a) but with geostrophic warm air advection shaded and ascent represented by the arrow.

Sawyer (1956)-Eliassen (1962) type circulations above the level of maximum winds and in the vicinity of the lower stratospheric front. In northwesterly flow, geostrophic cold air advection in the lower stratospheric cyclonic shear provided forcing for subsidence through the local jet core that weakened an initially intense lower stratospheric front, via tilting (conceptualized in Figure 3.1a). The lower stratospheric frontolysis was also associated with a decrease in the slope of the tropopause above the jet core. This weakening of the lower stratospheric front occurred in concert with the development of an intense upper tropospheric front that provided a precursor disturbance for a substantial surface cyclogenesis event. In the southwesterly flow case, QG forcing, in the form of geostrophic warm air advection in lower stratospheric cyclonic shear, promoted a plume of ascent on the cold side of the lower stratospheric front (conceptualized in Figure 3.1b). This vertical motion in the near-tropopause region resulted in

frontogenetic tilting, associated with both an enhancement of the frontal characteristics (e.g., cyclonic shear, static stability, temperature gradient) and an increased slope of the tropopause, above the jet core. Lang and Martin (2011) hypothesized that lower stratospheric frontogenesis processes can lead to substantial changes in the structure of the ULJF within which a lower stratospheric front is embedded. In addition, they noted that any changes to the midlatitude ULJF structure and tropopause slope can have potential consequences on the downstream development of sensible weather systems.

A leading characteristic of the southwesterly flow case presented in Chapter 2 was the vertical superposition of two distinct ascent plumes centered in (1) the near-tropopause upper troposphere, in association with lower stratospheric QG forcing; and (2) in the lower troposphere, in association with convection aligned along a surface cold front. That analysis suggested that when a surface cold front and a lower stratospheric front become nearly vertically aligned (common in southwesterly flow), the convection along the surface boundary can diabatically reduce the static stability of the upper troposphere. The reduced static stability can thereby produce a robust response to frontogenetical forcing for ascent in the vicinity of the lower stratospheric front. The present Chapter examines this hypothesis by considering the development of four robust southwesterly flow lower stratospheric fronts and the influence on the lower stratospheric frontogenesis process arising from coincident lower tropospheric ascent and associated latent heat release.

The Chapter is structured in the following manner. Section 2 provides an overview of each of the lower stratospheric front cases. The analysis of the four cases begins in Section 3,

with an overview of the common mechanisms associated with the development of the robust lower stratospheric fronts. Section 4 provides a cross sectional analysis of the cases, followed by a summary and discussion of the results highlighted in Section 5.

3.2. Case Overviews

In order to investigate the convective contributions to lower stratospheric frontogenesis in southwesterly flow, the present work highlights four ULJFs observed during the winter of 2008-2009 off of the east coast of North America. During that winter season, specifically the period between November 2008 to March 2009, the lower stratospheric and upper tropospheric frontal characteristics were documented and archived using data from the twice daily (0000 and 1200 UTC) analyses (00 h forecasts) from the $0.5^\circ \times 0.5^\circ$ grid of the National Center for Environmental Prediction's (NCEP) Global Forecast System (GFS) model. From this archive four events were selected to represent a sample of the strongest lower stratospheric front cases, each possessing a 200 hPa potential temperature gradient magnitude ($|\nabla\theta|$) exceeding $8 \text{ K (100 km)}^{-1}$ in the most intense phase of its life cycle in southwesterly flow.

Employing the GFS gridded model analyses, the following section provides a brief overview of the evolution of the lower stratospheric and upper tropospheric fronts in each of the ULJF cases. The evolution the 200 hPa $|\nabla\theta|$ will be used to represent the lower stratospheric front as 200 hPa was consistently located above the level of maximum winds of the southwesterly flow polar jet. The $|\nabla\theta|$ at 500 hPa serves as a measure of the intensity of the upper tropospheric front. Each of the overviews presented here corresponds to a period of

lower stratospheric frontogenesis that lasted at least 12 hours. Two times within the evolution are highlighted, one 12 hours prior to ($t = t - 12$ h), and a second at the time of ($t = 0$ h), the maximum intensity of each lower stratospheric front. In addition, this section provides a brief overview of the lower tropospheric synoptic environment at the $t = 0$ h period. The 950 hPa horizontal frontogenesis will be used to illustrate the forcing for lower tropospheric ascent in each case.

a. Case 1: 19-20 November 2008

At 1800 UTC 19 November 2008 a 200 hPa trough with a slight negative tilt characterized the flow off the east coast of North America (Figure 3.2a). Immediately downstream of the trough axis was a region of lower stratospheric baroclinicity, with a maximum $|\nabla\theta|$ of $6 \text{ K (100 km)}^{-1}$. The lower stratospheric front separated the higher potential temperatures ($\sim 360 \text{ K}$), characteristic of the lower stratosphere within the base of the trough from lower potential temperatures ($\sim 333 \text{ K}$), characteristic of the upper troposphere, in a band to the east of the baroclinic zone. At 500 hPa, an upper tropospheric front ($|\nabla\theta| \sim 6 \text{ K (100 km)}^{-1}$) extended from the base of a high amplitude trough northeastward through the eastern provinces of Canada (Figure 3.2b). The baroclinicity at this level was separated into two features, one in the vicinity of the base of the trough and the other downstream, within the southwesterly flow over eastern Canada. The region south of Nova Scotia with the strongest baroclinicity at 200 hPa, had relatively weak baroclinicity at 500 hPa.

By 0600 UTC 20 November, the trough at 200 hPa became more negatively tilted as the

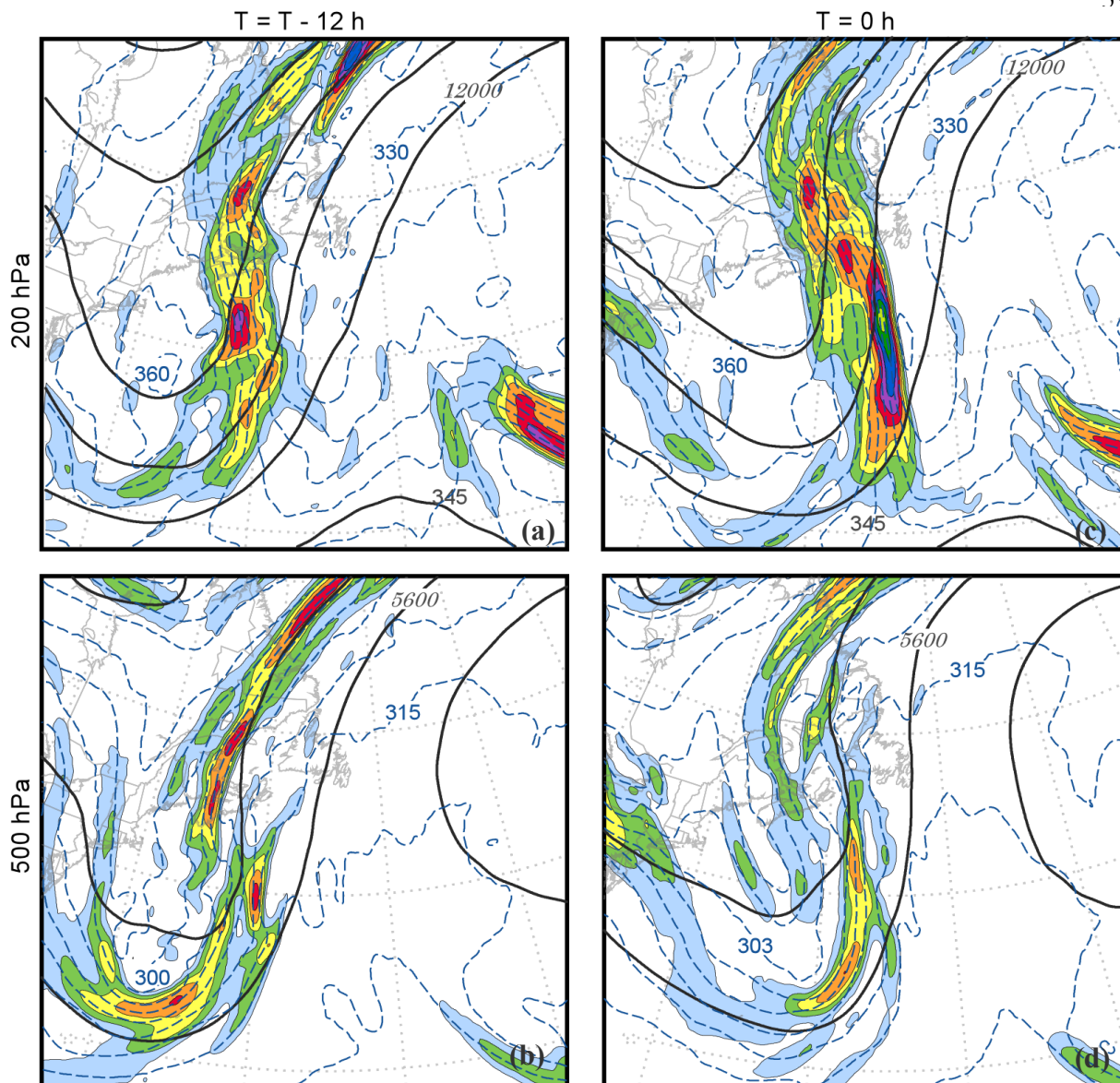
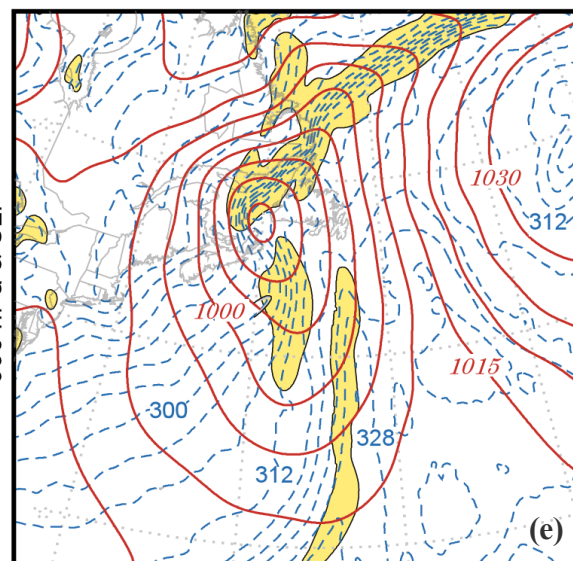


Figure 3.2. (a) 200 hPa geopotential height, θ , and $|\nabla\theta|$ from the GFS analysis valid at 1800 UTC 19 November 2008. Geopotential height (solid) is labeled in m and contoured every 200 m, θ (dashed) is labeled in K and contoured every 3 K, and $|\nabla\theta|$ is in units of $K (100 \text{ km})^{-1}$ shaded every $1 K (100 \text{ km})^{-1}$ beginning at $2 K (100 \text{ km})^{-1}$ (b) as in (a) but at 500 hPa, (c) as in (a) but from the GFS analysis valid at 0600 UTC 20 November 2008, and (d) as in (a) but from the GFS analysis at 0600 UTC 20 November 2008 and at 500 hPa. (e) Sea level isobars (solid), 950 hPa θ_e (dashed) and 950 hPa horizontal frontogenesis (shaded). Isobars labeled in hPa and contoured every 5 hPa, 950 hPa θ_e labeled in K and contoured every 4 K, and shading indicating 950 hPa horizontal frontogenesis exceeding $5 K (100 \text{ km})^{-1} (3 \text{ h})^{-1}$.



half wavelength between the trough and ridge shortened during the intervening 12 hours (Figure 3.2c). Within the southwesterly flow, the lower stratospheric front intensified, reaching a $|\nabla\theta|$ exceeding $9 \text{ K (100 km)}^{-1}$ south of Newfoundland. Directly to the east of the lower stratospheric front was a linearly oriented cold pool, with the lowest potential temperature ($\sim 330 \text{ K}$) flanking the maximum potential temperature gradient. At 500 hPa, the southwesterly flow was characterized by a broad region of baroclinicity that maintained the two separate upper tropospheric baroclinic features highlighted at the previous time (Figure 3.2d). In the vicinity of the lower stratospheric front, the upper tropospheric $|\nabla\theta|$ had weakened to a maximum of $5 \text{ K (100 km)}^{-1}$ in the region south of Newfoundland (Figure 3.2d). At this time, the lower stratospheric front was the more coherent and intense of the two frontal zones embedded within this southwesterly flow ULJF.

In the lower troposphere at this time, a sea level pressure (SLP) minimum ($\sim 985 \text{ hPa}$) was located over the Gulf of St. Lawrence (Figure 3.2e). The warm front that extended to the northeast of this SLP minimum was denoted at 950 hPa by an enhanced equivalent potential temperature (θ_e) gradient and a region of horizontal frontogenesis. Slightly east and extending south of the minimum in SLP, a second region of 950 hPa frontogenesis characterized the surface cold front. The southerly flow in the warm sector of this surface cyclone advected air with $\theta_e > 328 \text{ K}$ into the vicinity of the cold front where it was processed by the frontal circulation. At this time, a large section of this active cold front was positioned east of and parallel to the location of the 200 hPa lower stratospheric front.

b. Case 2: 8 December 2008

At 0000 UTC 8 December 2008 a broad trough at 200 hPa, centered over the northeast coast of North America, was characterized by a region of enhanced lower stratospheric baroclinicity extending from the base of the trough into the downstream southwesterly flow (Figure 3.3a). Within this baroclinicity, the maximum lower stratospheric $|\nabla\theta|$ was $7 \text{ K (100 km)}^{-1}$ east of Nova Scotia. This lower stratospheric front separated higher potential temperatures ($\sim 360 \text{ K}$) within the trough from lower potential temperatures ($\sim 324 \text{ K}$) in the broad ridge downstream. At 500 hPa, the upper troposphere was characterized by a trough with a notably sharper curvature than its 200 hPa counterpart (Figure 3.3b). Embedded within the flow through the base of the trough and extending into the downstream southwesterly flow was a broad region of baroclinicity. Within this broad baroclinic zone were two regions of enhanced potential temperature gradient. The first ($|\nabla\theta| \sim 4\text{-}5 \text{ K (100 km)}^{-1}$) in the vicinity of the location of the lower stratospheric front and the other ($|\nabla\theta| \sim 6 \text{ K (100 km)}^{-1}$) positioned within the base of the trough and to the cold side of the broader baroclinicity.

By 1200 UTC 8 December, the 200 hPa trough took on a more negative tilt as the downstream ridge amplified and the potential temperature within the peak of the ridge decreased to $\sim 321 \text{ K}$ just south of Greenland (Figure 3.3c). The robust portions of the lower stratospheric front within the southwesterly flow intensified, as $|\nabla\theta|$ increased to greater than $8 \text{ K (100 km)}^{-1}$. By this time, the lower stratospheric front had also expanded in the north-south direction, stretching from 40°N to 60°N roughly along 55°W . At 500 hPa, in the region south of Newfoundland, an upper tropospheric front ($|\nabla\theta| \sim 6 \text{ K (100 km)}^{-1}$) extended from the base

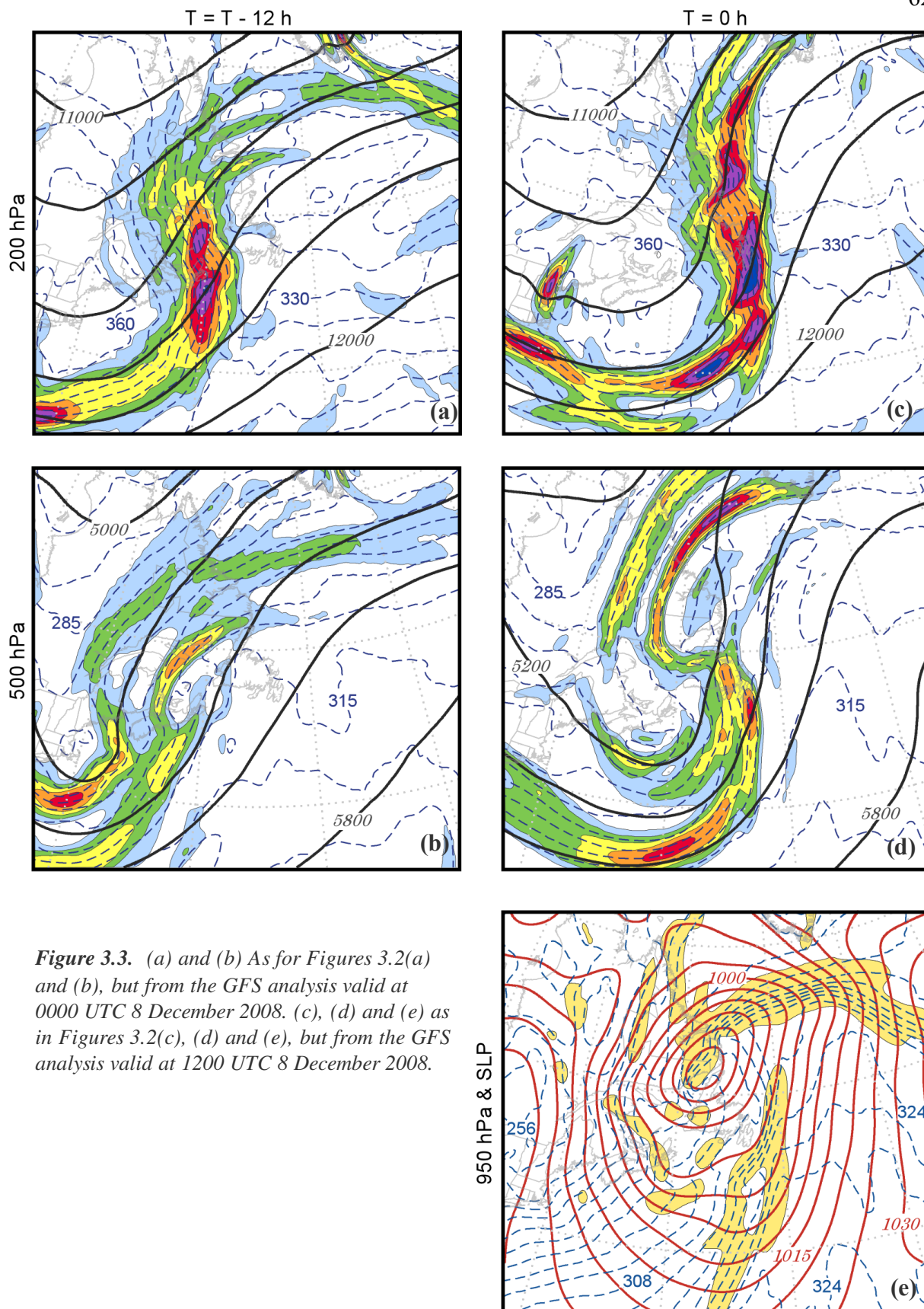


Figure 3.3. (a) and (b) As for Figures 3.2(a) and (b), but from the GFS analysis valid at 0000 UTC 8 December 2008. (c), (d) and (e) as in Figures 3.2(c), (d) and (e), but from the GFS analysis valid at 1200 UTC 8 December 2008.

of the trough northeastward (Figure 3.3d). North of the Gulf of St. Lawrence a second upper tropospheric front extended northeastward to the southern tip of Greenland.

At the surface, a deep cyclone (~ 975 hPa) was centered over eastern Quebec at 1200 UTC 8 December (Figure 3.3e). A pronounced frontogenetic region along the attendant surface warm front extended from the cyclone center to the northeast. The cold front and associated frontogenesis were located to the south and east of the SLP minimum. Though at 500 hPa the large scale upper tropospheric thermal field was characteristic of that associated with an occluding cyclone (see Figure 3.3d), the overall surface frontal structure associated with this cyclone was reminiscent of the T-bone frontal structure presented in the cyclone model of Shapiro and Keyser (1990). East of the surface cold front, moisture laden air characterized by $\theta_e \sim 320$ K, was advected into the region where it was subsequently ingested by the surface frontal circulation. As in *Case 1*, this region of active lower tropospheric frontogenesis was parallel to and east of the lower stratospheric front.

c. Case 3: 7 January 2009

Southwesterly flow at 200 hPa characterized the eastern half of the United States at 0600 UTC 7 January 2009 (Figure 3.4a). This flow, downstream of a broad trough centered over the central Plains and upstream of the axis of a weak ridge, was characterized by a notable lower stratospheric front with a maximum $|\nabla\theta|$ of $8 \text{ K (100 km)}^{-1}$. The lower stratospheric front represented a region of enhanced baroclinicity between the higher potential temperatures (~ 363 K) of the lower stratosphere near the base of the trough and the large region of lower

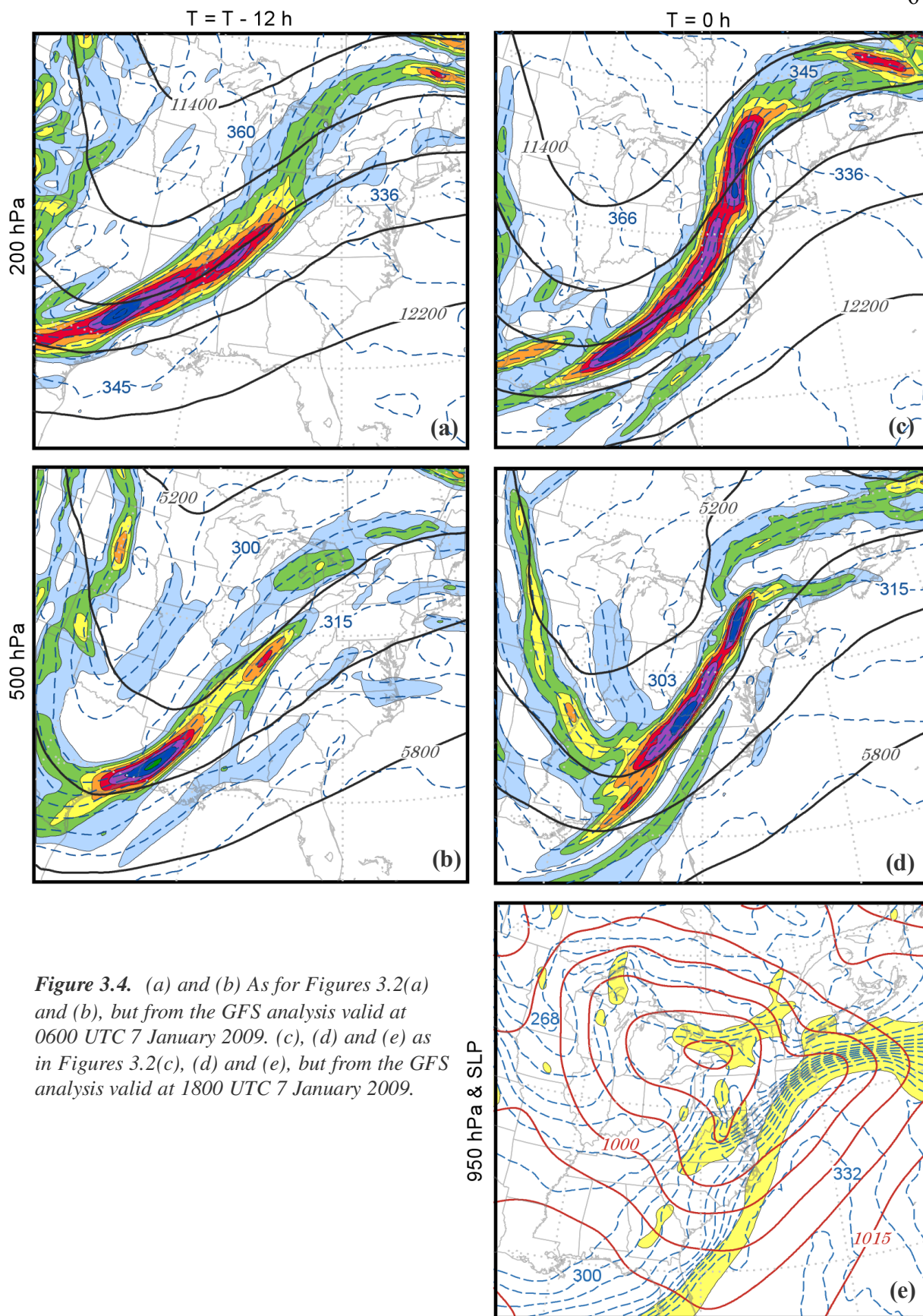


Figure 3.4. (a) and (b) As for Figures 3.2(a) and (b), but from the GFS analysis valid at 0600 UTC 7 January 2009. (c), (d) and (e) as in Figures 3.2(c), (d) and (e), but from the GFS analysis valid at 1800 UTC 7 January 2009.

potential temperatures (~ 336 K) of the upper troposphere located within the downstream ridge. At 500 hPa the upper tropospheric front was also characterized by a $|\nabla\theta|$ of $8 \text{ K (100 km)}^{-1}$ and extended from the base of the trough into the southwesterly flow (Figure 3.4b).

By 1800 UTC 7 January, the curvature in the downstream ridge increased as the half wavelength between the ridge and trough contracted in the intervening 12 hours (Figure 3.4c). Embedded within this ridge-trough couplet, the southwesterly flow lower stratospheric front intensified and elongated, as the region characterized by a $|\nabla\theta|$ of $8 \text{ K (100 km)}^{-1}$ expanded, stretching from the Gulf Coast states to Quebec. At 500 hPa, the upper tropospheric front also intensified, with the area of $|\nabla\theta| > 7 \text{ K (100 km)}^{-1}$ encompassing a more substantial geographic area, roughly located along the Appalachian Mountains (Figure 3.4d). To the southeast of this intense upper tropospheric front, a weaker region of baroclinicity stretched into the Gulf of Mexico. Though both of the concomitant frontal structures within the ULJF had $|\nabla\theta| > 8 \text{ K (100 km)}^{-1}$, the lower stratospheric front was the more spatially substantial of the two frontal structures at this time.

Also at 1800 UTC 7 January, a SLP minimum (~ 985 hPa) was located over southern Ontario (Figure 3.4e). East of, and removed from, this cyclone center was a southwest to northeast oriented region of frontogenesis. This frontogenetically active baroclinic zone consisted of both a warm front off of the New England coast and a cold front off of the southeast coast of the United States. The highest values of 950 hPa θ_e in the domain ($\theta_e > 328$ K) were located in the warm sector and in the vicinity of the frontogenetic forcing for ascent associated with the cold front. This cold front was located directly below the cold side of the

lower stratospheric front and nearly co-located with narrow band of lower potential temperatures at 200 hPa.

d. Case 4: 4 March 2009

At 0600 UTC 4 March 2009 a high amplitude flow pattern was evident over the northwest Atlantic consisting of a 200 hPa trough axis just off the east coast of North America and an associate downstream ridge (Figure 3.5a). Within the southwesterly flow characterizing this ridge-trough couplet, a lower stratospheric front with a maximum $|\nabla\theta|$ of $5 \text{ K (100 km)}^{-1}$ stretched from roughly 30°N to north of 55°N roughly centered on Nova Scotia. At 500 hPa, the baroclinicity in the southwesterly flow was less coherently organized than at 200 hPa, with regions of enhanced $|\nabla\theta|$ found in three distinct locations (Figure 3.5b). The eastern most of these was a narrow strip of enhanced baroclinicity ($|\nabla\theta| > 8 \text{ K (100 km)}^{-1}$) slightly east of the location of the lower stratospheric front. The second was a larger and wider region of weaker baroclinicity ($|\nabla\theta|$ of $5 \text{ K (100 km)}^{-1}$) that extended northeastward directly downstream of a shortwave trough which was embedded within the larger Rossby wave. The third region of baroclinicity ($|\nabla\theta|$ of $6 \text{ K (100 km)}^{-1}$) was found within the base of a trough located in eastern Quebec.

By 1800 UTC 4 March, the half wavelength between the ridge-trough couplet decreased (Figure 3.5c). Within the southwesterly flow that characterized the couplet, the intensity of the lower stratospheric front increased, having a $|\nabla\theta|$ of $8 \text{ K (100 km)}^{-1}$ just south of Newfoundland. This narrow lower stratospheric frontal feature was oriented nearly

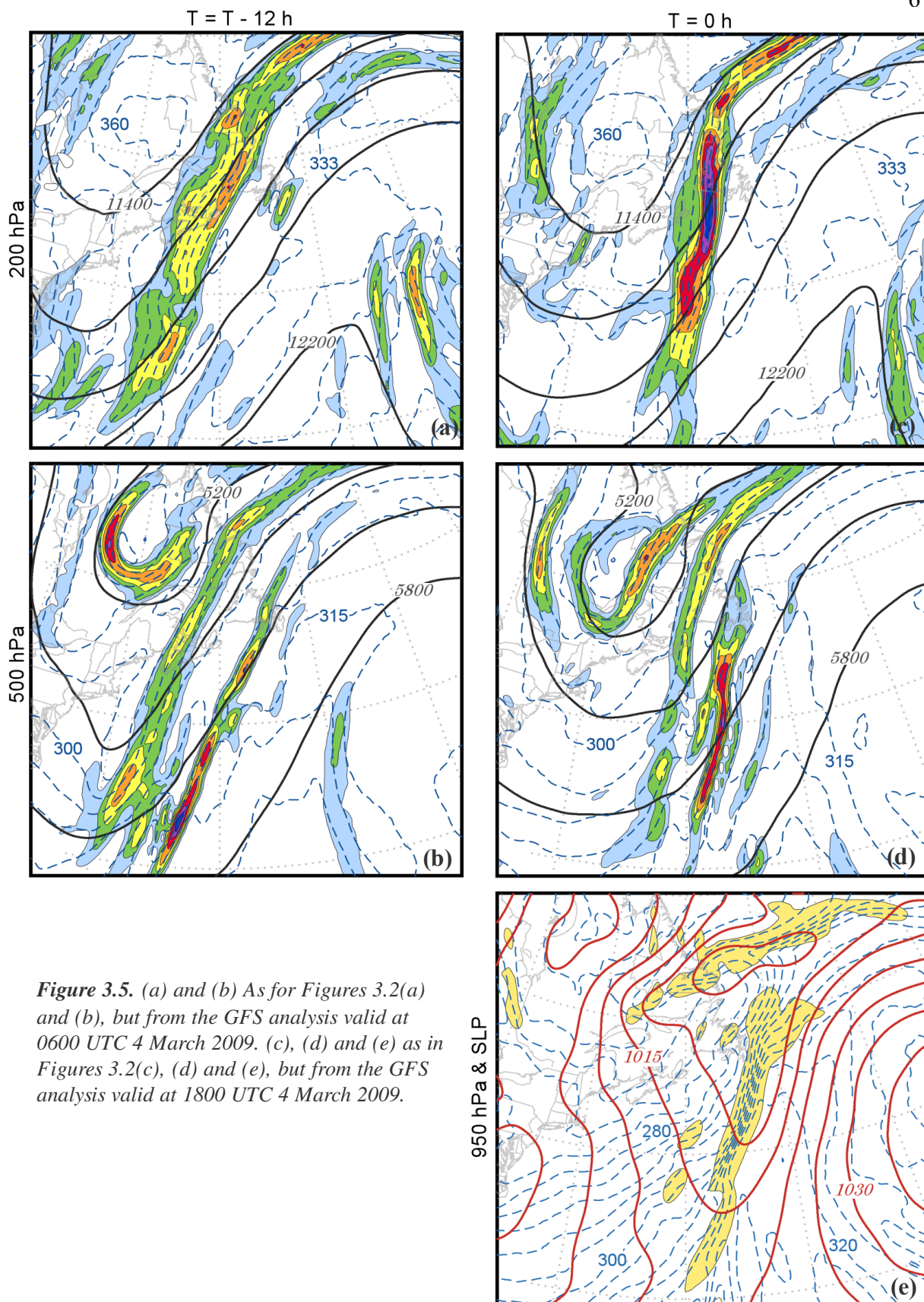


Figure 3.5. (a) and (b) As for Figures 3.2(a) and (b), but from the GFS analysis valid at 0600 UTC 4 March 2009. (c), (d) and (e) as in Figures 3.2(c), (d) and (e), but from the GFS analysis valid at 1800 UTC 4 March 2009.

meridionally along 60°W within the southwesterly flow. At 500 hPa, the three regions of upper tropospheric baroclinicity highlighted at the previous time were still discernible (Figure 3.5d). The most intense ($6 \text{ K (100 km)}^{-1}$) of those three regions was directly east of the location of the lower stratospheric front. Though both the upper tropospheric and lower stratospheric fronts were notable features, the lower stratospheric front was the more coherently organized of the two frontal features within this ULJF.

Also at 1800 UTC 4 March, an elongated minimum in SLP ($\sim 1005 \text{ hPa}$) was positioned just east of Labrador (Figure 3.5e). As in *Case 2*, this weak cyclone had a baroclinic structure reminiscent of the T-bone frontal model described by Shapiro and Keyser (1990). In the vicinity of the SLP minimum, the warm front and thermal ridge were characterized by a region of frontogenesis. South of the warm front, a cold front was associated with the largest gradients of θ_e in the domain and a region of enhanced 950 hPa frontogenesis. Immediately east of the cold front and in a region favorable for frontogenetic ascent, the warm sector was characterized by air with $\theta_e \sim 320 \text{ K}$. As in all the cases presented in this section, the frontogenetically active cold front was located slightly east of and parallel to the developing lower stratospheric front.

3.3. Analysis I: Overview of common dynamical processes

With the focus on connecting the lower tropospheric and lower stratospheric frontogenesis processes, this section highlights the common dynamical mechanisms that promoted the development of each of the robust lower stratospheric fronts presented in Section

2. The final time period ($t = 0$ h) highlighted in the Section 2 overview will be the focus of this analysis.

a. Diabatic Stability Tendency

In the Chapter 2 analysis, the southwesterly flow lower stratospheric frontogenesis process was dependent upon the magnitude of ascent in the cold upper troposphere, east of the lower stratospheric baroclinicity. Ascent in this region is a manifestation of the interplay between adjacent lower stratospheric forcing for ascent and the local upper tropospheric stratification. The subsequent analysis highlights this linkage in the lower stratospheric frontogenesis process by quantifying the impact of latent heat release on the upper tropospheric thermal and static stability fields by making use of the static stability tendency equation, which can be written as

$$\frac{d}{dt} \left(-\frac{\partial \theta}{\partial p} \right) = \left(\frac{\partial}{\partial t} + \mathbf{V} \cdot \nabla + \omega \frac{\partial}{\partial p} \right) \left(-\frac{\partial \theta}{\partial p} \right)$$

or

$$\frac{d}{dt} \left(-\frac{\partial \theta}{\partial p} \right) = -\frac{\partial}{\partial p} \left(\frac{d\theta}{dt} \right) - \frac{\partial \mathbf{V}}{\partial p} \cdot \nabla \theta - \frac{\partial \omega}{\partial p} \frac{\partial \theta}{\partial p}. \quad (1)$$

For each case, the rate of latent heating was obtained following the method employed by Emanuel et al. (1987), and is calculated as

$$\frac{d\theta}{dt} = \dot{\theta} = \omega \left(\frac{\partial \theta}{\partial p} - \frac{\gamma_m}{\gamma_d} \frac{\theta}{\theta_e} \frac{\partial \theta_e}{\partial p} \right), \quad (2)$$

where $\dot{\theta}$ corresponds to latent heat release, ω is the vertical velocity (in Pa s^{-1}), and γ_d and γ_m

are the dry and moist adiabatic lapse rates, respectively. By substituting both (2) and the fact that the thermal wind can not advect temperature, (1) becomes

$$\frac{d}{dt} \left(-\frac{\partial \theta}{\partial p} \right) = \underbrace{-\frac{\partial \dot{\theta}}{\partial p}}_a - \underbrace{\frac{\partial V_{ag}}{\partial p} \cdot \nabla \theta}_b - \underbrace{\frac{\partial \omega}{\partial p} \frac{\partial \theta}{\partial p}}_c, \quad (3)$$

where V_{ag} is the ageostrophic component of the horizontal wind. The static stability tendency equation (3) can be separated into three terms: *term a*, the diabatic static stability tendency; *term b*, the contribution from the tilting of horizontal temperature gradients into vertical temperature gradients (e.g., static stability) by the ageostrophic vertical shear; and *term c*, the contribution from the vertical stretching of isentropic layers. Together *terms b* and *c* represent the total contribution from the three-dimensional ageostrophic wind.

Focusing on the notion that lower tropospheric convective ascent can have a diabatic impact on the strength of the ascent in the vicinity of an ULJF, this section provides only an analysis of the diabatic contributions represented by *term a* in (3). At the $t = 0$ h time highlighted in each of these cases, *terms b* and *c* are roughly an order of magnitude smaller than *term a* and together contribute only a small percentage to the overall static stability tendency field. Of course, in the vicinity of a straight ULJF, the primary geostrophic flow provides forcing for secondary ageostrophic Sawyer-Eliassen circulations. When applying (3) in the vicinity of relatively straight ULJFs, such as those presented in this analysis, the contribution from *terms b* and *c* are directly related to the secondary Sawyer-Eliassen vertical circulation. The nature of contributions to the static stability tendency that arise from the total forced secondary circulations in (3) (*terms b* and *c*) is left to future work.

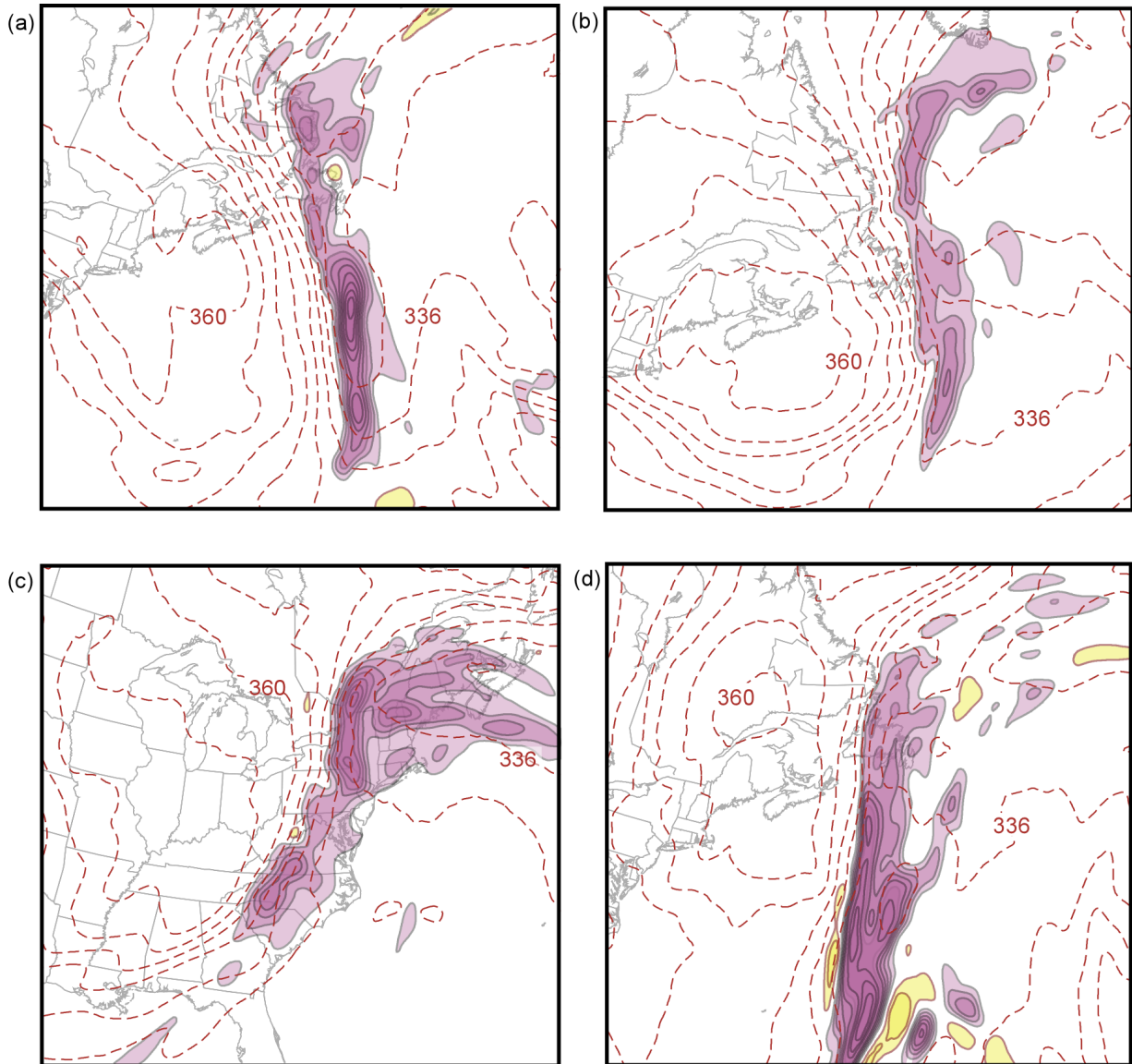


Figure 3.6. The 200 hPa potential temperature contoured every 4 K (dashed) and the diabatic static stability tendency at 250 hPa contoured every 1 K day⁻¹ with purple (yellow) shading corresponding to a decrease (increase) in static stability. From the GFS analysis valid at (a) 0600 UTC 20 November 2008, (b) 1200 UTC 8 December 2008, (c) 1800 UTC 7 January 2009, and (d) 1800 UTC 4 March 2009.

In all four cases presented in Section 2, the latent heat released in association with the lower tropospheric ascent allowed for a restructuring of the upper tropospheric static stability. Allowing for 10 minutes of latent heating from the convection in each case, Figure 3.6 shows

the distribution of the diabatic static stability tendency, *term a* in (3), at the 250 hPa level relative to the location of lower stratospheric front (isentropes) at 200 hPa for each of the four cases. Each of the cases shows similar impacts from the diabatic processes associated with the tropospheric ascent. The latent heating weakened the upper tropospheric static stability in a linearly oriented band immediately to the cold (upper tropospheric) side of the lower stratospheric front. The location and orientation of the reduction in static stability was such that, in each case it was located between the leading edge of both the lower stratospheric front and the lower tropospheric cold front. In the presence of forcing for vertical motion within the lower stratospheric frontal region, such a configuration of the static stability tendency would intensify the response to that forcing, particularly, ascent in the region on the cold side of the lower stratospheric front.

b. Lower stratospheric QG forcing, ascent, and tilting frontogenesis

Following the method employed in Chapter 2, the analysis uses the primary geostrophic forcing, in the form of geostrophic temperature advection in cyclonic shear, to diagnose regions of vertical motion in the vicinity of the lower stratospheric front. The tilting contribution to frontogenesis (F_{tilt}) at 200 hPa is calculated using the full model vertical motion from the GFS analyses, where

$$F_{tilt} = -\frac{1}{|\nabla\theta|} \left(\frac{\partial\theta}{\partial p} \left(\frac{\partial\omega}{\partial x} \frac{\partial\theta}{\partial x} + \frac{\partial\omega}{\partial y} \frac{\partial\theta}{\partial y} \right) \right). \quad (4)$$

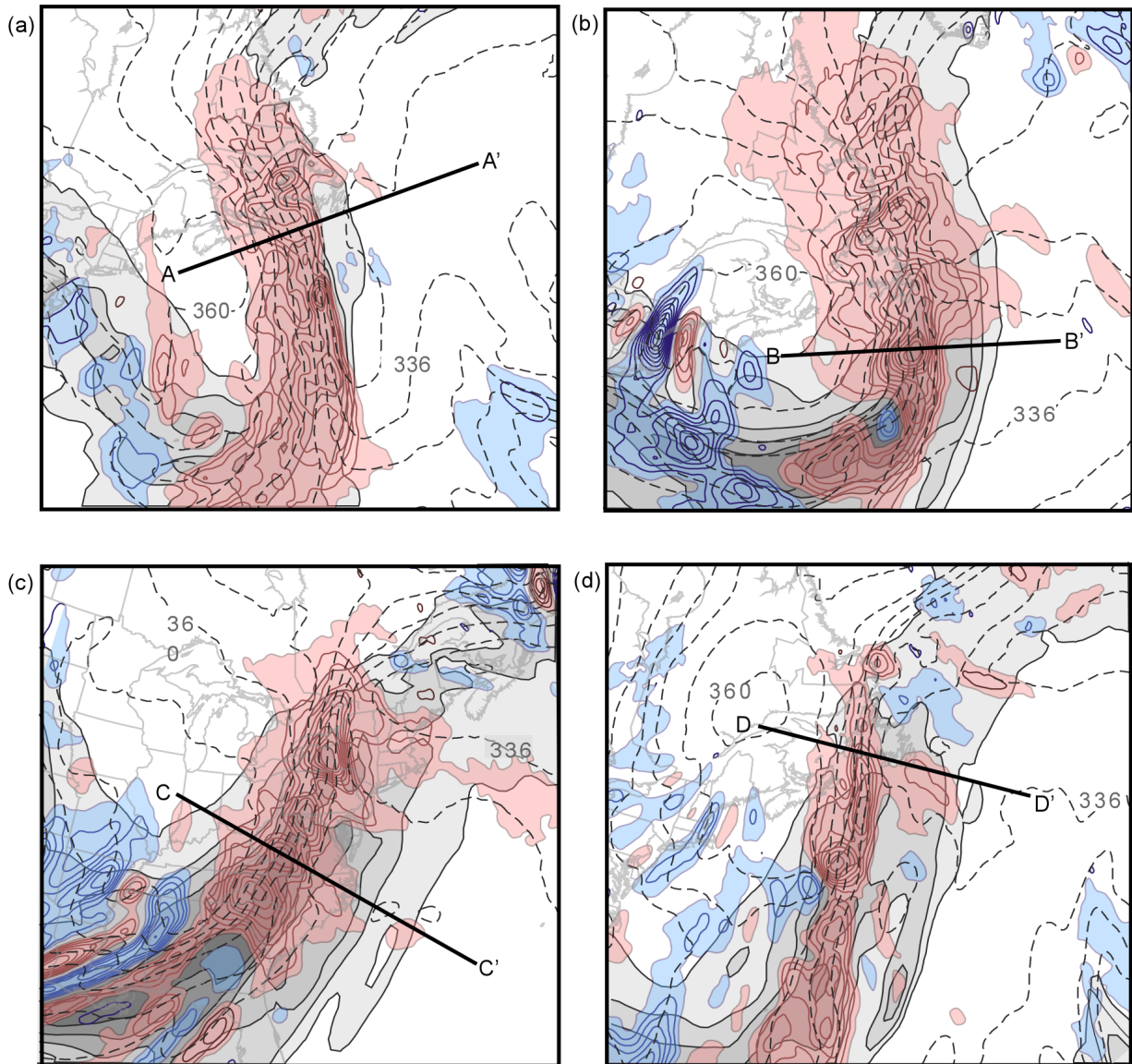


Figure 3.7. The 200 hPa potential temperature contoured every 4 K (dashed), the geostrophic isotachs every 10 m s^{-1} beginning at 40 m s^{-1} (solid), and the geostrophic temperature advection in pink (blue) shading above $3 \times 10^{-4} \text{ K s}^{-1}$ (below $-3 \times 10^{-4} \text{ K s}^{-1}$) and contoured every $3 \times 10^{-4} \text{ K s}^{-1}$. From the GFS analysis valid at (a) 0600 UTC 20 November 2008, (b) 1200 UTC 8 December 2008, (c) 1800 UTC 7 January 2009, and (d) 1800 UTC 4 March 2009.

The 200 hPa geostrophic temperature advection, at $t = 0$ h, for each of the cases is shown in Figure 3.7. In all four cases, a large elongated region of geostrophic warm air advection characterized the cyclonic shear side of the southwesterly flow. As conceptually illustrated by Figure 3.1b, geostrophic warm air advection in the lower stratospheric cyclonic shear promotes QG forced ascent through the local jet core, in the cold upper troposphere. While the geostrophic warm air advection varied in magnitude along the jet in each case, a maximum greater than $\sim 27 \times 10^{-4} \text{ K s}^{-1}$ was common at the 200 hPa level in each of the cases. In addition, the cold side of each of the regions of QG forcing was adjacent to the diabatic reduction in static stability (shown in Figure 3.6). With the QG forcing present in each case proximate to the regions of reduced static stability, a strong response in the form of robust ascent on the cold side of the lower stratospheric front can be expected.

Coincident with the lower stratospheric QG forcing (Figure 3.7) and the 250 hPa diabatic static stability reduction (Figure 3.6), the 200 hPa full model vertical motions reveal ascent oriented roughly linearly along the cold side of each of the lower stratospheric fronts (Figure 3.8). The strongest upward motion in each case was located directly to the east of the QG forcing, promoting adiabatic cooling on the cold side of the lower stratospheric front. The cooling response was particularly evident in *Case 1*, where at the 200 hPa level a narrow band of cold potential temperature was located in the regions of the maximum ascent along the lower stratospheric front (Figure 3.8a). Responding to the diabatic weakening of the static stability in the upper troposphere, the strong QG forced upward vertical motion led to a period of notable lower stratospheric tilting frontogenesis in each case (Figure 3.9).

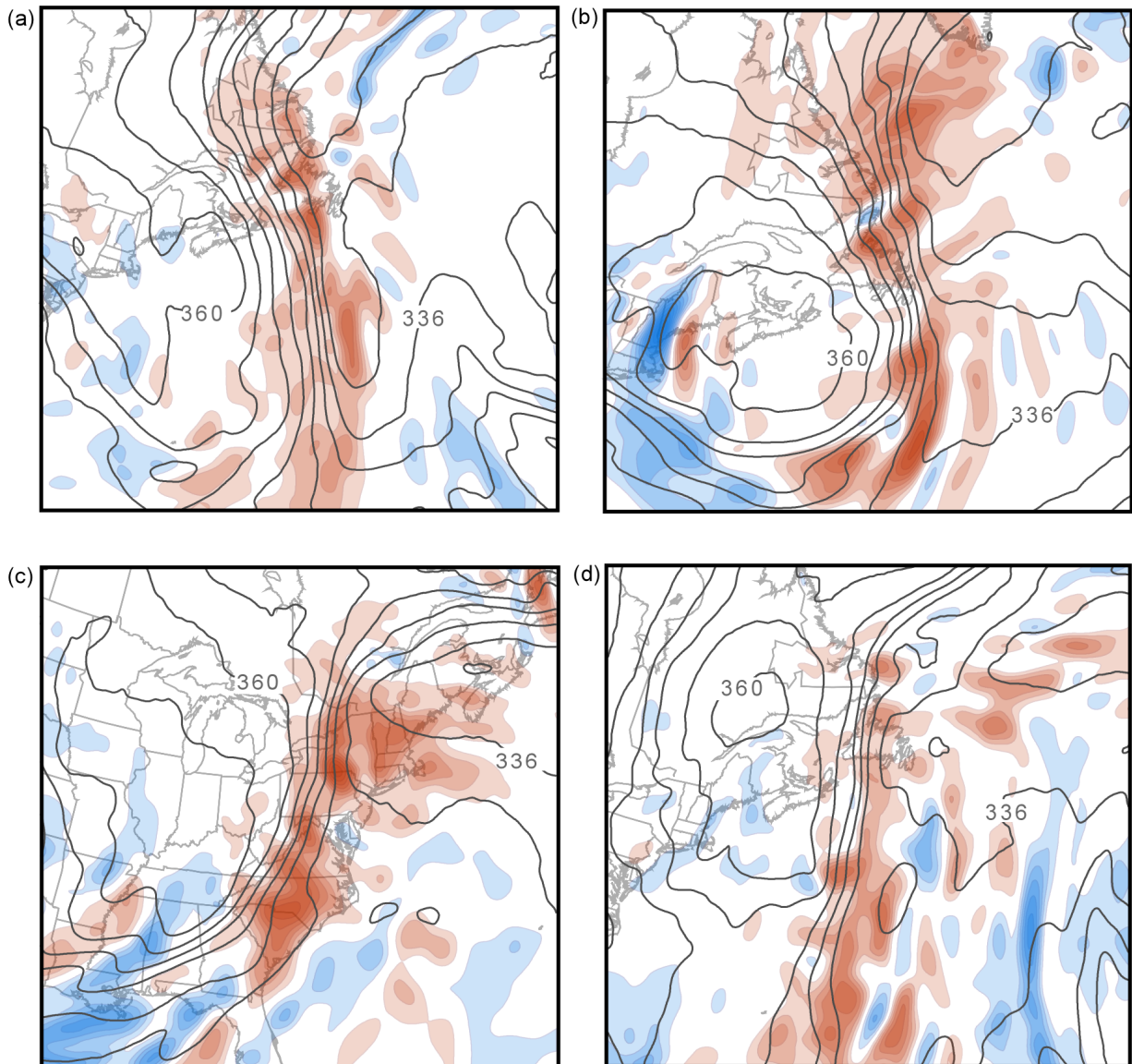


Figure 3.8. The 200 hPa potential temperature contoured every 4 K (solid) and vertical motion (shaded) from the model analysis every 2 cm s^{-1} beginning at 2 (-2) cm s^{-1} in red (blue). From the GFS analysis valid at (a) 0600 UTC 20 November 2008, (b) 1200 UTC 8 December 2008, (c) 1800 UTC 7 January 2009, and (d) 1800 UTC 4 March 2009.

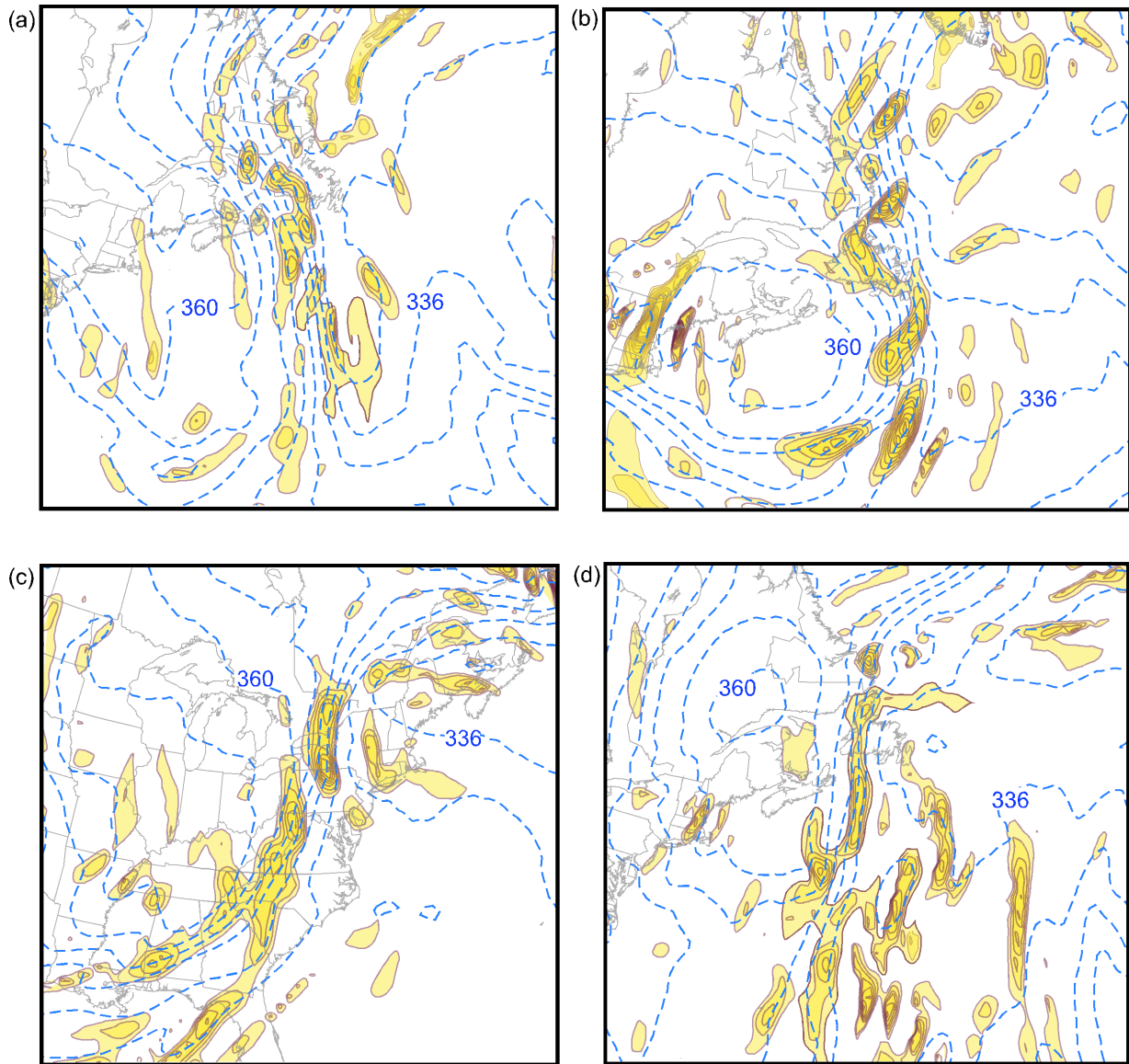


Figure 3.9. 200 hPa potential temperature contoured every 4 K (dashed) and positive tilting frontogenesis shaded and contoured every $4 \times 10^{-9} \text{ K m}^{-1} \text{ s}^{-1}$. From the GFS analysis valid at (a) 0600 UTC 20 November 2008, (b) 1200 UTC 8 December 2008, (c) 1800 UTC 7 January 2009, and (d) 1800 UTC 4 March 2009.

3.4. Analysis II: Vertical cross sections

This section highlights the lower tropospheric and lower stratospheric coupling through the analysis of a vertical cross section taken through the ULJF system in each of the four cases. The position of each cross section was selected in order to fully illustrate the separate, yet coupled, southwesterly flow lower stratospheric and lower tropospheric processes at the $t = 0$ h period in each case.

a. Case I

A cross section taken for *Case I* along the line A-A' in Figure 3.7a is shown in Figure 3.10. Below the level of maximum winds, the broad baroclinicity in the upper troposphere was characterized by weak geostrophic cold advection and associated subsidence. East of the location of the surface front was a plume of upright convective ascent (with a maximum of $> 20 \text{ cm s}^{-1}$) that reached from the surface to roughly the 300 hPa level, just above the 324 K isentrope (roughly the value of the surface θ_e). The lower stratospheric cyclonic shear was characterized by a region of geostrophic warm air advection ($\sim 12 \times 10^{-4} \text{ K s}^{-1}$). Within the weak static stability on the cold side of the lower stratospheric front, but to the west of the surface based ascent, was a second plume of ascent, with a maximum in upward vertical motion greater than 15 cm s^{-1} centered at 250 hPa. This second plume of ascent was a response to the Sawyer-Eliassen forcing associated with the lower stratospheric front.

As in the southwesterly flow case presented in Part I, the near-tropopause upper tropospheric ascent plume (Figure 3.10) acted to increase the slope of not only the isentropes,

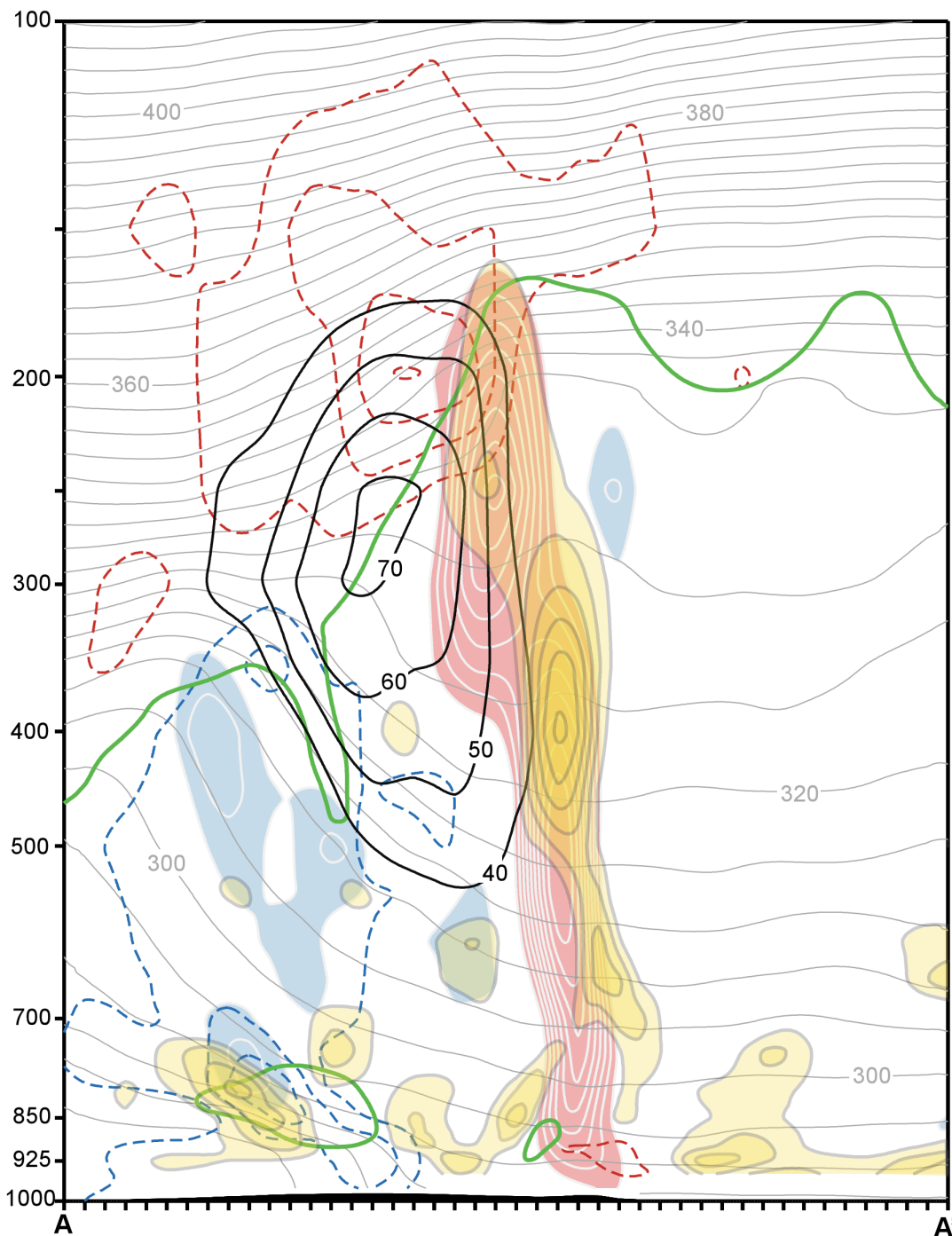


Figure 3.10. Vertical cross section along the line A-A' in Figure 3.7(a) of potential temperature, geostrophic isotachs, geostrophic temperature advection, vertical motions and diabatic stability tendency from the GFS analysis valid at 0600 UTC 20 November 2008. Potential temperature (thin gray lines) is labeled in K and contoured every 4 K. Geostrophic isotachs (thick black lines) labeled in m s^{-1} and contoured every 10 m s^{-1} beginning at 40 m s^{-1} . Vertical motion, with upward (downward) motion in the pink (blue) shading, is contoured in every 2 cm s^{-1} beginning at 4 (-4) cm s^{-1} then contoured every 5 cm s^{-1} after 20 (-20) cm s^{-1} . Geostrophic temperature advection (dashed lines) contoured every $3 \times 10^{-4} \text{ K s}^{-1}$ beginning at 3 (-3) $\times 10^{-4} \text{ K s}^{-1}$ in the red (blue). Negative diabatic static stability tendency contoured and shaded (yellow) in a every 1 K day^{-1} and beginning at -1 K day^{-1} .

but also the tropopause, above the jet core (positive tilting frontogenesis). The diabatic static stability tendency associated with the distribution of vertical motion, shows a reduction in static stability directly above the surface based ascent plume (Figure 3.10). However, the region of reduced stability associated with latent heat release extends into the region directly to the cold side of the lower stratospheric front. The stability within this upper tropospheric region is important as it plays a role in determining the magnitude of the ascent responding to the QG forcing associated with the lower stratospheric front. Thus, the distribution of latent heating in this case likely contributed to the development of robust ascent, responding to lower stratospheric QG forcing, by decreasing the stability in the near-tropopause upper troposphere. The strong ascent, located on the cold side of the lower stratospheric front, was well positioned to force a period of notable lower stratospheric frontogenesis via tilting.

b. Case 2

A cross section taken for *Case 2* along the line B-B' in Figure 3.7b is shown in Figure 3.11. Below the level of maximum winds, the troposphere was characterized by a region of weak geostrophic cold air advection. Immediately east of the location of the surface cold front, a plume of upright convection with a maximum in upward vertical motion greater than 30 cm s^{-1} , reached from the surface to 250 hPa, the vicinity of the 328 K isentrope (approximately the θ_e at the surface). The lower stratospheric cyclonic shear was characterized by an intense region of geostrophic warm air advection ($> 33 \times 10^{-4} \text{ K s}^{-1}$). On the cold side of the lower stratospheric front and in the vicinity of the jet core, was a second plume of upward vertical

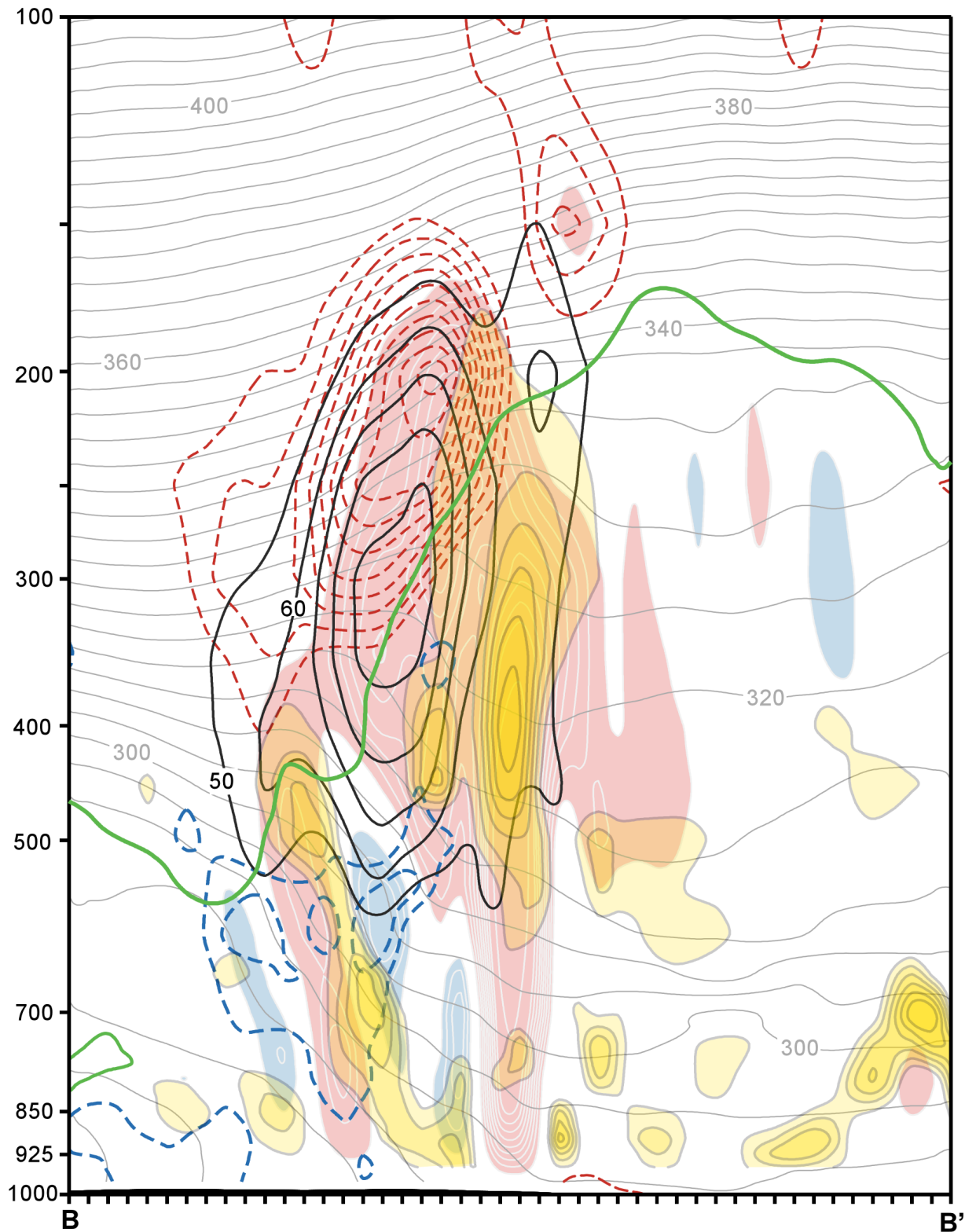


Figure 3.11. As for Figure 3.10, but from the GFS analysis valid at 1200 UTC 8 December 2008 and along the line B-B' in Figure 3.7(b).

motion (centered at ~ 250 hPa) with a maximum of ~ 15 cm s $^{-1}$. As in *Case 1*, these two plumes of ascent were associated with two separate forcing mechanisms, one in the form of lower tropospheric frontogenesis and the other in the form of lower stratosphere QG forcing. The diabatic static stability tendency plotted at this time illustrates that the reduction in the static stability above the surface based ascent plume extended into the vicinity of the tropopause level ascent plume. As the static stability in the near-tropopause upper troposphere was diabatically reduced, the strong lower stratospheric QG forcing was consequently able to produce robust ascent and was tied to a period of lower stratospheric frontogenesis.

c. Case 3

A cross section taken for *Case 3* along the line C-C' in Figure 3.7c is shown in Figure 3.12. Below the jet core, geostrophic cold air advection characterized a tropospheric deep cold front. Just east of the surface intersection of this cold front, a plume of ascent (15 cm s $^{-1}$) reached upward toward the 324 K isentrope at approximately the 500 hPa level. At upper levels, geostrophic warm air advection ($\sim 18 \times 10^{-4}$ K s $^{-1}$) in the lower stratospheric cyclonic shear was coincident with an ascent plume, centered at ~ 300 hPa, that extended from roughly the 320 K isentrope to the 360 K isentrope, a 250 hPa deep layer. This ascent plume, with a maximum of > 20 cm s $^{-1}$, was located to the cold side of the lower stratospheric front in a favorable configuration for frontogenetic tilting. Latent heating produced a reduction in the static stability immediately above the ascent associated with the surface front, which was also coincident with the lowest levels of the second plume of upward vertical motion. The elevated

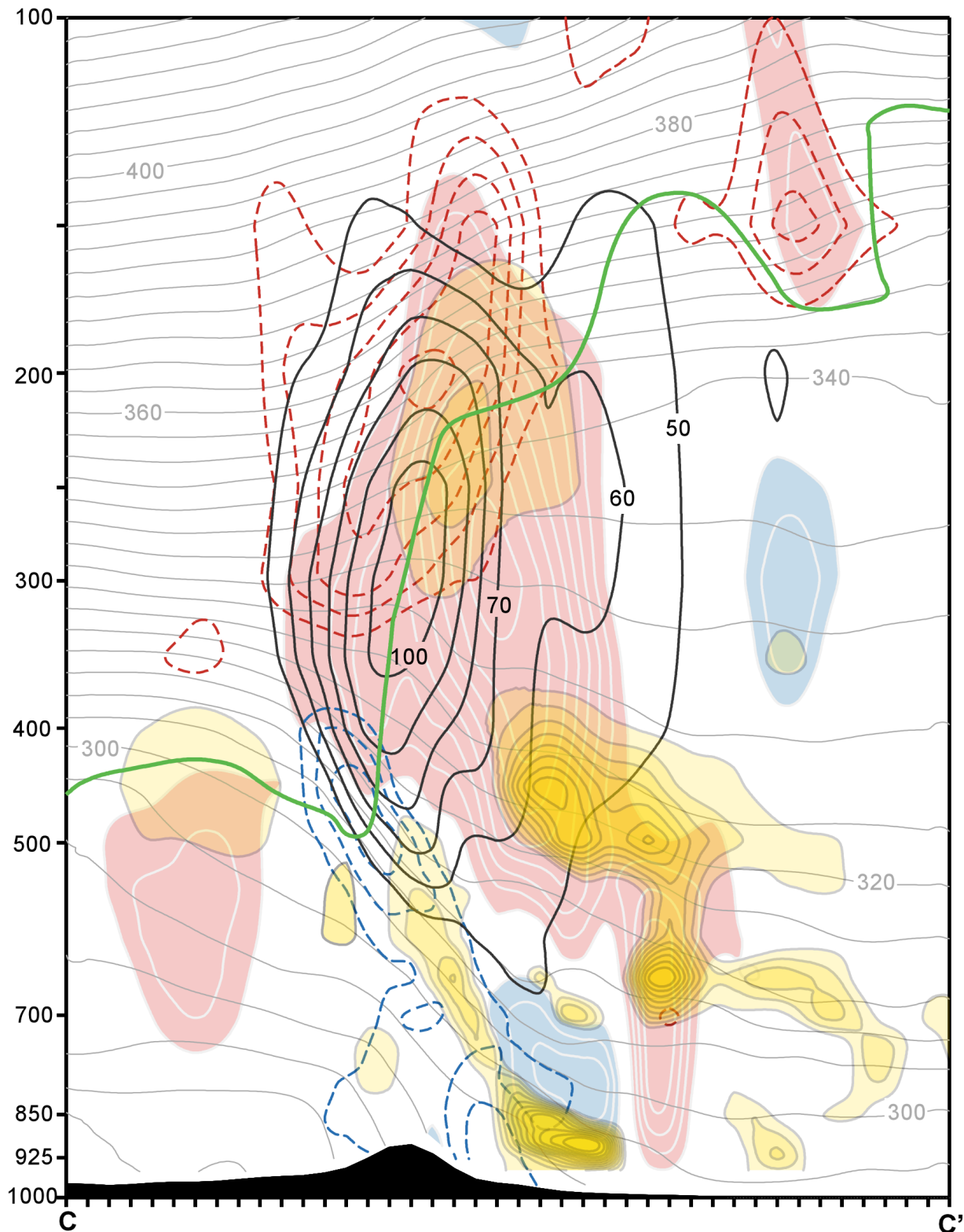


Figure 3.12. As for Figure 3.10, but from the GFS analysis valid at 1800 UTC 7 January 2009 and along the line C-C' in Figure 3.7(c).

ascent, drawing upon air from moist mid-troposphere, was associated with a diabatic reduction in stability maximized at roughly the 250 hPa level, on the cold side of the lower stratospheric front. Responding to the reduced static stability, the robust ascent in the cold upper troposphere was associated with a period of lower stratospheric tilting frontogenesis.

d. Case 4

A cross section taken for *Case 4* along the line D-D' in Figure 3.7d is shown in Figure 3.13. This cross section showed a double tropopause fold structure, in which the isentropes that defined the surface cold front were tied to the lower of the two folds, while the isentropes that defined upper tropospheric and lower stratospheric fronts were associated with more elevated of the two folds. The surface front was characterized by weak geostrophic cold advection in the lower troposphere. A frontogenetically forced upright plume of vertical motion east of the cold front reached from the surface to roughly the 400 hPa level, the vicinity of the 320 K isentrope. From roughly 450 hPa to 150 hPa and west of the surface based ascent plume was a second region of ascent with two maxima, one at the 350hPa level and the other at 250 hPa level. This second plume of upward motion, with its base in the mid-troposphere, reached into the region coincident with QG forcing in the form of geostrophic warm air advection in the lower stratospheric cyclonic shear (with a maximum of $\sim 15 \times 10^{-4} \text{ K s}^{-1}$).

Associated with these two plumes of ascent was a diabatic reduction in the static stability in the near-tropopause upper troposphere (Figure 3.13). Latent heating associated with lower level ascent was able to reduce the mid-tropospheric stability. Simultaneously, the

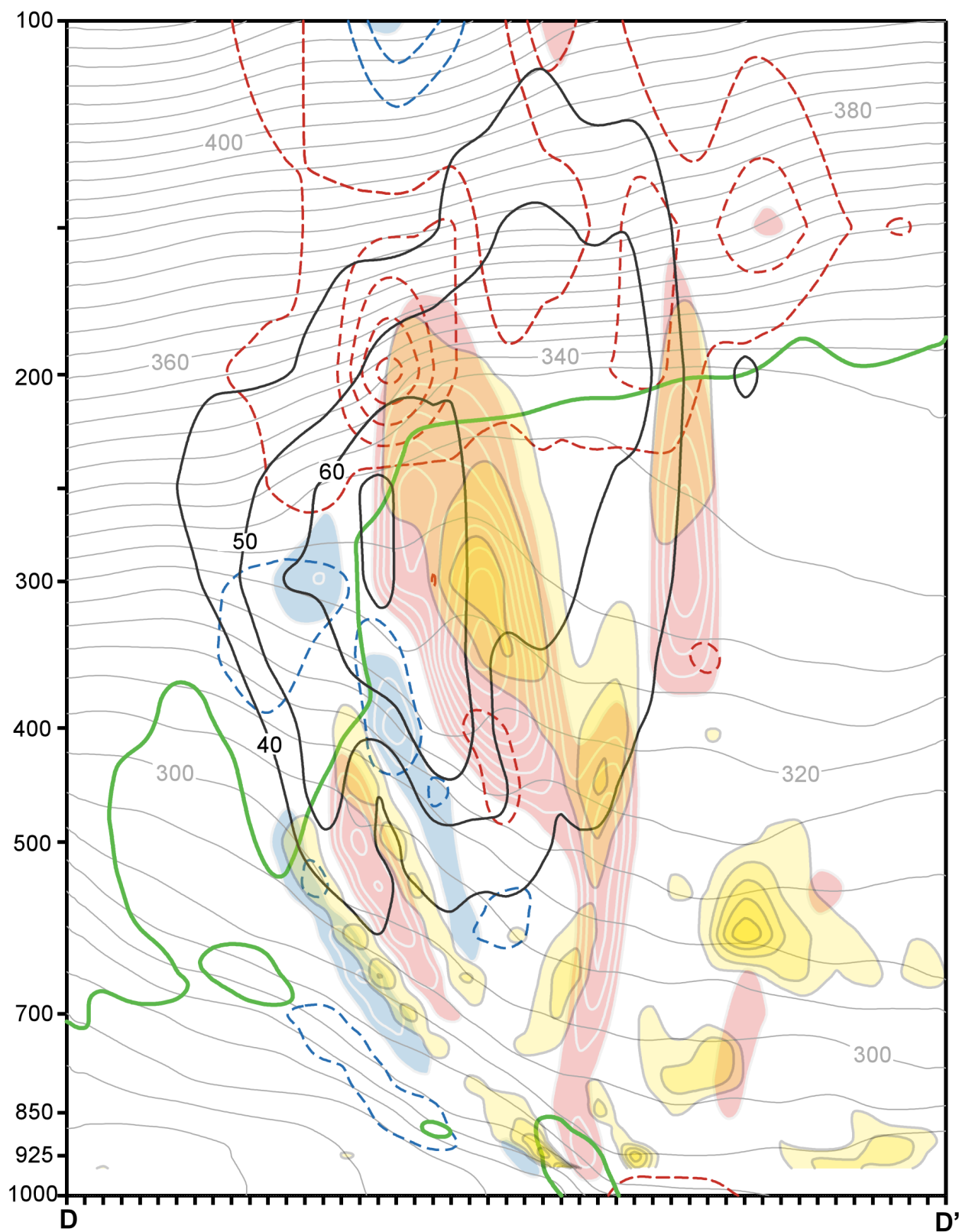


Figure 3.13. As for Figure 3.11, but from the GFS analysis valid at 1800 UTC 4 March 2009 and along the line D-D' in Figure 3.7(d).

latent heating within the elevated plume of ascent was associated with a distinct upper tropospheric region of diabatically reduced static stability (centered at 300 hPa). This reduction in stability was in sufficient proximity to the QG forcing for ascent in the lower stratosphere to likely enhance the response to that forcing and promote strong ascent in the upper troposphere that prompted a period of lower stratospheric frontogenesis.

3.5. Summary and Discussion

In an effort to investigate the connection between tropospheric convective ascent and the development of robust lower stratospheric fronts, four cases from the 2008-2009 winter were selected for diagnostic case study analysis. Though these four cases were selected based on the intensity of their lower stratospheric fronts ($|\nabla\theta| > 8 \text{ K (100 km)}^{-1}$), each case was also associated with lower tropospheric upright ascent forced by an active surface front. The accompanying surface front in each case was located roughly parallel to and east of the position of the lower stratospheric front, which was consistent with the results of the analysis of the southwesterly flow case presented in Section 4 of Chapter 2. By virtue of the near superposition of the surface and lower stratospheric fronts in the southwesterly flow cases, the analysis presented here illustrates that the diabatic impact of tropospheric convection (e.g., reduced upper tropospheric static stability) is consistently positioned so as to favor a robust response to lower stratospheric frontogenetic forcing for ascent on the cold side of the lower stratospheric frontal zone.

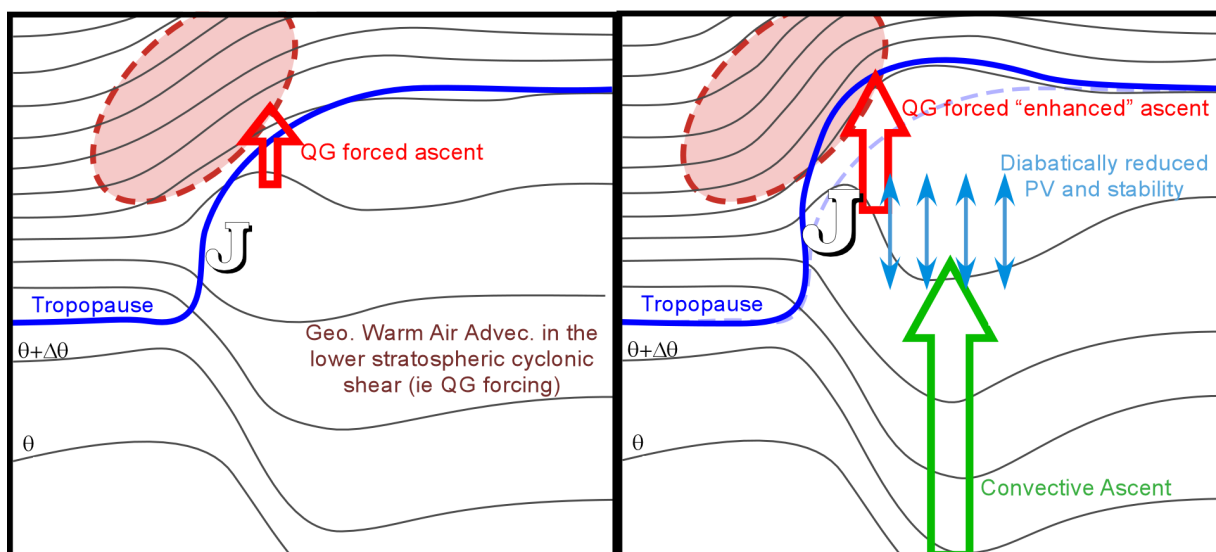


Figure 3.14. Conceptual model of the impact of convectively generated latent heat release on lower stratospheric frontal development as shown in idealized cross sections through jet-front systems (a) without convection and (b) with convection. (a) A dynamically active lower stratospheric front, characterized by geostrophic warm air advection in cyclonic shear (pink shading), forces ascent (red arrow) that can increase the slope of the isentropes (thin lines) and dynamic tropopause (blue line) above the jet core via frontogenetic tilting. (b) Convectively generated latent heat release reduces the stability in the near-tropopause upper troposphere and can enhance the ascent response to the lower stratospheric QG forcing (larger arrow) thereby intensifying the lower stratospheric tilting frontogenesis process, resulting in a steeply sloped tropopause and an intensified tropopause jet. See text for explanation.

This coupling between the lower tropospheric and lower stratospheric processes is conceptually illustrated in Figure 3.14 and summarized below. As convectively generated latent heat release associated with a surface frontal boundary reconfigures the potential temperature field (e.g., Emanuel et al. 1987) within the upper troposphere, the stability of the near-tropopause upper troposphere decreases. Such a distribution of the diabatic stability tendency directly influences the magnitude of the QG forced ascent on the cold side of the lower stratospheric front. The ascent that responds to the QG forcing, highlighted in each case, subsequently contributes to the intensification of a robust lower stratospheric front, and a

steeper tropopause above the jet core, via tilting frontogenesis.

The four cases analyzed in this paper illustrate several important synoptic-mesoscale dynamical links between tropospheric convection and lower stratospheric dynamics. The analysis suggests that: (i) the interaction of surface based convection and upper tropospheric static stability is likely able to influence the development of lower stratospheric fronts and substantially alter the structure of a midlatitude jet-front system by increasing the response to lower stratospheric QG forcing for ascent; (ii) an enhanced ascent maximum above the jet core can subsequently lead to an increase in the slope of not only the isentropes within the lower stratospheric front, but also the tropopause above the jet core, via tilting; and (iii) when latent heat release occurs in the vicinity of a ULJF with a dynamically active lower stratospheric front, the lower stratospheric frontal circulation may be able to enhance the mesoscale structure of the horizontal PV gradient (i.e., increase the tropopause slope) above the jet core.

The analysis presented here highlights the interactions between lower stratospheric frontal development and the reduction of static stability produced by in-situ moist convection along surface frontal zones. There are, of course, a variety of mechanisms whereby poorly stratified air may be delivered to the upper troposphere to similarly influence the lower stratospheric development. A particularly intriguing possibility for such delivery lies in the outflow from organized tropical convection, manifest either as tropical convective clusters, tropical plumes or tropical cyclones, which processes low PV, low static stability boundary layer air in convective updrafts and exhausts such air into the upper troposphere. If a pre-existing midlatitude jet becomes juxtaposed with such outflow, the convective outflow may be

linked to a period of lower stratospheric frontogenesis as well as changes in the slope of the tropopause above the jet core. Such changes, tied as they are to increases in lower stratospheric baroclinicity, must also be potentially energy generating and, thus, may provide a means by which energy released in the tropical convection might be stored for subsequent release downstream in space and time. A number of studies have recently highlighted a link between the convective tropical cyclone environment and associated changes in the structure of the midlatitude jet (e.g., Agustí-Panareda et al., 2004; Harr and Elsberry, 2000; Harr et al., 2000; Kitabatake, 2002, 2008; Klein et al., 2000, 2002). It is suggested that the analysis presented here provides insight into one of the mechanisms that may facilitate the observed tropical cyclone-extratropical jet interaction. Whether or not such interactions routinely manifest themselves in lower stratospheric frontal development is a topic for future inquiry.

Chapter 4

Future Research Directions

The results presented in Chapters 2 and 3 provide the fundamental groundwork for a variety of potentially fruitful research topics. This Chapter employs the concepts and results of Chapters 2 and 3 in an expanded description of future research directions. Section 4.1 provides an overview of three avenues of research that would benefit from the lower stratospheric front perspective presented in this dissertation, while Section 4.2 incorporates the concepts from the overview in a research proposal.

4.1. Overview of future research directions

The lower stratospheric frontal perspective presented in this dissertation would be beneficial to an exploration of a variety of atmospheric problems from observational, case study, and modeling approaches. Three topics relevant to current issues in atmospheric science will be elaborated upon in this section. The first of these topics (a) expands on the role of convection and the tropics in development and evolution of ULJFs from a lower stratospheric frontal perspective. The second topic (b) investigates the role of the lower stratospheric front in the development of upper level precursors to downstream sensible weather. With a more

coherent understanding of the evolution and development of lower stratospheric fronts, the third topic (c) interrogates the role of lower stratospheric fronts in altering the environment which determines propagation characteristics of atmospheric waves into the stratosphere.

a. Convection, the tropics and ULJFs

Chapters 2 and 3 illustrate that convection along a surface front can become vertically aligned with the vertical circulation involved in intensifying a lower stratospheric front. To the extent that lower stratospheric and lower tropospheric frontal circulations are vertically aligned, the kinetic energy released in any convective ascent along the tropospheric front can enhance the effect of the frontogenetic tilting already present in the lower stratospheric frontal circulation, thus further increasing the available potential energy being stored in an intensifying lower stratospheric front. The role that the kinetic energy released in association with tropospheric convection explicitly plays in the intensification of the thermal gradient (APE) in the lower stratosphere remains an outstanding question.

Understanding the role of frontal convection on the structure ULJFs will allow for greater insight into the nature of tropical/extra-tropical interaction processes. Much research attention has been given to the interaction between tropical cyclones and the extra-tropical environment. A number of studies have examined the critical role of positive vorticity advection by the thermal wind (PVA) and divergence, associated with the upper tropospheric portion of an ULJF, in the extratropical reintensification of tropical cyclones after recurving into the midlatitudes (DiMego and Bosart, 1982a, b; Sinclair, 1993; Foley and Hanstrum, 1994;

Harr et al., 2000). Likewise, Bosart and Lackmann (1995) illustrated that “tropopause lifting” can enhance the tropopause slope ahead of a weak upper tropospheric baroclinic disturbance and provide a mechanism by which tropical cyclones can shape the extratropical environment. Central to these studies is the role of the ULJF in facilitating the transition. Of particular interest is the idea of increasing the slope of the tropopause via lifting, this process will enhance the frontal characteristics of the environment above the jet core, within the lower stratospheric front, and will have impacts on the complete tropospheric and stratospheric structure of the ULJF. Fully interrogating this hypothesis from the more comprehensive ULJF perspective will shed light on the important and high impact process of tropical to extratropical transition and is elaborated upon in a proposal in Section 4.2.

b. Lower Stratospheric Fronts and Downstream Development

The initial inquiries into lower stratospheric fronts presented in the previous Chapters revealed that an apparent hand off in the baroclinic energetics occurs from the lower stratosphere (upper troposphere) to the upper troposphere (lower stratosphere) in northwesterly (southwesterly) flow. Investigating this suggested transfer from a baroclinic energetics perspective will be a step toward resolving the extent of this process and lead to a much more comprehensive view of the dynamics of the complete ULJF system. Explicitly connecting the lower stratospheric fronts to the energetics of upper tropospheric precursors provides a mechanism by which these features are connected to downstream sensible weather.

Understanding the energetics of the lower stratospheric front in the context of the

complete ULJF structure will provide a path toward answering questions pertaining to the dynamics involved in midlatitude weather systems. For instance, is the lower stratospheric geostrophic warm air advection in cyclonic shear tied to ridge building and blocking in the way that geostrophic cold air advection in the cyclonic shear within an upper tropospheric front is tied to upper level trough and cyclone development (Sanders, 1988; Rottuno, 1994; Schultz and Doswell, 1999; Lang and Martin, 2010)? The lower stratosphere, by its very nature, has a longer “memory” than the troposphere below it. Does the memory of the lower stratosphere allow a series of lower stratospheric frontogenesis cases to vastly alter downstream weather? Also of interest is the idea that the sloping midlatitude tropopause creates a horizontal potential vorticity gradient that acts as a wave guide for downstream energy propagation. The idea of PV frontogenesis (the temporal change in the magnitude of the horizontal potential vorticity gradient) was introduced by Davies and Rossa (1998) as an alternate view of upper tropospheric frontogenesis. Given the suggestion that the upper tropospheric and lower stratospheric fronts develop asynchronously, to what extent do these separate frontal processes manifest themselves in the life cycle of the important PV front?

c. Stratosphere-Troposphere Coupling

The importance of the lower stratospheric portion of midlatitude ULJF systems has, for the most part, only been considered in so far as it is manifested in a zonally averaged sense and on seasonal timescales. As summarized by Shepherd (2002), the zonally averaged meridional temperature gradient, associated with the sloping mid-latitude tropopause, is coupled (via

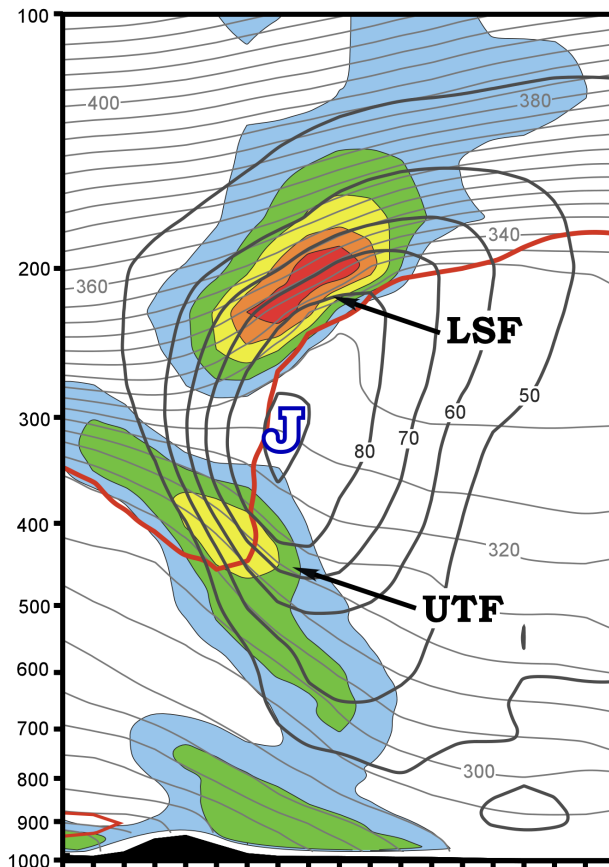
thermal-wind) to the zonal wind field at and above the tropopause which, in turn, determines the propagation characteristics of atmospheric waves into the stratosphere. Thus, it becomes pertinent to investigate whether a series of dynamically active lower stratospheric fronts, which alter the environment above the tropopause, exert an influence on the large scale stratospheric circulation and the seasonal scale stratosphere-troposphere exchange accomplished via the wave-driven Brewer-Dobson circulation. Fully understanding lower stratospheric frontogenesis has further implications for the coupling between the stratosphere and troposphere by potentially explaining some of the variation in the environment governing the vertical propagation of atmospheric waves. Perhaps consideration of lower stratospheric frontal processes will shed new light on the not-yet-completely-understood role of synoptic scale baroclinic waves in transmitting the downward propagating anomalies, associated with the Northern Annular Mode (NAM), from the stratosphere to the troposphere (e.g. Baldwin and Dunkerton, 1999, 2001; Haynes, 2005; Breiteig, 2008).

4.2. Research Proposal

North Pacific jet circulations during the extratropical transition of Western Pacific tropical cyclones

The subsynoptic scale structure of a jet-front system is characterized by a local wind speed maximum (i.e., the jet core) along the sloping mid-latitude tropopause surface. The regions of vertical shear located above and below the jet core are directly associated with attendant baroclinic zones (i.e., the fronts) via the thermal wind relationship (Figure 4.1). Recent work by Lang and Martin (2011) (Chapter 2) suggested that the upper tropospheric

Figure 4.1. A cross section the North Atlantic jet off the east coast of North America at 0000 UTC 28 November 2008, highlighting the jet core (marked with a “J”) and associated frontal structures. The upper tropospheric front is labeled “UTF” and the lower stratospheric front is labeled “LSF.” Isotachs are thick lines every 10 m s^{-1} beginning at 50 m s^{-1} , isentropes are thin lines every 4 K , and the magnitude of the horizontal potential temperature gradient is filled every $1 \text{ K (100 km)}^{-1}$ beginning at $2 \text{ K (100 km)}^{-1}$.



front (labeled “UTF” in Figure 4.1) and lower stratospheric front (labeled “LSF” in Figure 4.1) evolve asynchronously within the life cycle of a jet-front system. They showed that quasi-geostrophic (QG) forcing unique to the upper tropospheric or lower stratospheric cyclonic shear portion of the jet produced separate Sawyer (1956)-Eliassen (1962) type circulations (favorable for frontogenetic tilting) below or above the jet core, respectively. The magnitude of the vertical motion associated with these circulations is highly sensitive to the static stability (hereafter stability) of the environment in the vicinity of the jet-front system.

The analysis of intense lower stratospheric frontal cases (e.g., Figure 4.1) along the East Coast of North America (e.g., Chapters 2 and 3) suggests that convection along a surface boundary can become vertically aligned with the vertical circulation involved in strengthening

a lower stratospheric front. These analyses suggests that robust QG forced ascent, on the cold side of the lower stratospheric front, responded to the destabilization of the upper troposphere by surface based convection. As latent heat release associated with convection along the surface boundary redistributed the potential vorticity (PV; e.g., Hoskins et al. 1985) and reconfigured the potential temperature (e.g., Emanuel et al. 1987) fields within the upper troposphere, the stability of the near tropopause upper troposphere decreased. Such a configuration of latent heating was hypothesized to intensify the ascent responding to lower stratospheric QG forcing by decreasing the stability in the near tropopause upper troposphere. This vigorous ascent, located on the cold side of the lower stratospheric front, consequently lead to a notable period of lower stratospheric frontogenesis via tilting.

The preceding analyses suggests that (i) surface based convection is able to influence the development of lower stratospheric fronts and substantially alter the structure of a midlatitude jet-front system by increasing the response to lower stratospheric QG forcing for ascent; (ii) an enhanced ascent maximum above the jet core can subsequently lead to an increase in the slope of not only the isentropes, but also the tropopause above the jet core, via tilting; and (iii) when latent heat release occurs in the vicinity of a jet-front system with a dynamically active lower stratospheric front, the lower stratospheric frontal circulation may be able to enhance the mesoscale structure of the horizontal PV gradient above the jet core. These findings provide a basis for the idea that lower stratospheric frontogenesis is of consequence to midlatitude atmospheric dynamics and predictability insomuch as the structure of the jet is intimately linked to the tropopause slope and the midlatitude Rossby waveguide

associated with the horizontal PV gradient. The impact of convectively generated latent heat release on the lower stratospheric frontogenesis process is summarized in a conceptual model presented in Figure 3.15.

Tropical cyclones (TCs) that undergo extratropical transition (ET) in the vicinity of the North Pacific jet stream (e.g., Agustí-Panareda et al., 2004; Harr and Elsberry, 2000; Harr et al., 2000; Kitabatake, 2002, 2008; Klein et al. 2000, 2002) have the potential to vastly alter the subsynoptic scale structure of the jet. Subsequently, transitioning Pacific TCs can have high-impact consequences on the weather and predictability of the eastern North Pacific and North American continent (e.g., Agustí-Panareda 2008; Agustí-Panareda et al. 2005; Anwender et al. 2008; Harr et al. 2008; Harr and Dea 2009; Riemer et al. 2008). As recurving western Pacific TCs move poleward they encroach upon the enhanced baroclinicity associated with the North Pacific jet stream, characterized by frontal regions both in the upper troposphere and the lower stratosphere. The upper tropospheric front, and its concomitant frontal circulation, play a fundamental role in linking the jet with a variety of sensible weather phenomena, including the extratropical cyclone (EC) life cycle (e.g., Uccellini et al. 1985; Sanders 1988; Whitaker et al. 1988; Barnes and Colman 1993; and Lackmann et al. 1997) and, more specifically, the extratropical reintensification of remnant TCs (DiMego and Bosart 1982a,b; Sinclair 1993; Foley and Hanstrum 1994; Harr et al. 2000; Kitabatake 2002). The role of the lesser studied lower stratospheric front and its attendant frontal circulation (Lang and Martin, 2011) in the jet-front life cycle, as well as, their potential interaction with sensible weather systems are not well understood.

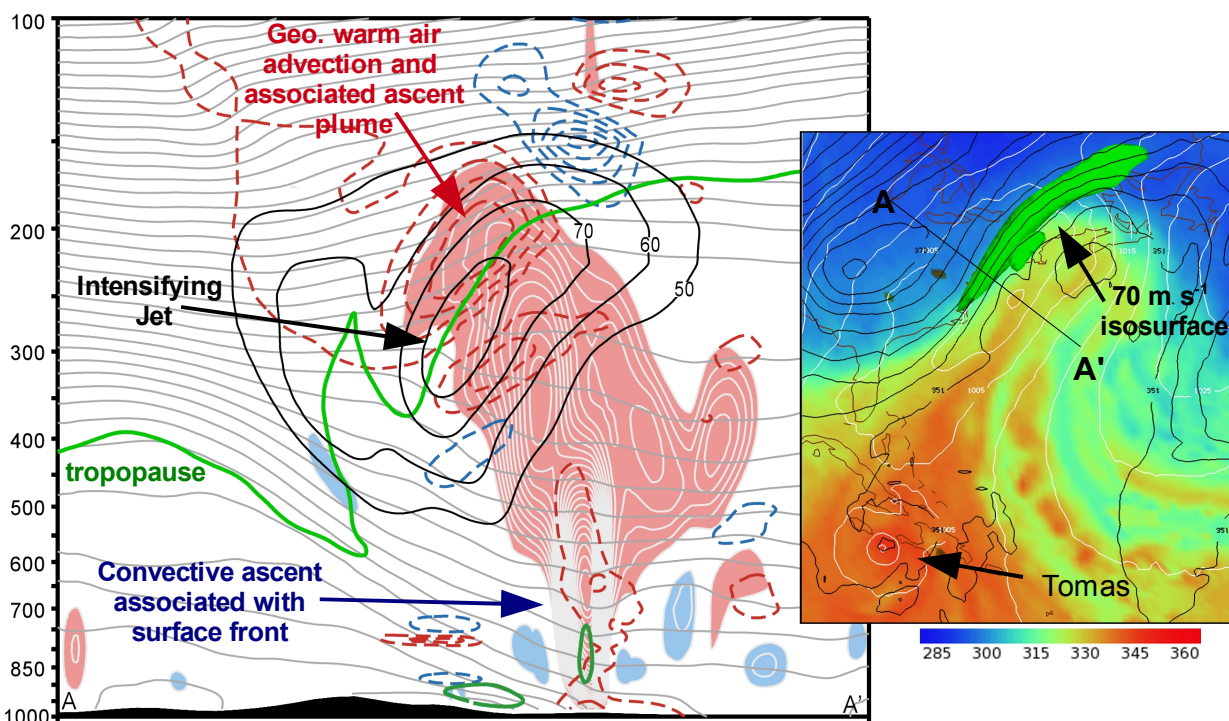


Figure 4.2. Valid at 0600 UTC 5 November 2010. Left: Cross section from A-A' in the right panel, with potential temperature every 4 K (gray lines), cross section normal wind speed every 10 m s^{-1} beginning at 50 m s^{-1} (thick lines), tropopause (1.5 PVU, green lines), geostrophic temperature advection every $5 \times 10^{-4} \text{ K s}^{-1}$ beginning at 5 (-5) $\times 10^{-4} \text{ K s}^{-1}$ in red (blue) dashed lines, vertical motion every 2 cm s^{-1} beginning at 4 cm s^{-1} (-4 cm s^{-1}) in pink (blue) fills. Right: 850 hPa equivalent potential temperature in K (fill), ~ 175 hPa potential temperature (black lines every 3 K), sea level pressure (white lines, every 5 hPa), and the 70 m s^{-1} isosurface (green).

As a TC recurves and interacts with the jet stream, a region of diabatically reduced PV and stability is introduced into the extratropical environment. Reduced stability in the vicinity of the jet stream can enhance the response to jet-front forcing for circulations. A recent example of such a TC-jet interaction occurred during early November of 2010 in the North Atlantic basin. On 29 October 2010, Tomas underwent TC genesis east of the Windward Islands and reached hurricane status on 30 October near the island of St. Vincent. As Tomas moved westward into the Caribbean, it encountered vertical shear and weakened to tropical

storm status on 1 November and tropical depression status for a brief period on 3 November. However, on 4 November Tomas began to recurve and by 5 November Tomas reintensified to Hurricane status over Haiti. During this recurvature period strong low-level southeasterly flow, between deepening Tomas and a strengthening Atlantic subtropical high, advected tropical air north of Tomas. This tropical air was ingested by the circulation associated with a surface frontal boundary, resulting in a linearly oriented band of convection off the east coast of North America (Figure 4.2). At upper tropospheric levels, the diabatically reduced stability associated with the upright convection along the surface front, as well as low PV outflow from Tomas, provided a means to reduce the stability directly to the cold side of a lower stratospheric front. It is hypothesized that the QG forcing within the lower stratospheric front was able to produce strong ascent within the cold upper troposphere in response to the reduced stability in that region. The upper tropospheric ascent consequently resulted in a period of robust lower stratospheric tilting frontogenesis, which corresponded to an enhancement of the tropopause slope, as well as the intensification of the southwesterly jet ($> 95 \text{ m s}^{-1}$ by 6 November) located between a trough-ridge couplet along the East Coast.

The analysis above suggests that the TC-jet interaction involving Hurricane Tomas and the North Atlantic jet had substantial downstream consequences on European weather. The exit region of the newly intensified jet in the Tomas case interacted with an arctic tropopause disturbance over Greenland to produce an explosively deepening cyclone ($\sim 995 \text{ hPa}$ to $\sim 960 \text{ hPa}$ in 18 h) that brought western Europe strong wind and waves, as well as heavy rain and unseasonably early snowfall. In addition, the uncertainty associated with the forecast of this

event resulted in 87 passengers being stranded on the NorthLink passenger ferry in the rough seas and unfavorable weather conditions off the coast of Scotland. The Tomas case is of particular relevance to the broader scope of this research, as not only was the upper level flow between the trough-ridge couplet straddling the East Coast amplified by processes associated with both Tomas and the jet-front circulations, but it was also associated with a Rossby wave train that was initiated upstream in the Western Pacific basin. A wave train that developed when Typhoon Chaba recurved and underwent ET as it interacted with the North Pacific jet stream between 20 October-1 November (Archambault et al. 2011).

The proposed project will emphasize the subsynoptic scale TC-jet interactions in cases involving major large-scale flow rearrangements over the western North Pacific, especially those cases that had consequent downstream impacts leading to reduced predictability over the eastern North Pacific and North America. Specifically, the investigation will highlight the evolution of the circulations associated with both the lower stratospheric and upper tropospheric fronts, as well as the processes involved in rearranging the structure of the North Pacific jet stream when remnant TCs experienced ET and reintensification as ECs. An example of a pertinent case study relevant to the proposed work occurred in November of 1996; ex-Super Typhoon Dale underwent ET and experienced a period of explosive reintensification when the subsequent EC appeared to “cross” the North Pacific jet stream. It is hypothesized that the diabatically generated outflow from ex-TC Dale was able to substantially alter the jet-level flow, via the subsynoptic scale jet circulations, resulting in jet stream redevelopment relative to the explosively deepening EC.

Research on the subsynoptic scale dynamics of jet-front systems, and the impact of the diabatic processes associated with TCs as they encroach on the North Pacific jet stream, will be accomplished through a variety of case study analyses. These case studies will allow for a diagnostic analysis of the separate dynamic forcing that occurred within the upper tropospheric and lower stratospheric components of the relevant jet-front systems. The diabatic reconfiguration of the stability field, along with the redistribution of the PV field, resulting from recurving and transitioning TCs will be highlighted. Of particular interest are the consequences of the jet-front forcing for vertical motion on the TC altered extratropical environment in the vicinity of the North Pacific jet. Cases such as (i) TC Malakas (2010), the recurvature of which directly excited a Rossby wave train that was associated with high impact weather in the eastern Pacific and North America; (ii) TC Chaba (2010) which during recurvature preconditioned the North Pacific jet into a configuration conducive to the excitation of a Rossby wave train (Archambault et al. 2011); and (iii) TC Dale (1996) and its associated explosively deepening EC. In addition, cases of interests from the recent past [TC Ioke (2006), TC Nari (2007), TC Bavi (2008)], as well as Nida (2009) and Megi (2010) will be considered.

Chapter 5

References

- Agustí-Panareda, A. (2008). The contribution of ex-tropical cyclone Gert (1999) toward the weakening of a midlatitude cyclogenesis event. *Mon. Wea. Rev.*, **136**, 2091-2111.
- Agustí-Panareda, A., C. D. Thorncroft, G. C. Craig, and S. L. Gray, (2004). The extratropical transition of hurricane Irene (1999): A potential-vorticity perspective. *Quart J. Roy. Met. Soc.*, **130**, 1047-1074.
- Agustí-Panareda, A., S. L. Gray, G. C. Craig, and C. D. Thorncroft (2005). The extratropical transition of tropical cyclone Lili (1996) and its crucial contribution to a moderate extratropical development. *Mon. Wea. Rev.*, **133**, 1562–1573.
- Anwender, D., P. A. Harr, and S. C. Jones (2008). Predictability associated with the downstream impacts of the extratropical transition of tropical cyclones: Case studies. *Mon. Wea. Rev.*, **136**, 3226–3247.
- Archambault, H., J. M. Corderia, R. A. Lazear, L. F. Bosart, and D. Keyser, (2011) “Reduced predictability and extreme weather events over North America following the recurvature of western Pacific tropical cyclones,” *15th Cyclone Workshop*, Monterey CA., Asilomar Conference Grounds.
- Baldwin, M.P., and T.J. Dunkerton, (1999). Propagation of the Arctic Oscillation from the stratosphere to the troposphere. *J. Geophys. Res.* **104**, 30937-30946.
- Baldwin, M.P., and T.J. Dunkerton, (2001). Stratospheric harbingers of anomalous weather regimes, *Science*, **294**, 581-584.
- Barnes, S., and Colman, B., (1993). Quasigeostrophic diagnosis of cyclogenesis associated with a cutoff extratropical cyclone - the Christmas 1987 storm. *Mon. Wea. Rev.* 121 (6) 1613-1634.
- Berggren. R. (1952): The distribution of temperature and wind connected with active tropical air in the higher troposphere and some remarks concerning clear air turbulence at high altitude. *Tellus*, 4, 43-54.

- Bjerknes, J. and H. Solberg (1922): Life Cycle of Cyclones and the Polar Front Theory of Atmospheric Circulation. *Geofys. Publik.* 3 (1) 1-18.
- Bjerknes, V. and E. Palmén (1937): Investigations of selectd European cyclones by means of serial ascents. *Geofys. Publik.* 12 (2) 1-62.
- Bosart, L. F., and G. M. Lackmann (1995). Postlandfall tropical cyclone reintensification in a weakly baroclinic environment: A case study of hurricane David (September 1979). *Mon. Wea. Rev.*, **123**, 3268-3291.
- Breiteig, T., (2008). Extra-tropical synoptic cyclones and downward propagating anomalies in the Northern Annular Mode. *Geophys. Res. Lett.* **35** L07809.
- Bryson, R. (1994): *Discovery of the Jet Stream*. Wisconsin Academy Review 40 (3) Madison, Wisconsin: Wisconsin Academy of Science, Arts, and Letters, Summer 1994.
- Danielsen, E. F. (1964). Project Springfield Report. Washington D. C., Defense Atomic Support Agency, DASA 1517, 97 pp. (DDC)
- Danielsen, E. F. (1968). Stratospheric-Tropospheric Exchange Based on Radioactivity, Ozone and Potential Vorticity. *J. Atmos. Sci.* **25**, (3), 502–518
- Davies, H. C. and A. Rossa (1998). PV frontogenesis and upper-tropospheric fronts. *Mon. Wea. Rev.*, **126**, 1528–1539.
- DiMego, G. J., and L. F. Bosar, (1982a). The transformation of Tropical Storm Agnes into an extratropical cyclone. Part I: The observed fields and vertical motion computations. *Mon. Wea. Rev.*, **110**, 385-411.
- DiMego, G. J., and L. F. Bosart (1982b). The transformation of Tropical Storm Agnes into an extratropical cyclone. Part II: Moisture, vorticity, and kinetic energy budgets. *Mon. Wea. Rev.*, **110**, 412-433.
- Dines, L. H. G., (1929) *The Dines balloon meteorograph and the method of using it*. H. M Stationery Office, London, UK.
- Eisele H, H. E. Scheel, R Sladkovic, and T. Trickl, (1999). High-Resolution Lidar Measurements of Stratosphere–Troposphere Exchange. *J. Atmos. Sci.* **56**, (4) 319–330
- Eliassen, A. (1962): On the vertical circulation in frontal zones. *Geof. Publ.* 24, (4) 147-160.
- Emanuel, K. A., M. Fantini, and A. J. Thorpe (1987). Baroclinic instability in an environment of small stability to slantwise moist convection. Part I: Two-dimensional models. *J. Atmos. Sci.*, **44**, 1559-1573.
- Foley, G. R. and B. N. Hanstrum (1994). The capture of tropical cyclones by cold fronts off the west coast of Australia. *Wea. and Forecasting*, **9**, 577-592.
- Harr, P. A., and R. L. Elsberry (2000). Extratropical transition of tropical cyclones over the

- western north Pacific. Part I: Evolution of structural characteristics during the transition process. *Mon. Wea. Rev.*, **128**, 2613–2633.
- Harr, P., R. L. Elsberry, and T. Hogan (2000). Extratropical transition of tropical cyclones over the western North Pacific. Part II: The impact of midlatitude circulation characteristics. *Mon. Wea. Rev.*, **128**, 2634-2653.
- Harr, P. A., D. Anwender, and S. C. Jones (2008). Predictability associated with the downstream impacts of the extratropical transition of tropical cyclones: Methodology and a case study of Typhoon Nabi (2005). *Mon. Wea. Rev.*, **136**, 3205-3225.
- Harr, P. A., and J. M. Dea (2009). Downstream development associated with the extratropical transition of tropical cyclones over the western North Pacific. *Mon. Wea. Rev.*, **137**, 1295-1319.
- Haynes, P. J. (2005). Stratospheric Dynamics. *Annu. Rev. Fluid Mech.* **37**, 263-293.
- Hobbs, P. V., J. D. Locatelli, and J. E. Martin (1990). Cold fronts aloft and the forecasting of precipitation and severe weather east of the rocky mountains. *Wea. Forecasting.* **5**, 613-626.
- Holton, J. R., P. H. Haynes, M. E. McIntyre, A. R. Douglass, R. B. Rood, and L. Pfister, (1995) Stratosphere-Troposphere Exchange. *Rev. Geophys.* **33**, 4. 403-439.
- Hoskins, B. J., M. E. McIntyre, and A. W. Robertson (1985). On the use and significance of isentropic potential vorticity maps. *Quart J. Roy. Met. Soc.*, **111**, 877-946.
- Keller, J. L. (1990). Clear air turbulence as a response to meso- and synoptic-scale dynamic processes. *Mon. Wea. Rev.*, **118**, 2228–2242.
- Kennedy, P. J., and M. A. Shapiro (1975). The energy budget in a clear air turbulence zone as observed by aircraft. *Mon. Wea. Rev.* **103**. 650-654
- Kennedy, P. J., and M. A. Shapiro (1980). Further encounters with clear air turbulence in research aircraft. *J. Atmos. Sci.* **37**, 986–993.
- Keyser, D, and M. A. Shapiro (1986). A review of the structure and dynamics of upper level frontal zones. *Mon. Wea. Rev.* **114**, 452-499.
- Keyser, D, and M. J. Pecneck (1985). A two-dimensional primitive equation model of frontogenesis forced by confluence and horizontal shear. *J. Atmos. Sci.* **42**, 1259-1282.
- Kitabatake, N., 2002: Extratropical transformation of Typhoon Vicki (9807): Structural change and the role of upper-tropospheric disturbances. *J. Meteor. Soc. Japan*, **80**, 229-247.
- Kitabatake, N., 2008: Extratropical transition of tropical cyclones in the western North Pacific: Their frontal evolution. *Mon. Wea. Rev.*, **136**, 2066-2090.
- Klein, P. M., P. A. Harr, and R. L. Elsberry (2000).: Extratropical transition of western North

- Pacific tropical cyclones: An overview and conceptual model of the transformation stage. *Wea. Forecasting*, **15**, 373-396.
- Klein, P. M., P. A. Harr, and R. L. Elsberry (2002). Extratropical transition of western North Pacific tropical cyclones: Midlatitude and tropical cyclone contributions to reintensification. *Mon. Wea. Rev.*, **130**, 2240-2259.
- Lackmann, G. M., D. Keyser, and L. F. Bosart (1997). A characteristic life cycle of upper-tropospheric cyclongenetic precursors during Experiment on Rapidly Intensifying Cyclones over the Atlantic (ERICA). *Mon. Wea. Rev.*, **123**, 1476-1504.
- Lamarque, J.-F., and P. G. Hess (1994). Cross-tropopause mass exchange and potential vorticity budget in a simulated tropopause folding. *J. Atmos. Sci.* **51**, 15 2246–2269
- Lang, A. A., and J. E. Martin (2010). The influence of rotational frontogenesis and its associated shearwise vertical motions on the development of an upper level front. *Q. J. Roy. Meteor. Soc.*, **136**, 239-252.
- Lang, A. A., and J. E. Martin (2011). The structure and evolution of lower stratospheric frontal zones. Part I: Examples in northwesterly and southwesterly flow. *Quart J. Roy. Met. Soc.*, **137**: 000-000 (*in press*)
- Martin, J. E. (2006). The role of shearwise and transverse quasigeostrophic vertical motions in the midlatitude cyclone life cycle. *Mon. Wea. Rev.* **134**, 1174-1193.
- Mohanakumar, K. (2008). *Stratosphere-Troposphere Interactions: An introduction*. Springer, Heidelberg, Germany.
- Newton, C. W., and A. Trevisan (1984). Clinogenesis and Frontogenesis in Jet-Stream Waves. Part I: Analytical Relations to Wave Structure. *J. Atmos. Sci.* **41**, 2717-2734.
- Palmén, E. (1948): On the distribution of temperature and wind in the westerlies. *J. Meteor.* **5** 20-27.
- Palmén, E. and K. M. Nagler (1949): Formation and structure of a large-scale disturbance in the westerlies. *J Meteor.* **6** (4) 227-242.
- Palmén, E. (1958): Vertical circulation and release of kinetic energy during the development of hurricane Hazel into an extratropical cyclone. *Tellus*, **10**, 1–23.
- Reed, R. J. (1955): A study of a characteristic type of upper-level frontogenesis. *J. Meteor.*, **12**, 226–237.
- Reed, R. J., and K. M. Hardy (1972). A case of persistent, intense, clear-air turbulence in an upper level frontal zone. *J. App. Metro.* **11**, 541-549.
- Reed, R. J. and F. Sanders (1953): An investigation of the development of a mid-tropospheric frontal zone and its associated vorticity field. *J. Meteor.*, **10**, 338–349.

- Riehl, H. (1948). Jet stream in upper troposphere and cyclone formation. *Trans. Am. Geophys. Union*, **29**, 175-186.
- Riemer, M., S. C. Jones, and C. A. Davis (2008). The impact of extratropical transition on the downstream flow: An idealized modeling study with a straight jet. *Quart. J. Roy. Meteor. Soc.*, **134**, 69–91.
- Rotunno, R., W. C. Skamarock, and C. Snyder (1994). An analysis of frontogenesis in numerical simulations of baroclinic waves. *J. Atmos. Sci.*, **51**, 3373-3398.
- Sanders, F. (1988). Life history of mobile troughs in upper westerlies. *Mon. Wea. Rev.* **116**, 2629–2648.
- Sawyer, J. S. (1952). Dynamical aspects of some simple frontal models. *Quart. J. Roy. Meteor. Soc.* **78** 170
- Schultz, D. M., and C. A. Doswell (1999). Conceptual models of upper-level frontogenesis in southwesterly and northwesterly flow. *Quart. J. Roy. Meteor. Soc.*, **125**, 2535-2562.
- Sinclair, M. R., (1993). Synoptic-scale diagnosis of the extra-tropical transition of a southwest Pacific tropical cyclone. *Mon. Wea. Rev.*, **121**, 941-460.
- Shapiro, M. A., (1976). The role of turbulent heat flux in the generation of potential vorticity in the vicinity of upper-level jet stream systems. *Mon. Wea. Rev.*, **104**, 892–906.
- Shapiro, M. A. (1980). Turbulent mixing within tropopause folds as a mechanism of the exchange of constituents between the stratosphere and troposphere. *J. Atmos. Sci.* **37**, 994-1004.
- Shapiro, M. A. (1981). Frontogenesis and geostrophically forced secondary circulations in the vicinity of jet stream-frontal zone systems. *J. Atmos. Sci.*, **38**, 954–973.
- Shapiro, M. A. (1982). *Mesoscale Weather Systems of the Central United States*. CIRES Univ. of Colorado/NOAA, Boulder, Colo, USA. 78 pp.
- Shapiro, M. A., T. Hampel, and A. J. Krueger (1987). The arctic tropopause fold. *Mon. Wea. Rev.* **115**, 2, 444–454.
- Shapiro, M. A., and D. Keyser (1990) Fronts, jet streams and the tropopause. *Extratropical Cyclones, The Erik Palmén Memorial Volume*, C. W. Newton and E. O. Holopainen, Eds., Amer. Meteor. Soc., 167–191.
- Shepherd, T. G. (2002). Issues in stratosphere-troposphere coupling. *J. Meteorol. Soc. Japan.* **80**, 769-792.
- Stohl, A., P. Bonasoni, P. Cristofanelli, W. Collins, J. Feichter, A. Frank, C. Forster, E. Gerasopoulos, H. Gäggeler, P. James, T. Kentarchos, S. Kreipl, H. Kromp-Kolb, B. Krüger, C. Land, J. Meloen, A. Papayannis, A. Priller, P. Seibert, M. Sprenger, G. J.

- Roelofs, E. Scheel, C. Schnabel, P. Siegmund, L. Tobler, T. Trickl, H. Wernli, V. Wirth, P. Zanis, and C. Zerefos. (2003). Stratosphere-troposphere exchange - a review, and what we have learned from STACCATO. STACCATO special section of *J. Geophys. Res.* **108**, 8516.
- Sutcliffe, R. C. (1947). A contribution to the problem of development. *Q. J. R. Meteorol. Soc.* **73**, 370-383.
- Trenberth, K. E. (1978). On the interpretation of the diagnostic quasigeostrophic omega equation. *Mon. Wea. Rev.* **106**, 131-137.
- Uccellini, L. W., D. Keyser, K. F. Brill, and C. H. Wash (1985). The President's Day cyclone of 18-19 February 1979: Influence of upstream trough amplification and associated tropopause folding on rapid cyclogenesis. *Mon. Wea. Rev.* **113**, 962-988.
- Whitaker, J. S., L. W. Uccellini, and K. F. Brill (1988). A model based diagnostic study of the Rapid development phase of the President's Day Cyclone. *Mon. Wea. Rev.* **116**, 2337-2365.